The tether model and the role of skin-derived laminin-332 (laminin-5) in sensory mechanotransduction

Inaugural-Dissertation
to obtain the academic degree of
Doctor rerum naturalium (Dr. rer. nat)
submitted to the Department of Biology, Chemistry and Pharmacy
of Freie Universität Berlin

by

Li-Yang Chiang

Born in Taichung, Taiwan

Berlin, July 2009

1st Reviewer: Prof. Dr. Fritz G. Rathjen

2nd Reviewer: Prof. Dr. Gary R. Lewin

Date of defense: 09 July 2009

Acknowledgements

First and for most, I would like to thank my parents, my wife and my sister for encouraging me in every step of the way. Without your absolute love and support, my education would not have been possible.

I would like to send my sincere gratitude to my supervisor Prof. Dr. Gary Lewin for guiding me throughout this work with all the advices and absolute optimism about this work and my postdoctoral fellow Dr. Jing Hu for useful suggestions and inspiring brainstormings. I really enjoyed working with you.

I am indebted to Dr. Bettina Erdmann for your help with EM techniques and Margit, Mariana, in the EM core facility group and Heike in our group for your technical support. I have learned a lot from you.

I am grateful to my colleagues in the MDC. We together have created a productive working atmosphere. I also want to thank Sören Markworth for your excellent translation of ZUSAMMENFASSUNG and Dr. Ewan Smith as well as Dr. Kate Poole for proofreading my thesis.

Declaration

This project was conducted and finished in the group of “Molecular physiology of somatic sensation” in the Max Delbrück Zentrum für Molekulare Medizin under the supervision of Prof. Dr. Gary R. Lewin. This thesis is submitted to the Department of Biology, Chemistry and Pharmacy of Freie Universität Berlin to obtain the academic degree of Doktors der Naturwissenschaften (Dr. rer. nat). It has not been submitted for any other degree of any examining body. Except where specifically mentioned, it is all the work of the author.

Berlin

SUMMARY

The skin is our largest sensory organ and required for the perception of the outside world using our sense of touch and pain. The underlying mechanism for sensory mechanotransduction at the molecular level is poorly understood. In sensory hair cells of the inner ear, extracellular protein filaments called tip links tethering mechanosensitive ion channels between stereocilia are required for mechanotransduction. In this study, we showed that a protein link, which is sensitive to the endopeptidases subtilisin and blisterase is necessary for the gating of mechanosensitive rapidly adapting (RA) currents in dorsal root ganglia (DRG) neurons. Using transmission electron microscopy (TEM), we demonstrated that a protein filament with a length of ~100 nm is synthesized by sensory neurons and may link mechanosensitive ion channels in sensory neurons to the extracellular matrix. This was the first evidence to show that an extracellular mechanotransducer link exists and that it maybe essential for normal mechanotransduction.

In this study we also investigated the role of the extracellular matrix (ECM) in sensory mechanotransduction. It was found that keratinocyte-derived ECM can profoundly inhibit the expression of RA current and delay gating of the mechanosensitive slowly adapting (SA) currents. We then identified a skin-derived protein laminin-332 as responsible for the inhibition of RA current expression but not for delaying SA current gating on keratinocytes-derived matrix. It was shown that laminin-332 is a potent inhibitory factor selectively for inhibition of RA current expression and TEM results showed that this can be

attributable to a lack of tether binding to the substrate, which is required for RA current gating. Microcontact printing and biochemical experiments revealed that laminin-332 is a local inhibitory factor not only for mechanosensitivity but also for neurite outgrowth in a manner independent of integrin. Our data suggests that laminin-332 inhibition of mechanosensitivity and of neurite outgrowth are likely two independent scenarios.

ZUSAMMENFASSUNG

Die Haut ist das grösste sensorische Organ des Menschen. Sie ist notwending für die Wahrnehmung unserer Umgebung durch Tasten und Schmerzempfinden. Über die zugrundeliegende sensorische Mechano-transduktion ist auf molekularer Ebene noch relativ wenig bekannt. In sensorischen Haarzellen des Innenohrs sind extrazelluläre Proteinfilamente, auch genannt „tip links“, zur Funktion der Mechanotransduktion notwendig. Diese Filamente verbinden mechanosensitive Kanäle zwischen den Stereocilia wie ein Spannseil. In diesem Projekt wurde gezeigt, dass ein Protein-link, der sensitiv gegenüber den Endopeptidasen Subtilisin und Blisterase ist, für mechanosensitive Ströme des RA Typs (RA=rapidly adapting) in DRG Neuronen notwendig ist. Mittels Transmissionselektronenmikroskopie (TEM) wurde beobachtet, dass sensorische Neuronen ein Protein-Filament mit einer Länge von ~100nm synthetisieren, welches mechanosensitive Inonenkanäle mit der extrazellulären Matrix verlinken könnte. Dies ist der erste Nachweis der

Existenz eines extrazellulären Mechanotransduktions-Links, der essentiell für eine normale Mechanotransduktion sein könnte.

In diesem Projekt wurde weiterhin die Rolle der extrazellulären Matrix (ECM) in sensorischer Mechanotransduktion untersucht. Vorherige Untersuchungen ergaben, dass von Keratinozyten abstammende ECM die mechanosensitiven RA-Ströme inhibiert und SA (slowly adapting)-Ströme verzögert. Wir konnten das Protein Laminin-332 identifizieren, das für die Inhibition der RA-Ströme, nicht aber für die Verzögerung der SA-Ströme auf Keratinozyten-ECM verantwortlich ist. Laminin-332 ist ein wirksamer selektiver Inhibitor des RA-Stroms und unsere TEM Ergebnisse zeigten, dass diese Inhibition durch eine fehlende Verbindung zum für die Erzeugung von RA-Strömen notwendigen Substrat verursacht werden könnte. Durch Microcontact Printing und biochemische Experimente konnte gezeigt werden, dass Laminin-332 ein lokaler Inhibitor nicht nur für Mechanosensivität ist, sondern Laminin-332 inhibiert ebenfalls das Axonwachstum unabhängig von Integrinen. Unsere Ergebnise sprechen dafür, dass die Inhibition der Mechanosensitivität durch Laminin-332 und die Inhibition des Axonwachstums zwei unterschiedliche Szenarien sind.

ABBREVIATIONS

NF	Neurofilament
TRPV	Transient receptor potential cation channel, subfamily V
DEG/ENaC	Degenerin/ epithelial Na^+ channel
EHS	Engelbreth-Holm-Swarm sarcoma
Laminin	Engelbreth-Holm-Swarm sarcoma-derived matrix
ECM	Extracellular matrix
EGF	Epidermal growth factor
ALs	Ankle links
KLs	Kinocilial links
SCs	Shaft connectors
TLs	Tip links
ULs	Upper lateral connectors
C. elegans	*Caenorhabditis elegans*
D. melanogaster	*Drosophila melanogaster*
E. Coli	*Escherichia coli*
O. Volvulus	*Onchocerca volvulus*
3T3	Mouse embryonic fibroblasts
SCC	Squamous cell carcinoma
DRG	Dorsal root ganglia
SCG	Superior cervical ganglia
BMZ	Basement membrane zone
JEB	Junctional epidermolysis bullosa

BAPTA	1,2-bis(o-aminophenoxy) ethane-N,N,N',N'-tetraacetic acid
PLL	Poly-L-Lysine
PIPLC	Phosphatidylinositol phospholipase C
TTX	Tetrodotoxin
PDMS	Polydimethylsiloxane
TEM	Transmission electron microscopy
RA	Rapidly adapting
IA	Intermediately adapting
SA	Slowly adapting
AP	Action potential

1 INTRODUCTION

Much of Aristotle's (384-322 BC) discussion of the soul concerns the topic of sense and perception. He discussed the physiology of each of the five senses, which are sight, tasting, smell, hearing and touch in detail and defines perception in general as the reception of the perceptible form of an external object in the soul. Simply speaking, senses are the physiological methods of perception. From the day we were born, we have been learning about the outside world through our five senses. The nervous system has a specific sensory system, dedicated to each sense. Each of the five senses can be subdivided by neurobiologists into a number of sub-senses based on differing definitions of what constitutes a sense.

It is known that smell, sight and much of taste are initiated by ligands binding to G-protein coupled receptors as the transduction molecule. Of these G-protein coupled senses, phototransduction is a process by which light energy is converted to a change in membrane potential. Rhodopsin serves as a photoreceptor protein, which undergoes a conformational change upon photoexcitation and activates a G protein, transducin, and eventually opens ion channels to excite/hyperpolarize photoreceptors (Hargrave 1992). Smell (olfaction) and taste (gustation) are both chemically activated sensations. They have evolved complex repertoires of chemosensory receptors, which are G-protein coupled receptors with a seven transmembrane domain structure. The mammalian mechanism for smell, which takes place in the olfactory bulb has been well studied and characterized. In the olfactory system, there are hundreds of olfactory receptors each binding to specific ligands (odor molecules or

odorants). Binding of odorants to the receptors on the cell surface stimulates adenylate cyclase to synthesize cAMP via a G-protein. cAMP then acts as a second messenger which subsequently opens a cyclic nucleotide-gated ion channel (CNG) depolarizing the cell by producing a cation influx (mostly Ca^{2+} and some Na^{+}) into the cell. The Ca^{2+} in turn opens a Ca^{2+}-activated chloride channel, leading to efflux of Cl^{-}, further depolarizing the cell and triggering an action potential (AP) (Storm 2003; Biel and Michalakis 2007). Taste is another chemically activated sensation, which involves many processes and each basic taste may use one or more of these mechanisms. Selective taste buds (peripheral taste receptors) concentrated on the upper surface of the tongue respond to a subset of taste cues such as saltiness, sweetness, sourness, bitterness and umami (taste of amino acids such as glutamate). Information of taste ligands is then coded in the periphery and taste cells are activated, which eventually evoke an AP in sensory afferents and transmit the information to the brain. Taste stimuli (or tastants) may (1) directly pass through ion channels (salt or sour), (2) bind to and block ion channels (sour and bitter), (3) bind to and open ion channels (some amino acids), or (4) bind to membrane receptors that activate second messenger system that , in return, open or close ion channels (sweet, bitter and umami). These are familiar processes, the functional building blocks of signaling in all neurons and synapses. (Laurent 1999; Mombaerts 2004; Drayna 2005; Scott 2005).

Hearing and touch are both considered mechanically activated sensations, and the underlying process is termed mechanotransduction, which is the conversion of a mechanical stimulus into an electrical signal. It reveals vital features of the

environment that an organism lives in. Mechanosensation is mediated by a wide variety of receptor types, from bristle receptors in flies and touch receptors in worms, to hair cells in the hearing apparatus and skin mechanoreceptors in vertebrates. In various mechanotransduction systems, mechanically sensitive cells play a crucial role and are essential for viability of a living organism. The scarcity of these cells and the uniqueness of their transduction mechanisms have conspired to slow cellular and molecular characterization of the molecular complexes that presumably mediate mechanotransduction. Recent progress in both invertebrates and vertebrates is beginning to reveal the identities of proteins essential for transduction and the mechanism.

1.1 Mechanosensation

Almost all living creatures respond to mechanical stimulation. Mechanical forces applied on an organism provide useful information about the world surrounding it. An organism detects mechanical information with a variety of cells that respond to force. Processing of the information that is received from the outer world relies on a unique subset of cells, named mechanosensory cells. One of the essential components in mechanotransduction complex is the mechanosensitive ion channels, which are gated by mechanical force and such mechanosensitive channels are thought to underlie mechano-electro transduction, which converts the mechanical forces into electrical signals.

Two models have been proposed for the gating of mechanosensitive channels: the membrane stretch-activated model and the tether model. In the first model changes in tension within the cell membrane directly open the ion channel through conformational changes in the channel protein (Fig. 1). Unicellular organisms like *Escherichia coli (E. coli)* as well as multicellular organisms require mechanisms that would protect their delicate cell membrane from potentially damaging mechanical stimuli. Bacteria have evolved a mechanism for sensing the extracellular environment change that subsequently regulates the cells to protect their plasma membrane from excessive dilation. The relevant force-transducing molecules, ie the mechanosensitive ion channels, have been identified in previous studies and are exemplified by and proven for the swelling activated bacterial channel MscL (Mechanosensitive channel of Large conductance) and MscS (mechanosensitive channel of small conductance) in which just the channel protein alone can be gated by membrane tension alone (Sukharev et al. 1994; Hamill and Martinac 2001; Kloda and Martinac 2002; Sukharev and Anishkin 2004; Kung 2005). Such channel proteins purified from bacteria sense forces from the lipid bilayer in the absence of other proteins. Recent evidence has shown that lipids are also intimately involved in opening and closing the mechanosensitive channels of fungal, plant and animal species. Patel and co-workers identified the polymodal K^{2+} channel of mammals, TREK-1, which is two-pore domain weak inward rectifying (TWIK)-related K^{2+} channel. It can be activated by both force and osmolarity change. Similar to MscS and MscL, it is also activated by bulge-forming amphipathic chemicals such as trinitrophenol, also termed crenaters, but inhibited by cup-forming amphipaths such as chlorpromazine (Patel 1998; Patel et al. 2001). It can be activated by the

cone-shaped lysophosphatidylcholine, whereas activated even more effectively by the exaggerated cone lysophosphatidylinositol (Patel et al. 2001).

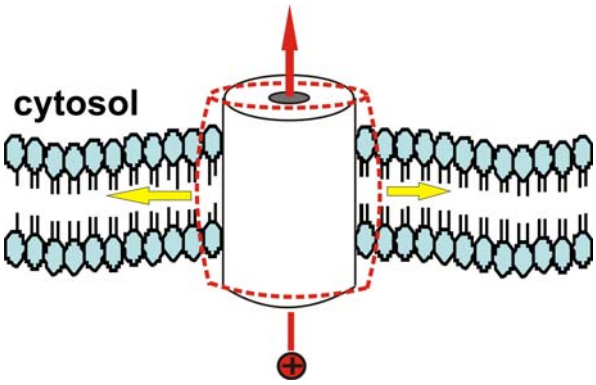

Figure 1. Model for stretch-activated mechanosensitive channel gating

In this model, bilayer tension could directly activate the channel. This occurs with prokaryotic stretch-activated channels such as MscL and MscS. No associated proteins are required. Some mammalian channels, such as TREK-1 and TRAAK are functionally defined by stretch activation may also be directly mechanically gated. These strech-activated mechanosensitive ion channels are capable of rectifying K^+ inward current (Hamill and Martinac 2001).

1.2 Sensory mechanotransduction

Sensory physiologists have proposed a somewhat different model based on the findings from sensory mechanotransduction complexes such as the invertebrate nematode *Caenorhabditis elegans (C. elegans)* and the hair cell in the inner ear. In spite of the structural differences, invertebrate mechanoreceptors, bristles of *Drosophila melanogaster (D. melanogaster)*, hair cells within the inner ear and cutaneous mechanoreceptors of the skin share many mechanistic features. One important feature is that these receptors maybe gated by a tether although this has not yet been shown for cutaneous receptors (Gillespie and Walker 2001)

(Fig. 2). In this model, the mechanosensitive channel binds to the extracellular matrix (ECM) or the intracellular cytoskeleton through a tether. Movement of this complex structure or mechanical force applied to the cell membrane is thought to be converted into tension and transmits or perhaps amplifies applied stresses to gate the channel (Gu et al. 1996; Itzhak and Driscoll 1999; Gillespie and Walker 2001; Hamill and Martinac 2001).

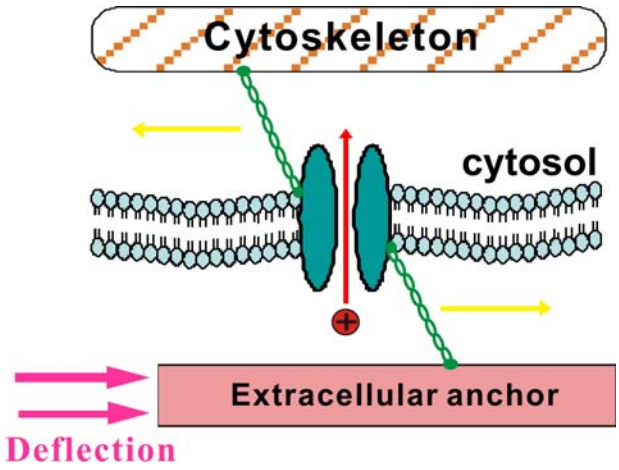

Figure 2. Schematic representation of tethered-model channel gating A transduction channel is anchored by intracellular and extracellular anchors to the cytoskeleton and extracellular structure to which forces are applied. In the resting state, components in the sensory mechanotransduction complex are at rest, maintaining the channel in its closed conformation. When pressure is applied on the extracellular structure, the transduction channel responds to tension in the system, which is increased by net displacements between intracellular and extracellular structures (Gillespie and Walker 2001).

For sensory hair cells of the inner ear it is thought that transduction channels located at the tips of stereocilia are gated by changes in tension within extracellular tip links that are attached to the channel. In essence the extracellular tip link was thought to act as a gating tether which binds to mechanosensitive ion channels and pull them open in response to mechanical stimulation (Markin and

Hudspeth 1995; Gillespie and Walker 2001). Independent of the above evidence, genetic screens carried out in both *C. elegans* and *D. melanogaster* have uncovered extracellular proteins, with functions reminiscent of hair cell tip links that are essential for the transduction of body touch and fly bristle movement respectively (Du et al. 1996; Chung et al. 2001; Ernstrom and Chalfie 2002). A number of candidate molecules that may fit with this model have been suggested to play a role in mechanotransduction in *C. elegans, D. melanogaster* as well as in mammals (Goodman and Schwarz 2003; Lewin and Moshourab 2004; Tobin and Bargmann 2004; Hu et al. 2006). Below, I will review the findings from the three well established tether model in *C. elegans*, *D. melanogaster* and the hair cell at its molecular level.

1.3 Molecular nature of sensory mechanotransduction in different systems

1.3.1 Invertebrate mechanoreceptor transduction model in *C. elegans* and *D. melanogaster*

A molecular model for cutaneous body touch in the nematode *C. elegans* emerged from studies by Chalfie and Sulston twenty years ago (Chalfie et al. 1981; Chalfie and Sulston 1981; Chalfie et al. 1983; Chalfie et al. 1985). They used classical mutagenesis approaches to screen mutants for aberrations in gentle touch sensation behavior along the body of the worms. Genes that were identified are named mechanosensitive *'mec'* genes, meaning mechanosensory

abnormal genes and their gene products are named MEC proteins. Among the identified genes that are related to the *C. elegans* sensory mechanotransduction complex, twelve genes are directly involved in touch receptor functioning and six other genes are important for mechanoreceptor cell development (Chalfie and Sulston 1981; Chalfie and Au 1989). The crucial component in the sensory mechanotransduction model derived from these studies is a mechanosensitive ion channel that is composed of MEC-4 and MEC-10, which are considered to form the pore of the heteromultimeric ion channel complex (Lai et al. 1996). The N- and the C-terminus of the channel proteins are cytoplasmic but their central regions are exposed to the extracellular side of the membrane and possibly attached to proteins of the ECM. Two accessory proteins which might be subunits of the ion channel itself, have been shown to modulate its activity (Chelur et al. 2002; Goodman et al. 2002). Three touch function genes: *mec-1*, *mec-5* and *mec-9* encode ECM proteins, a collagen (Driscoll and Tavernarakis) and an EGF/Kunitz repeat protein (Mec-9), which may also interact with each other in the mantle (Ernstrom and Chalfie 2002). On the intracellular side the ion channel seems to be linked to a specialized 15 protofilament microtubule network formed by MEC-12, a α-tubulin, and MEC-7, a β-tubulin, which are also shown to be essential for mechanosensation in *C. elegans* (Huang et al. 1995). In the absence of a mechanical stimulus the ion channel is normally closed. In response to mechanical forces, the two rigid structures of the mechanotransduction complex, i.e. the extracellular mantle and the intracellular microtubule network, presumably move relative to one another and subsequently force the channel to open (Fig. 3 and Table 1) (Garcia-Anoveros et al. 1995; Tavernarakis et al. 1997; Mianchi 2007).

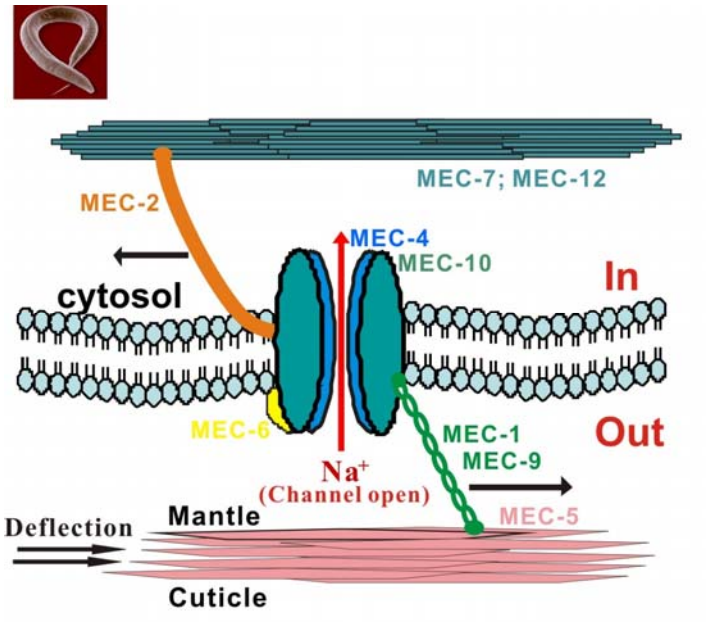

Figure 3. Schematic diagram of the sensory mechanotransduction complex in *C. elegans* touch receptor neurons. DEG/ENaC channel subunits MEC-4 and MEC-10 are at the core of the channel complex. They interact with accessory subunits MEC-2 and MEC-6 that selectively regulate channel activity for gating in response to mechanical force. On the intracellular side of the membrane, the α- and β-tubulins MEC-12 and MEC-7 form 15-protofilament microtubules that may interact directly or indirectly with the channel and help gate the channel when mechanical forces are applied. On the extracellular side of the membrane, extracellular proteins MEC-1 (a EGF/Kunitz repeat protein), MEC-5 (collagen), and MEC-9 (another EGF/Kunitz repeat protein) are part of the mantle and are required to cluster the MEC channel in puncta structures that are needed for function. These three proteins act as extracellular tether to pull the channel open (Chalfie and Sulston 1981; Chalfie and Au 1989; Gillespie and Walker 2001; O' Hagan et al. 2005).

Among all *mec* genes, *mec-4*, *mec-10*, *mec-6* and *mec-2* are proposed to form the mechanotransduction core complex (Chelur et al. 2002; Goodman et al. 2002; Zhang 2004; O' Hagan et al. 2005). The protein products of these four genes are co-expressed in touch neurons in *C. elegans* (Chelur et al. 2002; Goodman et al. 2002) and are also co-immuniprecipitated with one another when expressed in CHO cells (Chelur et al. 2002; Condrescu et al. 2002). In a recent paper it was

shown that MEC-2 and MEC-5 occupy overlapping but distinct domains in *C. elegans* touch receptor neurites. Although channels decorate all sides of touch receptor neurites; they are not associated with the distal endpoints of 15-protofilament microtubules hypothesized to be gating tethers. These specialized microtubules, which are unique to *C. elegans* touch receptor neurons, assemble into a cross-linked bundle connected by a network of kinked filaments to the neurite membrane. Thus it is speculated that the microtubule bundle converts external point loads into membrane stretch which, in turn, facilitates channel activation .

Gene/Protein	Homologues	Function	Phenotype
mec-1/MEC-1	EGF/Kunitz repeat protein	Mantle protein clusters the MEC channel in puncta	Touch insensitive. The mantle does not form and touch neurons are not attached to the cuticle
mec-2/MEC-2	Stomatin-like protein	Channel associated protein enhances channel function by acting on channel conductance or open probability	Touch insensitive. No transduction
mec-3/MEC-3	LIM domain binding protein	Specification of touch neurons differentiation	Touch insensitive. Touch neurons small and lacking processes. ALM and PLM touch cells misplaced
mec-4/MEC-4	Amiloride-sensitive DEG/ENaC channel subunit	Mechanosensitive channel protein conducts Na+ (Ca2+)	Touch insensitive. No transduction.
mec-5/MEC-5	Collagen	ECM protein, participates with MEC-1 in clustering of the MEC channel	Touch insensitive. The mantle is not stained by peanut lectin
mec-6/MEC-6	Paraoxonase-like protein	Channel associated protein enhances channel function by acting on channel conductance or open probability	Touch insensitive. No transduction.
	β tubulin	15-protofilament microtubule	Touch insensitive. Touch

mec-7/MEC-7		component	neurons lack 15 protofilaments microtubules
mec-8/MEC-8	RNA binding protein	RNA splicing (Lundquist 1996; Rowe 2002)	Touch insensitive. Disrupted fasciculation of amphid and phasmid channel cilia
mec-9/MEC-9	EGF/Kunitz repeat protein	Mantle protein required for MEC-1 localization in puncta around the touch cells processes	Touch insensitive.
mec-10/MEC-10	Amiloride-sensitive DEG/ENaC channel subunit	Mechanosensitive channel protein appears to act as accessory subunit of MEC-4	Touch insensitive. No transduction.
mec-12/MEC-12	α tubulin	15-protofilament microtubule component	Touch insensitive. Touch neurons lack 15 protofilaments microtubules. Increased transduction threshold
mec-14/MEC-14	Aldo-keto reductase	Controls MEC channel activity through an unknown mechanism	Partial touch insensitive. Temperature dependent
mec-15/MEC-15	F-box protein	Required for proper touch receptor neuron mechanosensation, morphology, and synapse development	Touch insensitive. Touch neurons lack 15 protofilaments microtubules
mec-16/MEC-16	Homeodomain protein	Required during early larval development for backward movement in response to anterior touch with a wire and during later larval stages, for response to gentle touch with a hair	Touch insensitive to metal wire in early development and to eye lash hair in later larval stages
mec-17/MEC-17	No distinct motif	Required for maintaining the differentiated state of the touch receptors component	Touch insensitive.
mec-18/MEC-18	AMP binding protein	May negatively regulate the MEC channel	Partially touch insensitive

Table 1. List of genes involved in sensory mechanotransduction complex in *C. elegans* as identified by Chalfie et al.

The *D. melanogaster* mechanosensory system is composed of two sets of mechano- receptors. Type I sensory organs have one to three sensory neurons, each with a single ciliated sensory dendrite, supported by accessory cells, whereas type II mechanoreceptor neurons have multiple nonciliated dendrites and no accessory cells. Genetic approaches in *D. melanogaster* has identified two of the genes: *nompA* and *nompC* (Kernan et al. 1994; Walker 2000; Chung et al. 2001), that are required for fly mechanoreceptor functioning. Like the results from the *C. elegans* screen, the screen from flies has identified an ECM protein and an ion channel. Mutations in the *nompA* gene, which eliminate mechanotransduction in *D. melanogaster* bristle receptors, were shown to disrupt contacts between neuronal sensory endings and cuticular sensory structures. Cloning and characterization of *nompA* revealed that it encodes a large transmembrane protein, exclusively expressed in type I sensory support cells of the peripheral nervous system (Chung et al. 2001). It has a modular extracellular segment that includes a zona pellucida domain and several plasminogen amino-modules. The NompA extracellular domain is localized specifically to the dendritic cap, an ECM protein that connects the sensory cilia to cuticular structures (in external sensory organs), or to attachment cells (Kernan et al. 1994), and transmits mechanical stimuli to the transduction apparatus (Chung et al. 2001). This suggests that NompA creates an extracellular mechanical linkage required for mechanotransduction. It shows similarity to a number of proteins, including the tectorins in mammals. Tectorins are extracellular proteins that transmit mechanical stimuli to mechanoreceptive hair cells in the vertebrate auditory system (Legan et al. 1997).

1.3.2 Vertebrate hair cell mechanotransduction model

In vertebrates, mechanotransduction is the basis for the perception of sound, acceleration, mechanical touch and pain. The vertebrate hearing system represents a well characterized tether model for hearing mechanotransduction mechanism. Vertebrates perceive sound and acceleration through the inner ear vestibular system. The auditory receptors are called 'hair cells' because each one has about one hundred "hairy looking" stereocilia extending from its top (Fig. 4A upper panel). The critical event in the transduction of sound into a neural signal is the bending of these cilia (Fig. 4A lower panel). Sound, acceleration or changes of the head position causes the deflection of the mechanosensitive ciliae of the hair cells, namely the hair bundles. Bundle deflection is postulated to stretch elastic linkages 'gating springs' that attach to the transduction channels and the resulting tension pulls the mechanosensitive cation channels open and the entry of predominantly potassium depolarizes the hair cell, which opens voltage-gated calcium channels and leads to the release of neurotransmitter from synaptic vesicles, which then diffuses to the postsynaptic spinal ganglion afferent nerve (Corey and Hudspeth 1983; Howard and Hudspeth 1988).

Fine, filamentous linkages are visible in electron micrographs extending from the tip of each stereocilium to the side of the next adjacent, taller stereocilium (Fig. 4B left panel). Tip links (denoted as TL) may be the structural correlates of the biophysically defined gating springs (Pickles et al. 1984; Assad et al. 1991). The tip links run parallel to the hair bundle's axis of bilateral symmetry and their oblique disposition indicates that they will be stretched or apply tension to an

attached channel only when the hair bundle is displaced in the excitatory direction, i.e., towards the kinocilium or the tallest row of stereocilia. Stereocilia with hair bundles are interconnected by lateral links of several other types. In addition to tip links, up to four other link types that are morphologically distinct are found between the stereocilia of vestibular hair bundles (Furness and Hackney 1985; Nagel and Thurm 1991; Goodyear and Richardson 1992). Kinocilial links (KLs) couple the tallest stereocilia in hair bundles to the kinocilia. Upper lateral connectors (ULs) connect the top of a shorter stereocilium to an adjacent longer stereocilium at a short distance below the tip links (Fig. 4B left panel). Shaft connectors (SCs) and ankle links (ALs) respectively connect the shafts and basal regions of neighboring stererocilia. (Hirokawa and Tilney 1982; Osborne et al. 1984) (Fig. 4B left panel). The roles of these different hair bundle links are not fully understood. Previous studies have suggested that these lateral links probably preserve hair bundle integrity and transduce forces between stereocilia. The tip-to-side connector (tip link) which consists of a filament joining the tip of a stereocilium with the side of an adjacent taller stereocilium was suggested to give rise to the mechanosensory transduction (Pickles et al. 1989; Langer et al. 2001). The other connectors probably serve to maintain the regular spatial arrangement of the hair bundle and the mechanical coupling of the stereocilia. However, the contribution of different link types to the overall stiffness still remains a puzzle. Previous studies of the pharmacological and biochemical characteristics of the hair bundle links have revealed some very important features (Assad et al. 1991; Goodyear and Richardson 1999; Bushtanov et al. 2004). It was found that different hair bundle link types have distinctive sensitivity to pharmacological and biochemical treatments and each link type is molecularly distinct (Table 2). Tip

links are sensitive to calcium chelation with BAPTA, an agent that disrupts transduction whereas they remain intact after treatment with the protease subtilisin (Fig. 4B and Fig. 4C) (Jacobs and Hudspeth 1990; Goodyear and Richardson 1999).

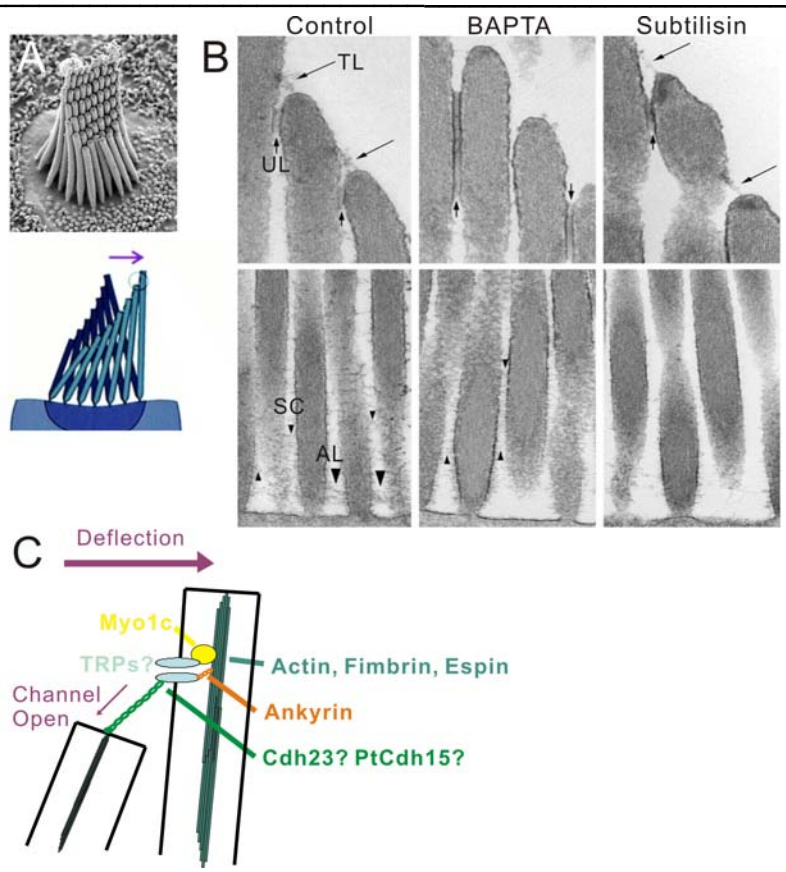

Figure 4. The hearing mechanotransduction system in the hair cell. In sensory hair cells of the inner ear, extracellular protein filaments called tip links tether mechanosensitive ion channels between stereocilia and are necessary for mechanotransduction. **A.** Scanning electron micrograph of the hair bundle in vertebrate inner ear cochlea. **B.** TEM micrograph clearly shows a 150nm tip link at the tip of stereocilia and selective sensitivity of different link types to calcium chelator BAPTA and endopeptidase subtilisin (Bushtanov et al. 2004). TL denotes tip link. UL denotes upper lateral links. SC denotes shaft connectors. AL denotes ankle links. Kinocilial links are not shown in this figure. **C.** Proposed molecular model for hair cell transduction apparatus and identified molecules involved in the transduction complex.

Treatment with subtilisin also does not appear to influence the amplitude of transduction currents (Michel et al. 2005). Kinocilial links have similar properties as tip links and are also BAPTA-sensitive, subtilisin-resistant structures (Fig. 4B and Fig. 4C) (Goodyear and Richardson 2003). The orientation and properties of the other link types, collectively referred to as lateral links, suggests that they are unlikely to be involved in the mechanotransduction process. They are aligned along three of the lattice planes of the hex-packed hair bundle and their relative sensitivities to BAPTA and subtilisin are not consistent with a role in gating the transducer channel (Fig. 4B; 4C and Table 2). ULs are resistant to both BAPTA and subtilisin. SCs are BAPTA-insensitive and subtilisin-sensitive. ALs are degraded by treatment with either agent (Goodyear and Richardson 1999).

	Kinocilial links (KLs)	**Tip links (TLs)**	**Upper lateral connectors (ULs)**	**Shaft connectors (SCs)**	**Ankle links (ALs)**
BAPTA	**+**	**+**	−	−	**+**
Subtilisin	−	−	−	**+**	**+**
Associated Anigens	Cdh23 Pcdh15(TLA)	Cdh23 Pcdh15(TLA)	?	Ptprq	Vlgr1(ALA) Usherin

Table 2. Pharmacological and biochemical properties of different link types in hair cells. Sensitivity of different hair bundle link types to the calcium chelators, BAPTA and the protease subtilisin. When links are sensitive to BAPTA or subtilisin, a plus (+) sign is marked. Otherwise, a minus (-) sign is marked. Associated antigens are also indicated. Cdh23 (cadherin-23) Pcdh15 (protocadherin-15). TLA (tip link antigen: avian Pcdh15). ALA (ankle link antigen: avian Vlgr1).

Biochemical studies using monoclonal antibodies (mAbs) that recognize components of the shaft connectors and the ankle links have revealed their biochemical components (Table 2) (Richardson et al. 1990; Goodyear and Richardson 1992; Goodyear and Richardson 1999). It is found that the 275 kDa

hair cell antigen (HCA) is a component of the shaft connectors (Goodyear and Richardson 1992). This hair-cell antigen (HCA) has been recently identified as a receptor-like protein tyrosine phosphatase, now known as protein tyrosine phosphatase receptor Q (Ptprq) (Legan et al. 2001). The tip-link antigen (TLA), a novel antigen that is associated with both tip links and kinocilial links that connect kinocilium to adjacent stereocilium has also been described (Goodyear and Richardson 2003). The very large G-protein coupled receptors 1 (Vlgr1) and usherin are associated with ankle links (Mcgee et al. 2006). Vlgr1 has been identified as the ankle link antigen (ALA) (Goodyear and Richardson 1999). Although the ALA is expressed throughout the lifetime of chick hair bundles, Vlgr1 is only expressed until P11 on hair bundles in the mouse inner ear. Ptprq, a shaft connector component, is expressed in the hair bundles of the vestibular organs throughout life (Goodyear and Richardson 2003). The disappearance of ankle links and Ptprq from the hair bundles of mouse cochlear outer hair cells is coincident with the appearance of the well defined horizontal top connectors characteristic for this cell type (Michel et al. 2005), suggesting that these junction-like connectors may play a key role in maintaining integrity of the hair bundle of the mature hair cells.

A properly formed hair bundle is essential for mechanotransduction. Among the identified proteins involved in hair cell mechanoreceptor machinery, actin, fimbrin and espin are the structural proteins. Actin has long been known to be the main cytoskeletal element of hair bundles, and fimbrin was identified as an important crosslinker in the hair bundle. More recently, espin was identified as a second crosslinker of stereocilia, responsible for the *jerker* mouse deafness mutation

(Flock et al. 1981; Tilney 1989; Zheng et al. 2000). Additionally, a human homologue of the *D. melanogaster* protein diaphanous is mutated in the nonsyndromic deafness DFNA1. Diaphanous is a ligand for the actin-binding protein profilin and is a target for regulation by Rho, which regulates cytoskeletal assembly in many cell types (Lynch 1997). The tip link can be manipulated with calcium chelator and proteases (Bashtanov et al. 2004). Müller and colleagues found that cadherin 23 binds to myosin-1c, the protein that sets the resting tension in tip links when both proteins are made together in non-hair cells. In addition to that, cadherin 23 mediates binding between adjacent cells that express the protein in culture. They have thus provided strong evidence that cadherin 23, although not the only molecular component is a major constituent of the tip link connecting adjacent hair cells. Recent evidence suggests that, apart from cadhrin 23, protocadhrin 15 collectively constitutes the hair cell tip (Siemens et al. 2004; Sollner et al. 2004; Kazmierczak et al. 2007). High-resolution electron micrographs reveal that the tip link is a double helix, 8–11 nm wide and 150–200 nm long, inelastic structure and that these links may be too stiff to constitute the gating spring (Kachar et al. 2000; Howard and Bechstedt 2004). Friedrich and his co-workers previously suggested that the channel TRPN1 is likely to mediate mechanotransduction in zebrafish. This channel has 29 ankyrin repeats, which form a thin helical structure that has been suggested to be elastic and to serve as a gating spring (Sidi et al. 2003; Howard and Bechstedt 2004). Therefore, ankyrin is suggested to have the appropriate stiffness and elongation and is speculated to be the internal gating spring in hair cell mechanoreceptor complex. Rapid progress has been made in our understanding of the molecular mechanisms underlying the process of hair bundle function due to studies of mouse and

zebrafish mutants and the discovery of genes required for hearing, many of which encode proteins required for the development and maintenance of hair bundle structure. Nonetheless, there is still much to be learned about the pathways that control the physiological properties as well as the development and final shape of each hair bundle.

1.3.3 Mammalian sensory mechanotransduction model

In vertebrates, the sensory terminals of touch receptors and proprioreceptors are far from the afferent neuron cell bodies, which are located in the dorsal root ganglia (DRG). The sensory nerve endings of DRG neurons are dispersed throughout the body and embedded in other tissues, impeding the electrophysiological recording of mechanoreceptor potentials and biochemical purification of components of the molecular machinery that mediates mechanosensation. Our senses of touch, mechanical pain, and proprioception all rely on the ability of primary sensory neurons to rapidly transform mechanical forces into electrical signals. This fundamental sensory transduction step still remains a puzzle at the cellular and molecular level (Gillespie and Walker 2001; Lewin and Moshourab 2004; Hu and Lewin 2006). It is widely agreed that mechanical forces on sensory nerve endings must directly open mechanically gated ion channels, which are located exclusively on the membrane of sensory nerve endings. Subsequently, a cation influx leads to depolarization of the cell membrane and a local receptor potential is generated (Loewenstein and Skalak 1966; Gillespie and Walker 2001). If the receptor potential breaks a certain

threshold, APs are initiated within milliseconds (Loewenstein 1959) and are propagated along the axon to the central nervous system (CNS) (Lynn 1975). Several genes have been identified in mice that are homologous with those required for normal touch sensation in *C. elegans.* The possible involvement of these genes in mechanotransduction has in some cases been evaluated (Mannsfeldt et al. 1999; Price et al. 2000; Garcia-Anoveros et al. 2001; Price et al. 2001; Alvarez de la Rosa et al. 2002). In recent years, research combining genetic, genomic and electrophysiological approaches has pushed forward our understanding of vertebrate sensory neuron mechanotransduction (Fig. 5). Candidate molecules include ion channel subunits of the transient receptor potential superfamily (TRP) (Zhang et al. 2004) as well as the degenerin/ epithelial Na^+ channels (DEG/ENaC) (Corey and Garcia-Anoveros 1996; Itzhak and Driscoll 1999; Price et al. 2001). Members of both families are widely expressed throughout the animal kingdom and are present in vertebrate sensory neurons. Recently, Lewin and his colleagues showed that a MEC-2 homologue, stomatin–domain protein named SLP3 (stomatin-like protein 3; 62% identical to stomatin in sequence similarity) is a key player in touch sensitivity in mice. SLP3 might act as an intracellular integrity mediating mechanosensitive channel gating (Fig. 5) (Wetzel et al. 2007). The mechanoreceptor endings are very fine structures often embedded in specialized end organs, which makes them very difficult to examine *in vivo* (Garcia-Anoveros and Corey 1997). In addition, mechano- sensitive ion channels are often very sparse and chemicals that interact with putative mechano- transducers with high affinity and high specificity are not yet known.

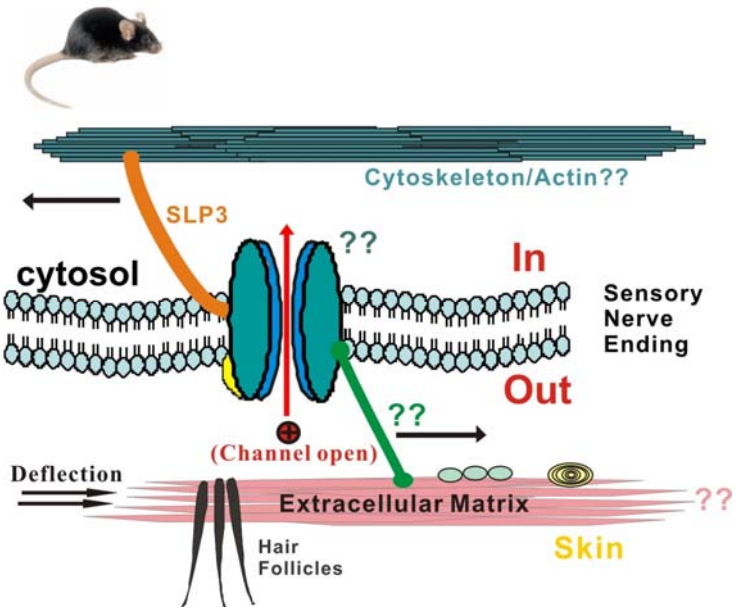

Figure 5. A possible molecular model for sensory mechanotransduction complex in mammals. Several homologues to the *mec* genes have been identified in mice and humans. Their possible involvement in mechanotransduction is in the process of being elucidated.

The inaccessibility and scarcity of sensory neuron membranes that contain transduction complexes preclude a straightforward biochemical investigation. Hu and Lewin have developed an *in-vitro* physiological assay to measure the activation of mechanosensitive channels in the neurites of acutely cultured sensory DRG neurons (Hu and Lewin 2006). It was found that cultured sensory neurons can be subdivided into different subtypes in accordance with the inactivation time constant of the mechanically activated currents. Measurement of reversal potential of cultured sensory neurons indicates that the rapidly-adapting (RA) current is sodium selective (consistent with a DEG/ENaCs channel) whereas the slowly adapting (SA) current is non selective (consistent with TRP like channel) (Hu and Lewin 2006). Using this *in-vitro* approach, It was demonstrated for the first time that distinct ion channel entities underlie the different

mechanically induced currents (Hu and Lewin 2006). Combining this *in-vitro* approach for measuring mechanotransduction with other methods such as cell culture, electron microscopy, microcontact printing and proteomic analysis, the aim of this project is to study the mammalian sensory mechanotransduction complex.

1.4 Objectives

It is hypothesized that the tether model, which may be applicable to sensory mechanotransduction process in *C. elegans*, *D. melanogaster* and the vertebrate hearing system also applies to mammalian sensory mechanotransduction system. To uncover the mechanism of sensory mechanotransduction in mammals, the first task of this project is to establish a cell culture system *in vitro*, simulating sensory neurons innervating defined cell types normally encountered in the skin. Recent studies have provided evidence that a mixture of laminins derived from Engelbreth-Holm-Swarm (EHS) sarcoma ECM extract, vital for supporting DRG neuronal neurite outgrowth in culture is required for cultured neuron mechanotransduction (Hu and Lewin 2006), suggesting an important role of ECM proteins in sensory mechanotransduction. The second task of this project is to study whether alteration of the ECM protein will modulate mammalian sensory mechanotransduction. Müller and colleagues (Siemens 2004) looked at the effects of buffers or ions that either chelate or displace Ca^{2+} ions; tip links are known to be severed by such treatment, but reappear in 5–10 hours (Assad et al. 1991; Zhao 1996). The biochemical properties of a putative extracellular protein

essential for mechanotransduction can be readily determined by pharmacologically manipulating the extracellular integrity of cultured neurons and measuring its effect on the functioning of sensory mechanotransduction. In comparison with an unequivocal visualization of an extracellular tip link required for mechanotransduction in hair cells using electron microscopy, there is so far no direct evidence showing whether an extracellular link is essential for mechanosensitive channel gating in mouse (Lewin and Moshourab 2004; Hu et al. 2006) or in *C. elegans* (Cueva et al. 2007). I hypothesize that if a tether is required for sensory mechanotransduction in mammals, I should observe such extracellular structures using electron microscopy. Since the 1950s it has been known that different sensory neuron subtypes innervate different cutaneous layers. The ultrastructure of the nerve terminal and its surrounding basement membrane has been visualized and classified (Halata 1975; Breathnach 1977). Recent scientific effort has been focused on studying the structural characteristics of axon terminals and the molecular concomitants of synaptic as well as organelle activity (Kruger 1996; Kruger et al. 2004). However, due to the complexity of connective tissues, cell-cell interaction, and cell-matrix interaction, the possibility to investigate the interface between sensory nerve endings and ECM protein has been precluded. Thus a clean culture system is needed to investigate the cell-matrix interaction. In this case an electron microscopic technique will be developed and optimized to visualize the extracellular integrities of cultured sensory neurites and cell-matrix interaction in culture system.

2 MATERIALS AND METHODS

2.1 Materials

2.1.1 Technical equipment

ADInstruments PowerLab/4s

BDK Laminar Flow Hood

Biometra TRIO-Thermoblock PCR machine

BioRad Mini Protean II

BioRad Mini Transblot Apparatur

BioRad PowerPac 300

Cryostat

DiATOME Ultra 35° diamond knife

Digitimer Ltd. NeuroLog Amplifier

Eppendorf Thermomixer Compact and 5436

EquiBio Easyject Electroporation Apparatus

EPC-9 amplifier, Heka

Forma Scientific -80°C Freezer

Forma Scientific Steri-Cult 200 Incubator

Gilson Minipuls 3 Peristaltic Pump

Hamamatsu Digital Camera C4742-95

Luigs & Neumann SM-5 CCD Camera

Eppendorf Centrifuge 5810

Reichert-Jung Ultracut machine

Diener Electronics Plasma Surface machine

Harnischmacher Labortechnik DNA Electrophoresis Chambers

Heidolph Duomax 1030 and Promax 1020 Shakers

Heraeus Biofuge 13

Heraeus Megafuge 1.0

Hereaus Biofuge 15R

Herolab E.A.S.Y 429K Digital Camera

Herolab UVT 2035 Transilluminator 302nm

Incubator Unitherm Hybridizationsoven or Thermo Hybaid

Ikamag Reo Magnetic Stirrer

Julabo MP and Medingen Waterbaths

Kleindieck Nanomotor

Leica DM 500B with Metamorph software

Leica DM RBE Upright Fluorescence Light Microscope

Leica KL 750 Fiber Optic Light Source

Leica MS5 dissecting microscope

Millipore Multiscreen Resist Vaccum Manifold

Mettler Toledo 320 pH Meter

Mitstbishi Video Copy Processor

MJ Research PTC 200 PCR machine

Harmacia Biotech Ultrospec 1000 Spectrophotometer

Plantar test, Ugo Basil

PerkinElmer Gene Amp PCR system 2400

Proscan 1k X 1k high speed slow scan CCD camera

Rotorod Test (TSE Systems)

Sartorius Weigh machine

Scientific Industries Vortex-Genie 2

Stratagene UV Stratalinker 2400

Tektronix TDS 220 Two Channel Digital Real Time Oscilloscope

Uni Equip Unitherm Hybridization oven 6/12

WAS02 automated perfusion system

Zeiss910 Electron Microscope

2.1.2 Analytical Software

AnalySIS 3.2 Software, Soft Imaging System

Lasergene Software, DNAStar Inc.

MetaVue v6.2, Universal Imaging Corp.

Openlab 3.0.4

Pulse and PulseFit software, HEKA

iTEM imaging sofeware, Olympus Soft Imaging

Origin8, OriginLab

GraphPad Prism, GraphPad Software

2.1.3 Chemicals and reagents

Reagent and chemical	**Company**
10 x PCR buffer	Invitrogen Life Technologies
100bp and 1kb ladder	Gibco

20x TaqMan Gene Expression Assay	Applied Biosystems
2x TaqMan Universal Master Mix	Applied Biosystems
5x First-strand buffer	Invitrogen Life Technologies
5x Second-strand buffer	Invitrogen Life Technologies
APES	Sigma-Aldrich
Aqua-Polymount	Polyscience Inc.
BAPTA	Tocris Bioscience
Bovine Serum Albumin (BSA)	Invitrogen Life Technologies
Cacodylate	Electron Microscopy Sciences
Cell strainer	BD Falcon
dNTPs (10mM each)	Invitrogen Life Technologies
DTT	Invitrogen Life Technologies
ECL	Amersham Bioscience
ExpressHyb solution	Clontech
Fetal bovine serum	Biochrom
Gelatine	Sigma-Aldrich
Glygogen	Promega Corporation
Glutaraldehyde	Sigma-Aldrich
Horse serum	Biochrom
Lead Citrate	Serva
MES Free Acid Monohydrte Ultra pure	Sigma-Aldrich, P/N M5287
MES sodium salt	Sigma-Aldrich, P/N M5057
Paraformaldehyde	Sigma-Aldrich
Phenol/chloroform/isoamyl alcohol	Roth
PetriPerm35 petridish	VivaScience AG
Propylene oxide	Polysciences Inc.
Toluidine blue	Sigma
Tetrodotoxin	Seojin International Corporation
Tissue Tek	Miles, Elkhart, Ind. USA
Triton X-100	Sigma-Aldrich
Trizol	Roth
Tween-20	Pierce Chemical
Ruthenium red	Sigma-Aldrich
Uranyl acetate	Serva

Further chemicals were obtained from Biomol, Merck, Roth and Sigma-Aldrich

2.1.4 Solutions and buffers for general use

Buffer and solution	**Composition**
10x MOPS	200mM MOPS 500mM Na-acetate 10mM EDTA pH 7.0
10x TBS	0.5M Tris/HCl pH 7.9 1.5M NaCl
4% PFA	4% paraformaldehyde in PBS pH 7.4
5x Lämmli buffer	60mM Tris/HCl pH 6.9 10% SDS 10% β-mercaptoethanol 50% glycerol 1.5% bromphenolblue
Acetate buffer	Na-acetate 10 mM pH 5
Homogenization buffer	0.1M PBS
Patch clamp buffer - intracellular solution	110 mM KCl 10 mM Na^+ 1 mM $MgCl_2$ 1 mM EGTA 10 mM HEPES pH7.3, adjusted with KOH
Patch clamp buffer - extracellular solution	140 mM NaCl 1 mM $MgCl_2$ 2 mM $CaCl_2$ 4 mM KCl 4 mM glucose 10 mM HEPES pH 7.3, adjusted with NaOH
PBS	PBS Dulbecco w/o Ca^{2+}, Mg^{2+}
Phosphate buffer	0.1M KH_2PO_4 0.1M Na_2HPO_4 x $2H_2O$
SDS PAGE running buffer	25mM Tris/HCl pH 8.3 190mM Glycine

	0.1% SDS
Silverstaining developer	30g Na_2CO_3 250µl Formalin (37%) 10ml pre-incubation solution Ad 500ml H_2O
Silverstaining staininer	1g $AgNO_3$ 376µl Formalin(37%) Ad 500ml H_2O
Silverstaining fixation	50% Methanol(250ml) 12% Acetic Acid (60ml) 0.05% Formalin (37%) (250µl) Ad 500ml H_2O
TE buffer	10mM Tris pH 8.0 1mM EDTA
Silverstaining ore-incubation solution	100mg $Na_2S_2O_3$*$5H_2O$ (Natriumthisulfatpentahydrat) Ad 500ml H_2O
RIPA buffer	50mM Tris-HCl pH7.4 150mM NaCl 1mM EDTA 0.5% DOC 1% Triton X-100 0.2% SDS 1.5mM DTT Protease inhibitors

2.1.5 Culture media

DRG culture medium (also applicable to superior cervial ganglia culture):

20% Horse serum (Biochrom)

2mM glutamine (Gibco)

100u penicillin/100µg/ml streptomycin (Gibco)

D-MEM/F12 (Gibco)

Normal growth medium:

10% Fetal bovine Serum (Biochrom)

100µg/ml penicillin, streptomycin, gentamicin (Gibco)

D-MEM/F12 (Gibco)

SCC25 culture medium

Ham's F12 and DMEM 1:1

0.4µg/ml hydrocortisone

15% Fetal bovine serum

Kerationocytes culture medium:

100µg/ml penicillin, streptomycin (Gibco)

Defined keratinocyte-SFM (Gibco)

Defined keratinocyte growth supplement (Gibco)

2.1.6 Purified proteins, antibodies and enzymes

Products	**Providers**
Laminin (EHS-derived matrix)	Invitrogen
Purified laminin-332	Invitrogen
Purified laminin-111	M. Koch, Uni Köln
Nf200 mAb	Biocompare
TRPV1 polyclonal antibody	Abcam
Col28 antibody (mAb) VWA1 and VWA2	M. Koch, Uni Köln

Laminin-332 antibody (mAb) CM-6 against rat laminin-332 integrin binding	Santa Cruz Biotechnologies
Laminin-332 antibody (mAb) BM-2 against human laminin-332 integrin binding	M. Koch, Uni Köln
Laminin β_3 subunit	M. Koch, Uni Köln
Laminin γ_2 subunit	M. Koch, Uni Köln
Antibody against tenurin I, II, III, IV	Fässler Lab, München
CD29 mAb	Sigma-Aldrich
Alexa 488	Invitrogen
Alexa 555	Invitrogen
Trypsin	Gibco
Collagenase type IV	Gibco
Subtilisin	Sigma-Aldrich
Blisterase	New England Bio Labs
PIPLC	Sigma-Aldrich

2.1.7 Consumables

Products	**Company**
15ml and 50ml tubes	Falcon, Greiner
Cell culture dishes	Falcon
Centricon	Millipore
Coverslips	Roth
Dissection scissors	FST
Dissection forceps	FST
Dounce homogenizer	Roth
Eppendorf tubes	Eppendorf
Glass rod	In house made
Hybond-N	Amersham
Hybridization plates	Multiscreen TM- MAHVS4510
Insect needles	FST
Micro spin columns	Amersham
MicroAmp Optical 96 well reaction plate	Applied Biosystems

Needles	Sterican
Quartz cuvettes	Roth
Pipettes and multichannel pipettes	Eppendorf or Biohit
Slides and coverslips	Roth or Menzel-Gläser
Sterile filters	Nalgene, Millipore
Syringes	Braun
Whatman filters	Schleicher & Schuell

2.1.8 Animals

C57BL/6N mice were obtained from Charles River Breeding Laboratory, Inc. and kept in the animal house of the MDC until they were used for experiments.

2.2 Methods

2.2.1 Molecular biology

Standard methods were performed according to Sambrock et al. (1989) and Asubel et al. (1997).

2.2.2 Cell cultures

2.2.2.1 Cultivation of afferent sensory neurons and efferent sympathetic neurons

Mouse DRGs or Superior Cervical Ganglia (SCGs) were dissected and collected in a 1.5ml tube in PBS on ice. Ganglia were washed once with PBS before incubation with 1µg/ml Collagenase TypeIV in 1ml PBS at 37°C for 30 min. Ganglions were centrifuged briefly (170 x g), the supernatant was removed and DRGs were incubated with 100µl 0.5% Typsin in 1ml PBS at 37°C for 30 min. The supernatant was removed and 1ml D-MEM/F12 medium was added. The suspension was passed through 1-2 different siliconised Pasteur pipettes to dissociate them into single cells and centrifuged at 170 x g for 4min. The supernatant was removed and cells were resuspended in 1ml culture medium. Cells were plated on laminin (EHS-derived laminins) coated coverslips, which were pre-coated with Poly-L-Lysine (PLL) (about 60-120 µl of cell suspension per coverslip) to let the cells attach to the coverslip. After 4 hours an additional 150µl of the DRG medium was added to the coverslips. Cells were cultured for 24h at 37°C in a Steri-Cult 200 incubator. No nerve growth factor or other neurotrophin was added to the medium.

2.2.2.2 Culture of mouse embryonic mouse fibroblast cell line (3T3 cells)

The fibroblast cell line (mouse NIH 3T3 cells) was maintained in Dulbecco's modified Eagle's medium (DMEM), supplemented with 10% fetal bovine serum, and 1% penicillin, streptomycin and glutamine. Each week, the confluent cells were subcultured and excess cells irradiated as a suspension with 60Gy (6000 rads) γ-irradiation. The cells are then used as feeders for keratinocytes

2.2.2.3 Culture of squamous cell carninoma 25 (SCC25)

SCC25 was obtained from ZITHROMAX. To subculture, cells were disaggregated to single cells when the culture is preconfluent. Medium was removed and cells were rinsed with 0.25% trypsin and 0.03% EDTA solution. Solution was then removed and an additional 1-2 ml of trypsin-EDTA solution was added. The flask was allowed to sit at 37°C until the cells detached. Fresh medium was then added into new flask then aspirated and dispensed. For co-culture, cells were disintegrated (by enzymes: collagenaseIV and trypsin, mechanical pippetting) and pre-plated on clean coverslips. Neurons were then cultivated on matrix produced by confluent SCC25 layer.

2.2.2.4 Culture of primary mouse keratinocytes

Primary mouse keratinocytes were cultured using a modification of a previously described method (Paladini and Coulombe 1998). Newborn mice (postnatal day 1-3) were decapitated and their limbs and tails removed. After washing with 70%

ethanol, trunk skin was removed, stripped of fat, and floated (epidermis upwards) overnight at 4°C in a petri dish containing 0.25% trypsin. On the next day the epidermis was peeled from the underlying tissue. Keratinocytes were harvested from both surfaces of the epidermis by flushing with medium or gentle scraping, harvested cells were then placed in a defined serum free keratinocyte medium (Gibco-Invitrogen, Germany). Cells were pelleted and resuspended in the same medium. Keratinocytes were then plated either on glass cover slips pre-coated with 0.67 µg/cm^2 Collagen IV or cultured together with lethally irradiated 3T3 cells acting as an adhesion layer.

2.2.2.5 Co-culture and conditioned-matrix culture systems

DRG neurons were plated on top of the keratinocytes or 3T3 monolayer or SCC25 instead of on PLL/laminin substrate when co-cultured with keratinocytes or 3T3 cells or SCC25. Whole-cell recordings began 24 hours after plating. For keratinocyte-derived matrix, cultured monolayer of keratinocytes were treated with 0.1% Triton X-100 for 5 to 120 minutes, then the keratinocytes were washed away and the DRG neurons were plated on the left matrix.

2.2.3 Protein chemistry

2.2.3.1 Immunostaining of cultivated neurons

Cultured DRG neurons were fixed with 4% paraformaldehyde (p-f-a) in PBS for 10 min and then washed with PBS. Then neurons were permeabilized with 0.05%

Triton X-100 in PBS for 5min and then washed with PBS. In case of staining extracellular proteins, Triton X-100 permeabilization was skipped. Non-specific binding was blocked by incubating the neurons in 3% normal goat serum in PBS for 30min. Cells were incubated with the primary antibodies (diluted 1:200 in 3% goat serum) overnight at 4°C. The staining was detected using secondary antibodies ie. Alexa 488 or Alexa 555 (dilution 1: 200, incubation for 1 h at RT, wash 3x with PBS. Fluorescent light emission was captured with the XF22 filter (excitation 535nm, emission 605DF50, Omega Optical)

2.2.3.2 ECM Protein isolation

A simple extracellular protein isolation method was used by bursting cells and collecting remaining substances to strengthen mass spectrometry results. Cultured cells were removed by adding diluted PBS (1/5PBS+4/5 H2O) + 0.5% DOC (sodium deoxycholate) into a dish to burst cells. ECM proteins that remained on the dish were immersed in RIPA buffer (lysis buffer), scraped off and collected (for 10cm dish, add 2ml of RIPA buffer). The collected supernatent was centrifuged 20mins, max speed at 4^0C to spin down undissolved proteins. For storage, supernatent (proteins in RIPA) was kept at -20^0C. Protein concentration can be determined at this step. To precipitate proteins, 1/100 vol. 2% DOC was added, then vortexed and left on ice for 30mins. Then 1/10 vol. 100%TCA (stocks stored at 4^0C room) was added into the tube and left on ice for 30mins. After samples became cloudy, tubes were centrifuged 20mins at max speed 4^0C. Proteins were then precipitated at bottom. Clear supernatant above the cloudy layer at the bottom was carefully discarded. To remove DNA, RNA and other

non-protein products, samples were washed with acetone and centrifuged 20mins at max speed 4^0C. This step was repeated 3 times. The final pellet was very acidic. To run gel, pellet was dissolved in Alkaline SDS-PAGE sample bugger (50mM Tris pH8.0, 2% SDS, 100mM DTT, 10% glycerol) then boiled 5 minutes and loaded for gel running.

2.2.3.3 SDS-PAGE

Utilizing a SDS polyacrylamid gelelectrophoresis (SDS-PAGE) in a mini-apparatus (Mini Protean II from BioRad) proteins were separated according to their molecular mass under reducing conditions (2% β-mercaptoethanol) at 110-130V (Lämmli, 1970). The size of protein bands was determined by comparing them to a molecular mass standard (BioRad).

2.2.3.4 Western blotting

Proteins were transferred from the SDS gel to a nitrocellulose membrane for 1h at 150V at 4°C in the Mini Transblot Apparature from BioRad. Membranes were quickly rinsed with distilled H_2O and protein bands detected with a 3% Ponceau red solution. After washing twice with H_20, the membrane was transferred into WB blocking buffer for 1h at RT to quench nonspecific interactions. Primary antibodies were usually diluted 1:500 in blocking buffer and incubated overnight at 4°C. Membranes were washed several times. The appropriate secondary antibody, conjugated to horse radish peroxidase (HRP), was diluted 1:2000 in WB blocking buffer and applied to the membrane for 1h at RT. Protein bands were

detected using SuperSignal® ULTRA chemiluminescent substrate from Pierce and visualized on Kodak Scientific Imaging Film X-Omat™ Blue XB-1.

2.2.4 Electrophysiology

Whole-cell patch clamp recordings were made as previously described (Hu and Lewin 2006) and demonstrated in Figure 6. Sensory DRG neurons were recorded using fire polished glass electrodes with a resistance of 4-9 MΩ. During recordings, cells were kept in extracellular buffer and electrodes were pre-filled with intracellular solution. For most experiments, 0.1% lucifer yellow was included in the electrode to stain the whole neurons with neurites. Cells were perfused with drug containing solutions by moving an array of outlets in front of the patched cells (WAS02). Tetrodotoxin (TTX) was prepared to a final concentration of 1 μM in extracellular solution. Observations were made with an Axiovert 200 microscope equipped with a TILL imaging system (Till Vision GmbH), including the polychome V, a CCD camera and the imaging software TILLvisION. Membrane current and voltage were amplified and acquired using an EPC-9 amplifier sampled at 40 k Hz, acquired traces were analyzed using PulseFit software (HEKA). For most experiments the membrane voltage was held at –60mV with the voltage clamp circuit. Mechanical stimuli were applied using a heat-polished glass pipette (tip diameter 2-5μm), driven by the MM3A micromanipulator system (Kleindiek), positioned at an approximate angle of 45º to the surface of the dish. There are two different movements for the Nanomotor®: 'fine mode' and 'coarse mode'. Fine mode movement from any position is limited

to about 740nm in each direction the Z-axis (calibrated by a Piezo actuator calibration device LL10PZT (LASERTEX). Coarse mode steps (1 step about 740nm) can be executed in any direction until the micromanipulator reaches its physical limits. The probe was positioned near the neurite or cell body, moved forward in steps of 740 nm for 500 msec and then withdrawn. If there was no response, the probe was moved forward by 1 step coarse mode. And the same procedure was repeated until a mechanically activated inward current was recorded. The probe was moved at a speed of 1.4 μm/ms for finemode and 7.5 μm/ms for coarse mode. For the analysis of the kinetic properties of mechanically activated current, traces were fitted with single exponential functions using PulseFit software. Data are presented as mean ± SEM.

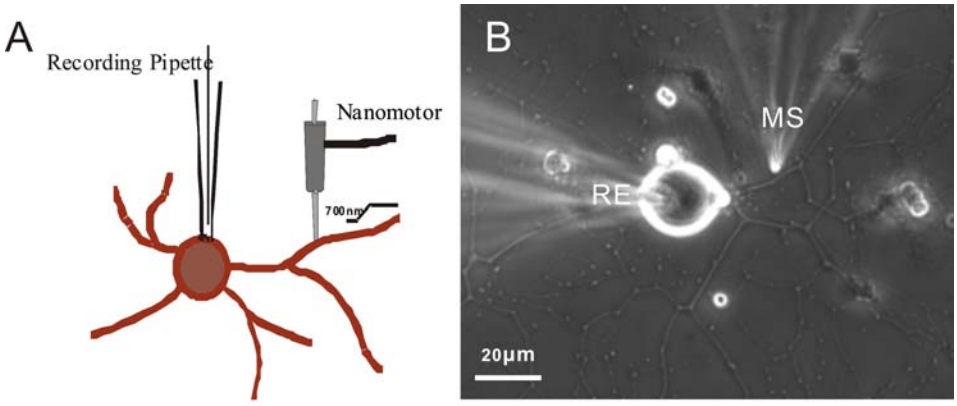

Figure 6. Method of recording mechanotransduction from sensory neurons

A. Schematics of the *in-vitro* recording method. The sensory neurites are stimulated by a nanomotor with displacement of 740 nm each step and evoked mechanically gated currents are recorded from cell soma. **B.** Light micrograph of a cultured sensory neuron with abundant neurite process being recorded in response to mechanical stimuli on the sensory neurite. RE denotes recording pipette and MS denotes mechanical stimuli.

2.2.5 Electron microscopy

DRG or SCG neurons were isolated and cultivated on laminin-coated petriPERM dishes using standard culture conditions (Hu and Lewin 2006) (petriPERM35, Vivascience AG, Germany). After 24hrs, cells were washed twice with 0.1M cacodylate buffer (Electron Microscopy Sciences, PA, USA) and fixed in 2.5% glutaraldehyde for 4 hrs and stained with OsO_4 (Osmium Tetroxide) (Sigma-aldrich Co. Ltd.) in the presence of Ruthenium Red (Fluka) to enhance the electron density of extracellular proteins (Hasko and Richardson 1988). The fixed samples were dehydrated through a series of graded ethanol exchanges and infiltrated in mixture of Poly/Bed^R 812 epoxy resin and propylene oxide (Polysciences Inc, Warrington, PA), then embedded in Poly/Bed^R 812 epoxy resin. Embedded samples were randomly sectioned (50nm thick) then contrasted with uranyl acetate and lead citrate (Serva, Germany) and examined with a Zeiss 910 electron microscope. Digital micrographs were taken with a 1kx1k high speed slow scan CCD camera (Proscan) at an original magnification of 10000 X and analyzed with iTEM software (Olympus Soft Imaging Solutions, Münster, Germany). For quantification, all attachments between neurite and underlying substrate were identified and length of each attachment was measured and plotted on a two dimensional coordinate using random number generator.

2.2.6 Microcontact printing

Recently a microcontact printing method has been proposed to guide neurite growth on a graded pattern (von Philipsborn et al. 2006). To begin the

experiment, stamps with a stripe pattern needed to be prepared. Silicon masters with desired patterns of mirror image were provided by Dr. Siegmund Schroeter (Institute of Photonic Technology, Jena, Germany). In order to use silicon as a master to mold Polydimethylsiloxane (PDMS) from, the master was rendered hydrophobic by submerging the master for 10 minutes in a 1 mM trichloro (octadecyl) silane solution in heptane, then well-mixed PDMS prepolymer was poured on the master. A small piece of clean glass was placed on top of the PDMS. Mold was then fixed with metal weights and polymerized at 60°C overnight then the polymerized PDMS is ready for use. To prepare coverslips for stamping, glass coverslips were carefully cleaned to avoid debris interference during the printing process. For a thorough cleaning, coverslips were washed three times respectively with ultrapure H_2O; 50% ethanol and ultrapure ethanol. Washed coverslips were then incubated overnight in 1:1 ethanol-acetone solution. The following day, coverslips were washed three times in ultrapure ethanol. The coverslips were dried in a clean place for printing. To print laminin protein on coverslips, the stamps were covered with laminin proteins at concentration of 20 µg/ml. Laminin proteins were mixed with 2 µg/ml Alexa 488 (Cy2 equivalent) or Alexa 555 (Cy3 equivalent) fluorescence for detecting printing ink and incubated at 37°C. After 45 minutes, the stamps were rinsed with ddH_2O and dried using nitrogen then quickly placed onto a glass coverslip. The previous steps were repeated by vertically printing other laminin proteins. After the process mentioned above, DRG neurons were dissected and trypsinized as previously decribed then plated for guided neurite outgrowth.

3 RESULTS

3.1 Identification of an extracellular tether required for mechanosensitive channel gating

3.1.1 Mechanotransduction and the tether model

Our senses of touch and pain rely on the afferent sensory neurons, which innervate to our skin to rapidly transform mechanical stimuli into an electrical signal. However, the mechanism by which the mechanical-electrical transduction takes place still remains a puzzle at the cellular and molecular level. The mechanoreceptor endings are very fine structures often embedded in specialized end organs, which makes them very difficult to examine *in vivo*. So far, the only mechanoreceptors in mammals from which a mechanically gated receptor potential has been measured *in vivo* are Pacinian corpuscles and muscle spindle afferents (Hunt and Ottoson 1973; Loewenstein and Skalak 1996). The extreme inaccessibility of sensory nerve endings has precluded direct biophysical recordings of the nerve terminal within the cutaneous layer. An alternative approach to address this question was established by recording from sensory neurons cultured on PLL/laminin (EHS-derived matrix) substrate using patch-clamp techniques combined with a mechnical stimulation method by a fire-polished glass pipette powered by a nano-motor, which can move the glass

tip at sub-micron displacement (see Methods). Mechanically activated currents evoked by mechanical stimulation of the sensory neuron neurite in culture (740 nm amplitude displacement) were measured using whole-cell recording from the cell body in the presence of TTX (1μM) to block interference of action potentials (APs) as previously described (Hu and Lewin 2006). Consistent with previous findings by Hu et al (Hu and Lewin 2006; Wetzel et al. 2007), three major types of mechanosensitive currents were observed and classified in accordance with their inactivation time constant into rapidly adapting currents (RA), intermediately adapting currents (IA) and slowly adapting currents (SA) (Fig.1A) (Hu and Lewin 2006). Using such stimuli >93% of isolated sensory neurons (n=45) possessed one of three mechanically activated currents, RA (inactivation in <5 ms), IA (inactivation in <50 ms) and SA (no adaptation during a 230 ms stimulus). These three mechanically activated current types account for approximately 40% (18/45), 5-10% (5/45); and ~40% (19/45) of all cultured neurons respectively. There were few neurons (~6%; 3/45) that were unresponsive to mechanical stimuli (Fig. 7B). Usually neurons possessing RA currents have a relatively narrow AP (width < 1 ms; measured by 1/2 AP duration) and large soma size (> 25 μm). Cells that were not responding to mechanical stimuli all have very wide AP (> 2.5 ms) with a hump and very small soma size (< 25 μm), characteristic of nociceptors (Koerber et al. 1988; Lawson 2002). Cells possessing SA and IA mechanosensitive currents often have relatively smaller soma size and wider AP with a hump, which suggests that these cells might be putative nociceptors (Fig. 7B & Fig. 7C).

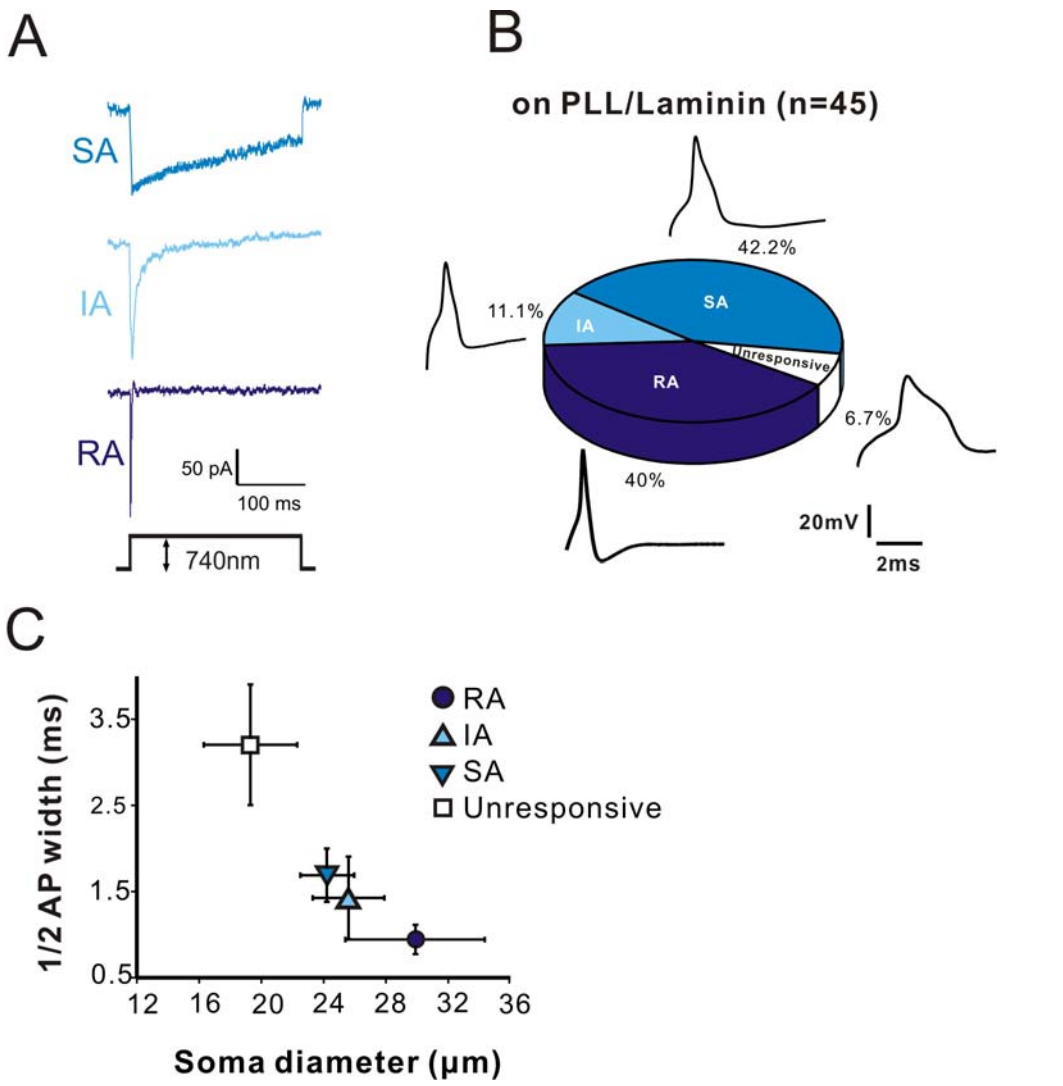

Figure 7. Mechanosensitive currents classification and the proportion. A. Mechanical stimulation of neurites evokes three types of mechanosensitive currents. Current trace example: RA currents (inactivation in <5 ms), IA currents (inactivation in <50 ms) and SA currents (no adaptation during a 230 ms stimulus). **B.** Distribution of these three currents approximately account for 40%, 5-10%; 40% of all cultured neurons respectively. There are few neurons (~5-10%) which do not respond to mechanical stimuli. Example traces of the measured AP configuration for each current type are shown. **C.** The AP width is plotted against the soma diameter for cells displaying different currents. Cells with RA often have big soma size and narrow AP and cells with IA and SA currents had smaller soma size and broader AP. Unresponsive neurons have very small soma size and very wide AP with a hump.

In mammals, adult sensory neurons can be authoritatively classified into mechanoreceptive neurons and nociceptive neurons by their AP configuration (Koerber et al. 1988; Djouhri et al. 1998; Lawson 2002). Low threshold mechanoreceptors with myelinated axons, which innervate dermal layer of the skin normally have very narrow AP spikes (Fig. 8A upper panel) (Koerber et al. 1988). The small to medium-sized neurons are high threshold nociceptors, which in the adult are characterized by wider APs that exhibit an inflection or 'hump' on the falling phase of AP spikes (Koerber et al. 1988; Lawson 2002; Lechner et al. 2009). The first derivative of each humped spike (dV/dt) exhibits two relative minima as compared to one minimum in mechanoreceptors (Fig. 8A lower panel). All recorded cultured neurons, if not unresponsive to mechanical stimulation, possess one of the three types of mechanically activated currents that can be distinguished on the basis of their inactivation kinetics, biophysical properties and pharmacological sensitivity. The RA-type mechanosensitive current is found in mechanoreceptors and nociceptors, whereas almost all IA and SA currents are exclusively found in nociceptors (Drew et al, 2002; Hu and Lewin, 2006) (Fig. 8B & 8C left panel). The morphology and physiology of recorded neurons in culture can be linked to the biophysical properties of cutaneous mechanoreceptors (Fig. 8B & 8C right panel).

Cutaneous mechanoreceptor classification is based on the receptor morphology and physiology and functional properties can be linked to neurochemical and biophysical features (Koerber 1992; Lawson 1992). Physiologically, there are in principle two distinct responses: 1. afferent fibers discharge only during stimulus application (ramp phase); 2. afferent fibers continue firing during the static

maintenance of a mechanical stimulus (static phase). Large diameter neurons in the DRG are thickly myelinated Aβ-fibres that conduct very rapidly (>10 m/s in mice (Koltzenburg et al. 1997). These neurons represent low threshold mechanoreceptors that can be divided into two groups, namely RAM (rapidly-adapting mechanoreceptors), which are preferentially excited only during ramp phase and SAM (Slowly-adapting mechanoreceptors), which are preferentially excited during both ramp and static phase (Fig. 8B right panel).

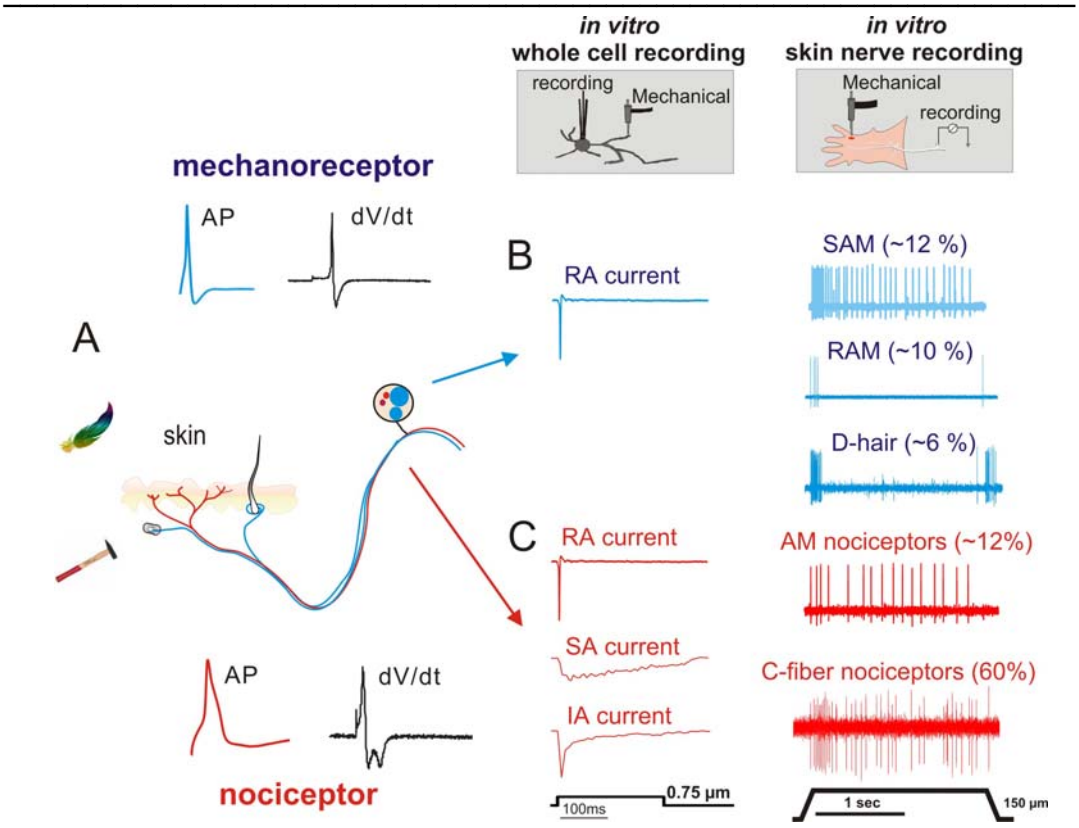

Figure 8. Morphological and biophysical properties of mechanoreceptors and nociceptors A. Example AP traces. The first derivative of humped spikes (dV/dt) exhibit two relative minima. **B.** Biophysical properties of low-threshold mechanoreceptors in culture and in skin. **C.** Biophysical properties of high-threshold nociceptors in culture and in skin.

A-mechanonociceptors (AM) and D-hairs have medium size axons that are thinly myelinated conducting in the Aδ-range with velocities between 1-10 m/s in mice

(Koltzenburg et al. 1997). AM fibres are excitable by either pressure of very high intensity, pinching the epidermis or cutting the skin with sharp objects (Fig. 8C lower panel), whereas D-hairs belong to low threshold mechano- receptors and conduct exclusively during the movement phase of the mechanical stimulus (Fig. 8C upper panel). C-fibres nociceptors make up the largest group of cutaneous receptors in mice (60%). These fibers lack a myelin sheath therefore conduct very slowly, i.e. below 1.0 m/s in mice (Fig. 8C lower panel) (Koltzenburg et al. 1997)

In collaboration with Dr. Jing Hu in the lab, it was asked if a tether model applies to mechanotransduction in mammalian sensory DRG neurons that mediate gating of mechanosensitive channels. Only the terminal endings of sensory neurons in the skin are mechanosensitive *in vivo*, and thus it is needed to establish a model of the cellular milieu found at the receptor ending *in vitro*. To this end, Dr. Jing Hu has developed a co-culture system by cultivating sensory neurons on a monolayer of mouse 3T3 cells. Sensory neurons grow neurites on a monolayer 3T3 cells and mechanical stimulation of these neurites (740 nm amplitude displacement) evokes mechanosensitive currents. It was hypothesized that if mechanosensitive ion channels are gated by a tether linking them to the fibroblasts or matrix surrounding the fibroblast, then mechanical displacement of the fibroblast adjacent to the neurite may evoke fast mechanosensitive currents in sensory neurons. Gating kinetics were measured based on latency (time window between mechanical stimuli and onset of mechanosensitive current) and activation time constant (τ_1; activation time exponential fit). It was found that short latency, fast activating mechanosensitive currents were indeed evoked in sensory neurons when adjacent fibroblasts were mechanically stimulated (Supplementary

paper. Fig. 1a & 1b left panel. Hu, Chiang et al. 2009). Compared to neurons cultured on PLL/Laminin substrate, the latency and activation time constant of the mechanosensitive current was virtually identical after direct stimulation of neurites and stimulation of the adjacent fibroblast (Supplementary paper. Fig.1b right panel. Hu, Chiang et al. 2009). These findings suggest that the existence of a physical link might transfer force from the stimulated fibroblast to mechanosensitive ion channels in the sensory neuron.

I next prepared sensory neuron/fibroblast co-cultures for transmission electron microscopy (TEM) using a standard protocol for sample preparation. TEM micrographs show that the interface between different cell types is highly diverse. To correctly identify sensory neurons from fibroblasts at the ultrastructural level, several criteria were considered: their relative orientation between different cell types, cell morphology and intracellular composition. From my observations, sensory neurons were usually round and rich in mitochondria. Neurofilaments (NFs), intermediate filaments that represent the most abundant cytoskeletal element in large, myelinated axons were observed occasionally. These neurofilaments run in parallel along the axon and interact through electrosteric forces mediated by their unstructured sidearm domains (Ohara et al. 1993; Draberova et al. 1999; Kumar et al. 2002). As far as orientation is concerned, sensory neurons were usually embedded on a layer of flattened fibroblast. Underneath the fibroblast cell layer, a thin layer of secreted ECM proteins was observed, suggesting that fibroblasts are capable of secreting ECM proteins needed for cell attachment and growth. However, no electron dense objects were visualized in the interface between sensory neuron and fibroblast when standard

preparation protocols were applied (Fig. 9A). In a standard EM preparation, biological samples are fixed (by glutaraldehyde or other fixans) and stained by osmium tetroxide then contrasted by uranyl acetate and lead citrate. Using a standard protocol, the lipid bilayer of cells and organelles can be clearly observed as shown in Fig. 9A, however, the cell/cell or cell/matrix interface is not clearly visualized thus an improved EM preparation protocol was required.

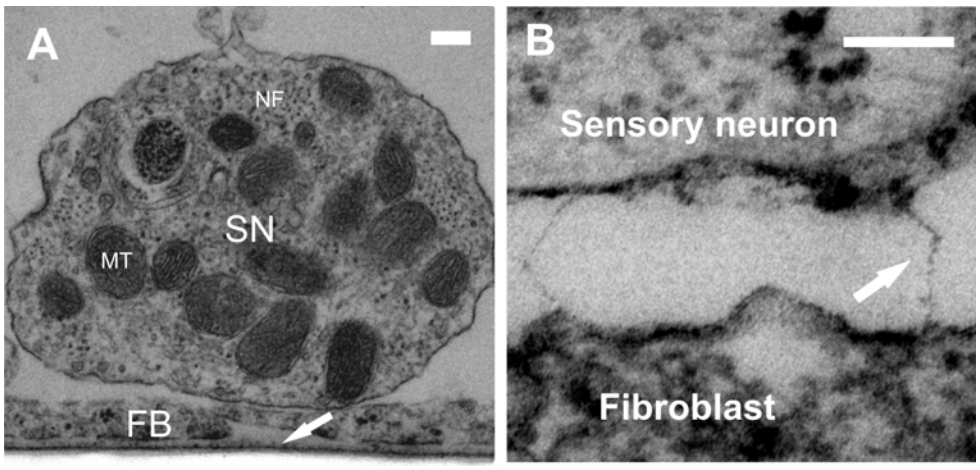

Figure 9. TEM micrograph of sensory neuron/fibroblast co-culture.

A. A sample TEM micrograph of the interface between fibroblast (FB) and sensory neuron (SN). In this case, the axon was round and rich in mitochondria (MT) and neurofilament (NF) and was embedded on a flattened fibroblast, in which neurofilament is absent. Underneath the fibroblast was a thin layer of electron dense material indicated by an arrow, suggesting ECM proteins secreted by fibroblast. Scale bar is 100 nm. **B.** In presence of ruthenium red, the electron density of sensory neuron/fibroblast interface was enhanced. Arrow indicates sporadic 100nm long electron dense extracellular filaments which links neurites to fibroblast. Scale bar is 100 nm.

To enhance the electron density of the sensory neuron/fibroblast interface, I introduced a fixation and staining procedure optimized to visualize extracellular proteins (see Methods 2.2.5). During sample preparation, cultured sensory neurons were fixed in glutaraldehyde and stained with osmium tetroxide

(Sigma-aldrich Co. Ltd.) in the presence of ruthenium red (Sigma-Aldrich) to enhance the electron density of extracellular proteins (Hasko 1988; Goodyear and Richardson 1992). Interestingly, additional electron dense objects in neuron/fibroblast interface were observed using this method. Using the same criteria to distinguish neurons from fibroblasts, examination of TEM-sections from such preparations revealed occasional long tether-like links of 100 nm between fibroblasts and sensory neurites (Fig. 9B). Such tethers are candidate entities for transferring force from matrix produced by fibroblasts and mechanosensitive channels.

3.1.2 Pharmacological and biochemical manipulation of the tether

The mechanosensitive currents found in sensory neuron/fibroblast co-cultures are identical to those found in sensory neurons cultured on laminin or on purified laminin-111 (also known as Laminin-1, which is the major component of Engelbreth-Holm-Swarm sarcoma laminins; highly purified trimeric laminin $\alpha_1\beta_1\gamma_1$-nidogen complex provided by Manuel Koch) (Paulsson et al. 1987; Aumailley and Yurchencho 2005) (Supplementary paper. Fig. 2a right panel. Hu, Chiang et al. 2009). It was asked whether tethers are necessary for channel gating in this reduced system. Using sensory neurons cultured on laminin, a series of experiments were conducted to examine the effects of manipulating ECM integrity or cell-matrix interaction on the mechanosensitive current. Interestingly, the hair cell tip link proteins are rapidly disrupted by Ca^{2+} chelation, consistent with the calcium dependence of cadherin interactions(Assad et al.

1991; Zhao et al. 1996). However, depleting extracellular Ca^{2+} ions with the calcium chelator 1,2-bis (o-aminophenoxy) ethane-N,N,N',N'-tetraacetic acid (BAPTA), blocking integrin signalling with the CD29 antibody(Mendrick and Kelly 1993; Tomaselli et al. 1993), and cleaving glycosyl phosphatidylinositol (GPI) membrane anchors with the enzyme phosphatidylinositol-specific phospholipase C (PIPLC), all did not affect the kinetic properties (data now shown), integrity and expression of mechanically activated curents in sensory neurons. (Supplementary paper. Fig. 2a right panel. Hu, Chiang et al. 2009)

The sensory neuron cultures were then treated with the endopeptidase subtilisin, which does not cleave the hair cell tip link (Osborne and Comis 1990; Goodyear and Richardson 1999) or with the subtilisin-related, site specific protease blisterase from parasite *Onchocerca volvulus* (*O. volvulus*), this protease cleaves a tetrabasic sequence with the motif RX(K/R)R (Catherine B. Poole 2003). Experiments were carried out on populations of cells treated with subtilisin (50 µg/ml, 120s, 37^{o}C) or blisterase (10-75 units/ml, 5-200 min, 37^{o}C) and observed that between 0 to 3 hours after treatment the proportion of cells found with an RA-type mechanosensitive current was reduced from 55% (23/42 cells) in control to just 16% (6/36 cells) in subtilisin treated cultures, and 12.5% (3/24) in blisterase treated cells χ^2–test $p<0.001$. The number of neurons with an SA-type mechanosensitive current remained unchanged after subtilisin and blisterase treatment. The SA current is found exclusively in nociceptors and is pharmacologically and biophysically distinct from the RA-type current. (Hu and Lewin 2006; Drew et al. 2007). Following ablation of the hair cell tip link mechanotransduction is lost, but transduction currents return 24 hours later, after

new tip link protein is re-targeted to the bundle (Zhao et al. 1996). Thus, Mechanosensitive currents were measured in populations of cells 17-30 hours after subtilisin removal. At these time points the incidence of the RA type mechanosensitive current had returned to control values. (Fig. 10A) (experiment carried out by Dr. Jing Hu).

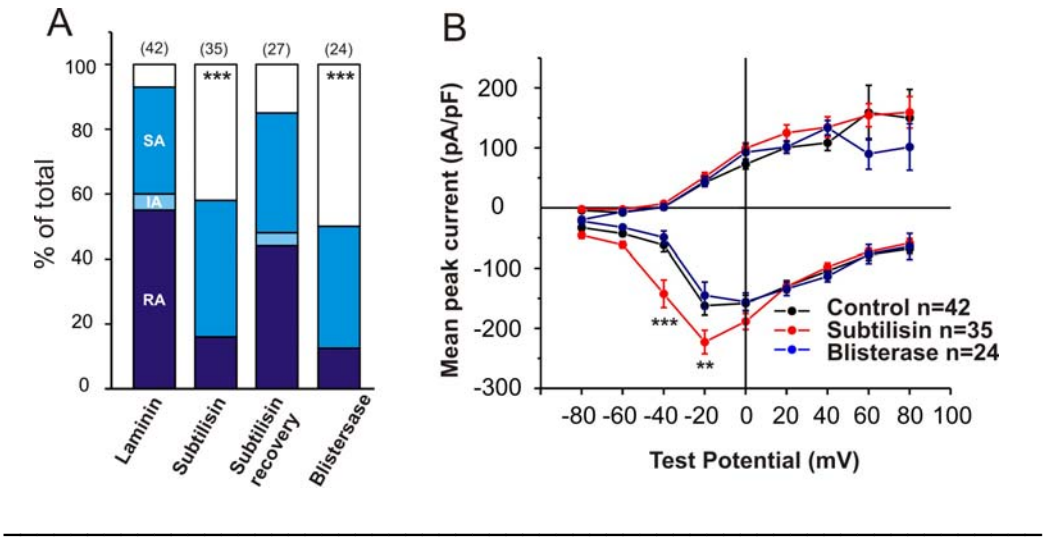

Figure 10. Subtilisin or blisterase selectively abolished RA mechanosensitive currents.

A. Stacked histogram shows that after two mins treatment of subtilisin/blisterase in whole culture, the population of rapidly currents is significantly reduced. The proportion of mechanosensitive currents recovered to control level when culture was allowed to recover for 30hrs (Chi-square test. $P<0.001$). **B.** I-V curve shows that subtilisin/blisterase treatment does not significantly alter the relation of inward and outward current in each group, suggesting that ion channels are not substantially cleaved by either protease (experiment carried out by Dr. Jing Hu).

After subtilisin or blisterase treatment 70-80% of the cells with a large cell body and a narrow AP characteristic of mechanoreceptors lacked mechanosensitive current (subtilisin 8/10 tested; blisterase 7/10 tested). In control cultures all mechanoreceptors possess a RA-mechanosensitive current (19/19 cells with narrow APs tested) (Hu and Lewin 2006). Many of the cells lacking

mechanosensitive currents after subtilisin or blisterase treatment (subtilisin 7/15 tested; blisterase 5/12 tested) were putative nociceptors with humped APs (Lewin and Moshourab 2004). The I-V relation for inward and outward currents was not markedly altered by blisterase treatment suggesting that the mechanosensitive ion channels integrities are not substantially cleaved by the specific enzyme (Fig. 10B) (experiment carried out by Dr. Jing Hu).

3.1.3 TEM quantification of identifiable extracellular attachments

I next asked whether anatomically identifiable protein tethers, that are subtilisin/ blisterase sensitive, are responsible for RA-current gating. To address this question, I have developed a quantitative TEM analysis method by comparing electron dense attachments between the neurite membrane and the laminin substrate in four conditions; control, subtilisin treated acute (3 mins) or subtilisin-treated 30 hour recovery and blisterase-treated acute (25 mins). From patch clamp data it was found that the RA current is sensitive to subtilisin/ blisterase endopeptidase and the TEM micrograph of the sensory neuron/fibroblast interface shows an electron dense ultrastructure which might be a candidate entity for mechanosensitive channel gating. Cultures for control and subtilisin treatment recovery (30 hours) were prepared, fixed and labelled using a method optimized for observing extracellular structures (see Materials and Methods) and then imaged using TEM. The aim was to observe the interface between cultured sensory neurites and underlying coated laminin substrate as illustrated in Figure 11A.

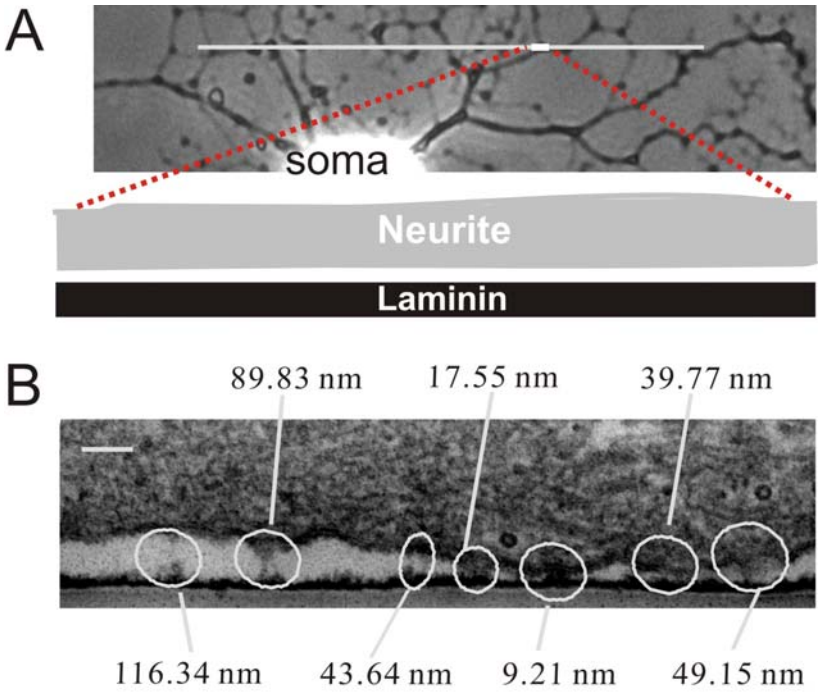

Figure 11. Schematic diagram of TEM quantification method and the interface between sensory neurite and laminin substrate. A. Light photomicrograph of a cultured sensory neuron with neuritic tree. TEM photomicrographs were generated from ultrathin sections from blocks of tissue with dimensions in the range illustrated by the white rectangle at the end of red dotted lines. Sample electronmicrographs of the neurite/matrix interface in control. **B.** Sample TEM micrograph shows the heterogeneity of sensory neurite/laminin interface. All electron dense objects are identified and measured for analysis. Scale bar is 100nm.

An electron dense laminin matrix 17 ± 1 nm in depth could be visualized on the surface of the culture dishes with a variety of tight and loose electron-dense connections between the neurite membrane and this matrix (Fig. 11B). I next investigated 4 groups: control, 3 minutes subtilisin treatment, 25 minutes blisterase treatment and 30 haours recovery after subtilisin treatment. All electron dense connecting objects were identified and measured for analysis. The area of measured membrane contact was 7.5 μm^2, 4.7 μm^2, 5.4 μm^2 and 5.5 μm^2 respectively in each group (Table 3). I then calculated and superimposed the

frequency distribution of all electron dense objects in the interface between cultured neurons and underlying laminin substrates from control, subtilin and subtilisin recovery groups. From the frequency distribution, two bell distributions (Gaussion fit) could be observed below 75 nm. The tethers above 75 nm were sporadic as no red peaks were observed above 75 nm thus 75 nm was selected as a criterium for quantification (Fig. 12).

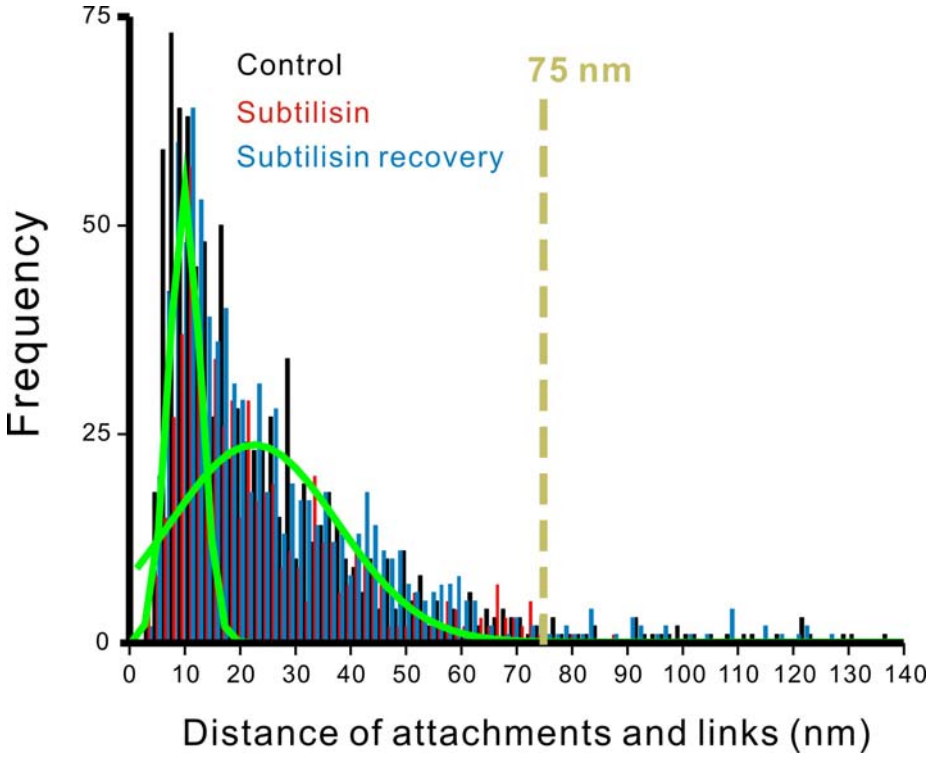

Figure 12. Frequency distribution of electron dense objects in neurite/laminin interface
Frequency distribution from control (DRG on laminin), subtilisin treatment (3 mins) and subtilisin recovery (30 hrs) groups were calculated and superimposed. Below 75 nm, two bell distriutions were observed (Gaussian fit). Above 75 nm, tether presence is sporadic and no peak from the subtilisin treatment group was observed. Thus 75 nm was chosen as the criterium for long tether considering absence and reappearance of the long links across different groups

These data were quantified by randomly photographing microscopic fields from 58 to 99 ultrathin sections (thickness: 50 nm) from at least 3-4 cultures in each

group (Table.1) and measured the number and length of electron dense objects that linked the neurite membrane to the laminin substrate. The length of each object was then randomly plotted in 2-dimensional space (Fig. 13I). The longest connecting objects were similar in length (~100nm) and shape similar to those observed in TEM of sensory neuron/fibroblast co-cultures (Fig. 13B; Fig. 9B). The longest protein tethers were rarely observed in subtilisin or blisterase treated cultures but the incidence was essentially the same in both the control and subtilisin-treated 30 hour recovery groups (Fig. 13A-H). The average distance of less than 75 nm short links in control, subtilisin, blisterase, and 30 hours subtilisin recovery is 22.6 ± 0.5 nm, 24.1 ± 0.7 nm, 23.1 ± 0.6 nm and 23.5 ± 0.5 nm respectively, comparable with length of integrin receptors, suggesting that these links might be integrin or integrin-related entities, which mediate cell-ECM interactions (Takagi 2002; Walz 2003; Adair et al. 2005; Iwasaki et al. 2005). These short links are unafftected by subtilisin/blisterase endopeptidase treatment. It clearly shows from this representation of the raw data that links with a length of between 5 and 75 nm were largely unaffected by subtilisin/blisterase treatment. However, electron dense objects >75 nm in length, presumably corresponding to protein filaments were selectively abolished after subtilisin/blsiterase treatment but reappeared in cultures allowed to recover for 30 hrs after subtilisin treatment (Fig. 13). The subtilisin/blisterase-sensitive protein filaments identified in these TEM experiments are always present under conditions when mechanically activated RA currents are intact and disappear under conditions when RA current is absent. This highlights a strong correlation between mechanically activated RA current and the TEM-identifiable subtilisin/blisterase-sensitive protein filament.

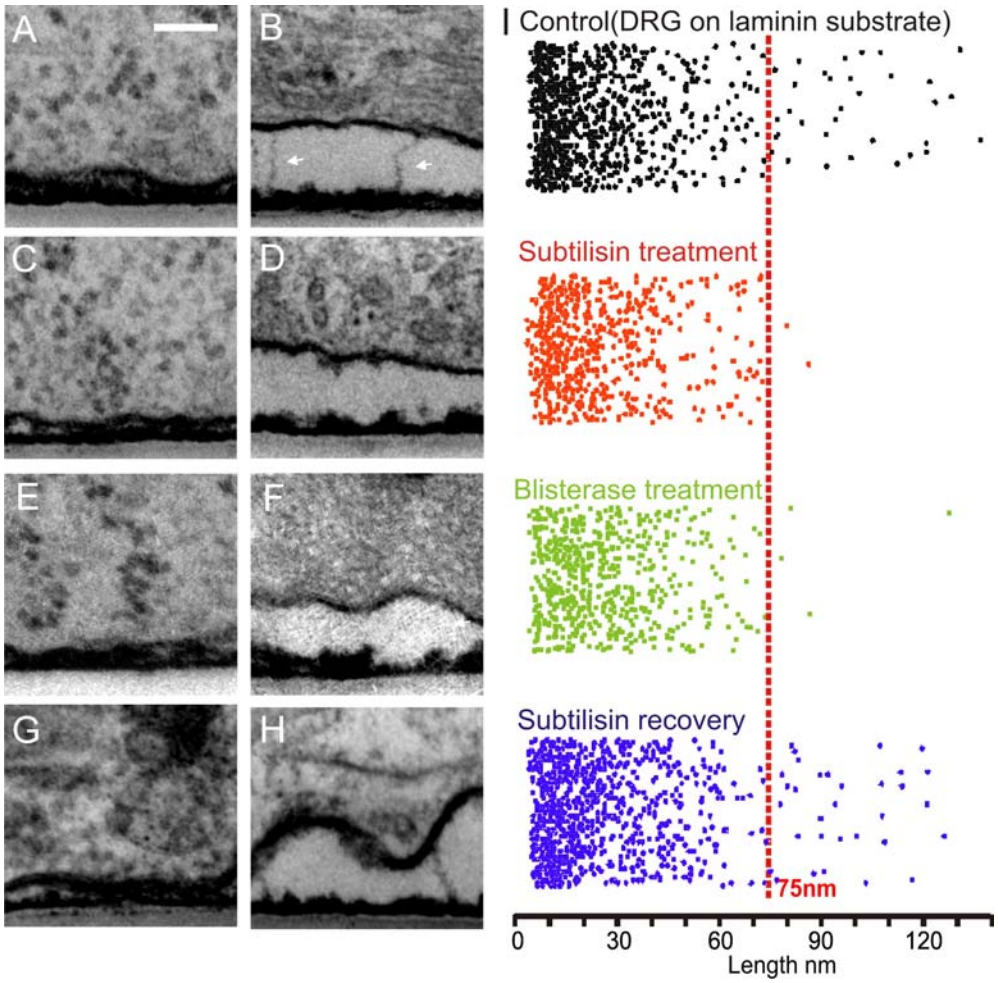

Figure 13. TEM reveals a protein filament necessary for RA current. A.B. Sample TEM micrographs of the neurite/matrix interface in control (DRG on laminin substrate) **C.D.** Sample TEM micrographs of the neurite/matrix interface in control after 3 minutes subtilisin treatment. **E.F.** Sample TEM micrographs of the neurite/matrix interface in control after 25 minutes blisterase treatment **G.H.** subtilisin treated cells after 30 hour recovery. **I.** The length of each measured attachment is plotted in a two dimensional space to illustrate the range of attachment lengths observed. Each dot represents the measured length of each linking object. Note the almost complete absence of long tether like proteins greater than 75 nm in length after subtilisin/blisterase treatment and their reappearance after recovery. Means are shown ± s.e.m. Scale bar is 100 nm.

To confirm the specificity of this effect, I cultured SCG neurons on laminin. SCGs are located opposite the second and third cervical vertebræ. They contain efferent neurons that supply sympathetic innervation to the face and have been reported not to possess mechanosensitive currents (Drew et al. 2002); this makes SCG neurons an ideal model as a negative control because in the tether model it could be predicted that the tethers could be absent. Good neurite outgrowth of SCG neurons was observed on a laminin substrate after 24 hours in culture medium (Fig. 14A). However, comparing with DRG culture the soma size of efferent sympathetic SCG neurons is clearly smaller than sensory DRG neurons (Fig. 14B).

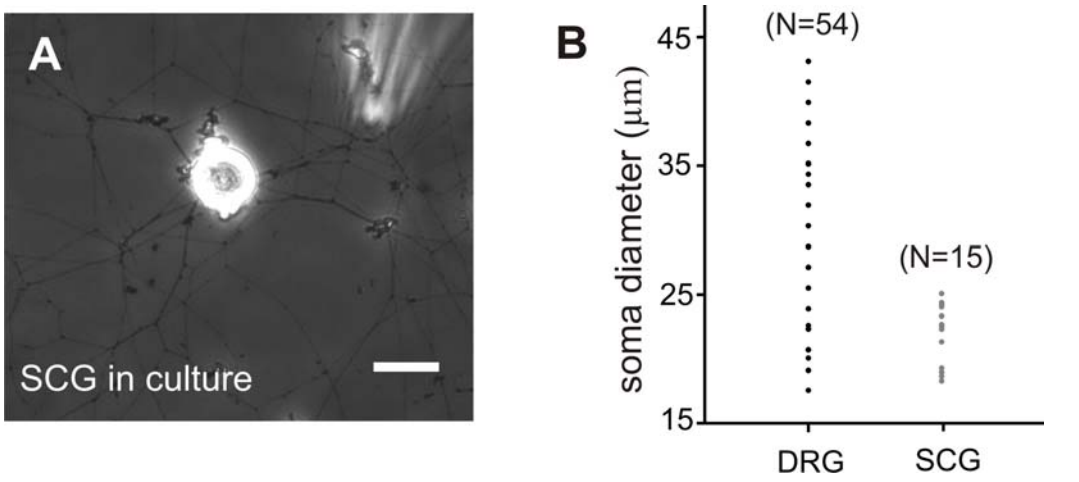

Figure 14. Superior cervical ganglion neurons in culture

A. Bright field micrograph of a culture SCG neuron. Good neurite outgrowth could be observed after 24 hours in medium. **B.** In comparison with DRG neurons which have cell size between 15 µm and 45 µm, most SCG neurons are smaller than 25 µm. Scale bar is 20 µm.

Recordings were made from cultured SCG neurons and could confirm that no RA-mechanosensitive currents were observed (Fig. 15A), although I did observe rare (2/15; ~13%), small amplitude, SA mechanosensitive currents in such cells (Fig. 15B) (n=15; Chi-square test).

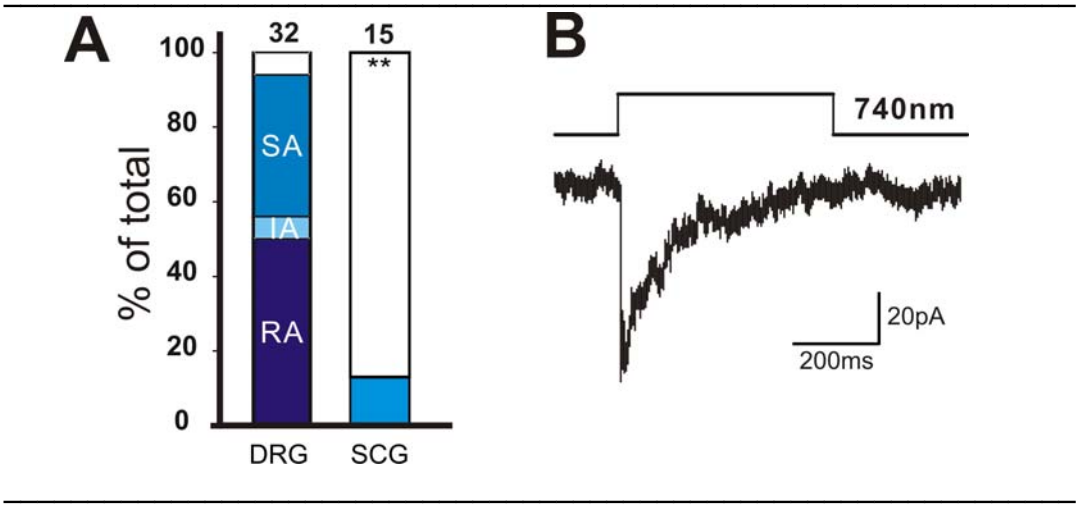

Figure 15. Mechanosensitive currents in cultured SCG neurons

A. The proportion of mechanosensitive currents on SCG neurons. The stacked histogram shows that RA currents are absent in SCG neurons. Most SCG neurons are silent to mechanical stimulation although I did observe rare SA currents (Chi-square test). **B.** Example current trace of mechanosensitive-SA current recorded from SCG.

A detailed TEM study of SCG cultures showed that no extracellular protein filaments are found that are greater than 75 nm in length (Fig. 16). The average length of short links less than 75 nm is significantly lower in DRG neurons 22.6 ± 0.5 nm (from 1030 sections) compared to 19.4 ± 0.3 nm in SCG neurons (from 1071 sections), suggesting that the membrane protein composition is different between SCG and DRG neuron types (Table 4). Measurement of electron dense objects greater than 75 nm in sensory neuron cultures showed that these objects

are on average 100 ± 3 nm in length and occur with a density of 4.9 ± 1.3 filaments per μm^2 of membrane (Table. 2).

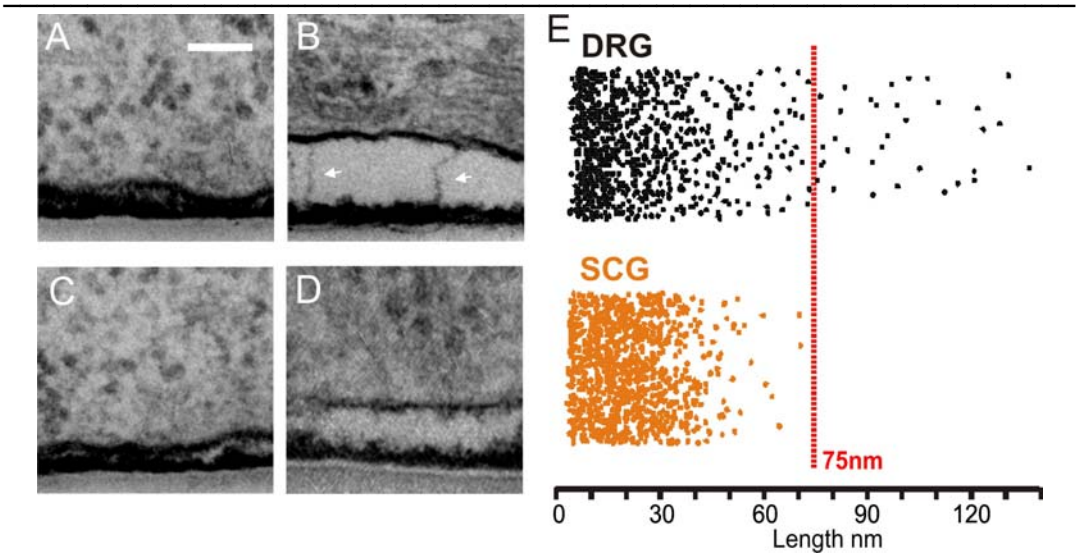

Figure 16. TEM study of SCG neurons confirms the absence of a protein filament necessary for RA current expression.

A.B. Sample electronmicrographs of the neurite/matrix interface in DRG **C.D.** sample electronmicrographs from cultivated SCG neurons where no long tethers were observed. **E.** Quantification of the electron dense attachments in many sections from control DRG and SCG cultures. The length of each measured attachment is plotted in random 2D space to illustrate the range of attachment lengths observed. Each dot represents the measured length of each linking object. Note the absence of long tether like proteins greater than 75 nm in SCG and an average position shift to the left of plotted dots in SCG. Means are shown ± s.e.m. Scale bar is 100 nm.

These data suggest that a subtilisin/blisterase-sensitive protein filament links the mechanosensitive complex in the membranes of sensory neurons to a laminin containing matrix. Furthermore, this protein tether is synthesized by sensory neurons as evidenced by the fact that protein filaments reappeared when allowed for recovery after 30 hours in the absence of other cell types in the culture. Most strikingly the absence and reappearence of RA-mechanosensitive current is

correlated with absence and reappearence of the protein filament, which strongly suggests that the protein tether is most likely necessary for the gating of the RA-mechanosensitive current.

	Total Measured Area (μm^2)	Density of attachments <75nm (unit/ μm^2)	Density of attachments >75nm (unit/ μm^2)	Average distance of attachment <75nm(nm)	Average distance of attachment >75nm(nm)
DRG Control (prep=4)	7.5 μm^2	150.3 ± 7.0 (N=1030)	4.9 ± 1.3 (N=31)	22.6 ± 0.5 (N=1030)	100.0 ±3.1 (N=31)
DRG Subtilisin (prep=3)	4.7 μm^2	156.1 ± 9.2 (N=581)	0.5 ± 0.4** (N=2)	24.1 ± 0.7 (N=581)	83.6 ± 3.2 (N=2)
DRG Blisterase (prep=3)	5.4 μm^2	159.5 ± 7.1 (N=869)	1 ± 0.6** (N=4)	23.1 ± 0.6 (N=869)	91.9 ±11.4 (N=4)
DRG Recovery (prep=3)	5.5 μm^2	167.3 ± 9.1 (N=836)	5.8 ± 1.8 (N=32)	23.5 ± 0.5 (N=836)	97.1 ±2.7 (N=32)
SCG (prep=3)	9.4 μm^2	142.7 ± 5.2 (N=1071)	0 (N=0)	19.4 ± 0.3** (N=1071)	0 (N=0)

Table 3. Quantification of TEM data. These data show results from control experiments (preparation=4) and from experiments where neurons in culture were treated with subtilisin 3-8 minutes (prep=3) and cultures left for 30hrs recovery (prep=3), cultures treated with specific protease Blisterase for 30mins (prep=2) and superior cervical ganglion neurons (prep=3). For each experiment, the total measured area was summed. Density and average distance of short and long links respectively are calculated. No significant differences in density of short attachments were noted between control neurons and the treatment groups as well as sympathetic SCG neuron. In subtilisin- and blisterase-treated group, the long links were significantly decreased and in the SCG group, the long links were not observed. In DRG cultures, the average distance of short and long links were conserved across different experiments. In the

SCG group, the average length of short links is reduced. N=number of identified attachments. Prep=number of preparations. Unpaired t-test (*P<0.05; **P<0.01; ***P<0.001)

3.1 Summary

The mode of gating of mechanosensitive ion channels in vertebrate touch receptors is largely unknown. Here it is shown that a protein link is necessary for the gating of mechanosensitive RA currents in the DRG neurons. Using TEM, I have demonstrated that a protein filament with a length of ~100 nm is synthesized by sensory neurons and may link mechanosensitive ion channels in sensory neurons to the ECM. Brief treatment of sensory neurons with the endopeptidase subtilisin, or the site specific protease blisterase, destroys the protein tether and abolishes mechanosensitive currents in sensory neurons without affecting electrical excitability. The role of stretch-activated channels in mechanoreceptors is controversial and these data show that it is unlikely that membrane stretch is, by itself, sufficient to gate mechanosensitive channels required for touch perception. Thus, like hair cells, an extracellular protein tether is required for mechanosensitive channel gating of sensory neurons.

3.2 Role of ECM in sensory mechanotransduction

ECM proteins are important for cell growth, attachment, and proliferation, however little is known about the role of the ECM in sensory mechano-transduction. Genetic screens carried out in both *C. elegans* and *D. melanogaster* have suggested that extracellular proteins are essential for the transducton of body touch and fly bristle movement respectively (Du et al. 1996; Chung et al. 2001; Chalfie 2002). There is no direct evidence showing that extracellular factors are crucial for the gating of somatic mechanotransduction channels in vertebrates. Due to the inaccessibility of sensory nerve endings at the cutaneous layer, an experimental model was desired to reproduce the extracellular environment of the skin *in vitro*. It was asked whether altering the substrate might change the physiological properties of mechanically gated currents or whether different extracellular environments modify the transduction of mechanical stimuli by DRG neurons.

3.2.1 Co-culture system and reproduction of sensory nerve ending at cutaneous layer *in vitro*

In order to address the role of different extracellular environments on mechanotransduction, recordings were made from sensory neurons cultured on PLL alone. As expected from previous work (Tomaselli et al. 1993) growth on such substrate was poor although in some cases neurons with a few short neurites were found. Mechanically activated currents were evoked in only 9/14

cells tested under such conditions. But it is difficult to exclude the possibility that this was because the neurons simply do not thrive on such a substrate. Furthermore, it was noticed that cells on a PLL substrate only usually thrived when fibroblasts were growing nearby thus it was speculated that the stimulated neurites may be exposed to extracellular factors produced by non-neuronal cells. Therefore a modified approach was introduced: a co-culture system of sensory neurons with defined cell types normally encountered in the skin was established.

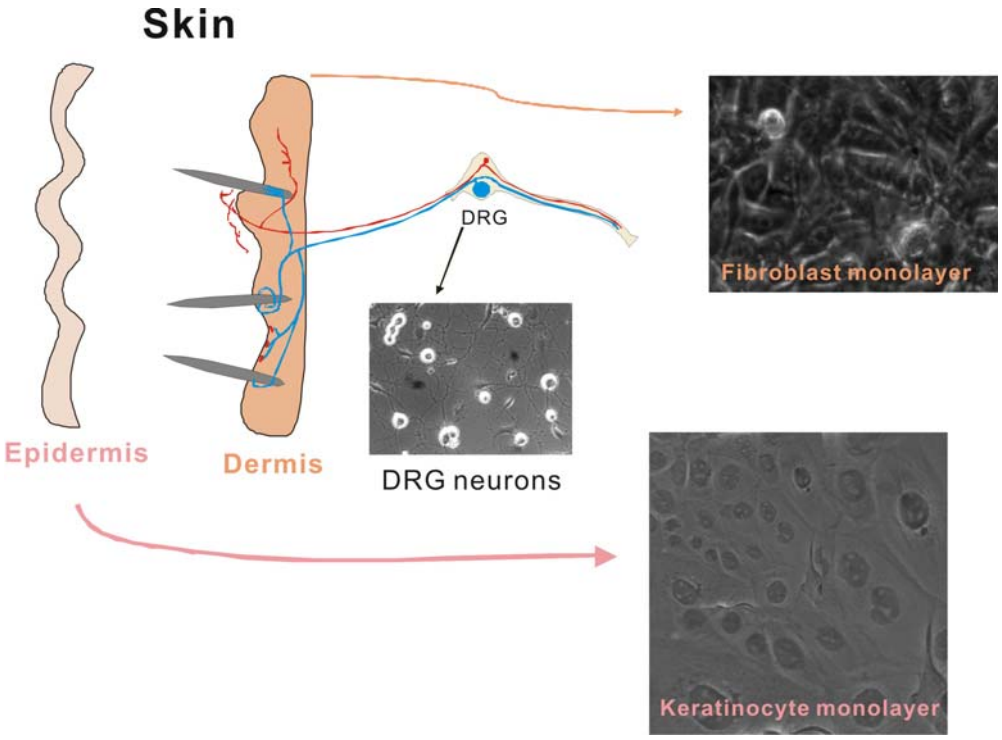

Figure 17. Schematics of reproduction of epidermis and dermis *in vitro*

Keratinocytes, the main component of epidermis and mouse fibroblasts (3T3 cells), important components of dermis were cultured. 3T3 cells were first grown on coverslips as the supporting layer for keratinocytes growth. When cells reached confluence, neurons were cultured on the cell monolayer to simulate the nerve ending innervating the skin. Blue color denotes low threshold mechanoreceptors which innervate mainly the dermal layer. Red color denotes high threshold nociceptors which innervate the epidermal layer.

The primary mouse skin keratinocytes were chosen because they are the main component of the skin epidermal layer, which is innervated by free nerve endings. Mouse fibroblast (3T3), which is an important component of the skin dermal layer was grown in a monolayer on a glass coverslip as a feeding layer for keratinocytes (Fig. 17). Sensory neurons were seeded on top of these monolayers and recordings made once they had established neurites on top of the monolayer 24 hrs later. Both cellular substrates supported good neuritic growth and there was no indication that sensory neurons processes avoided growing on keratinocytes or fibroblasts (Fig. 18).

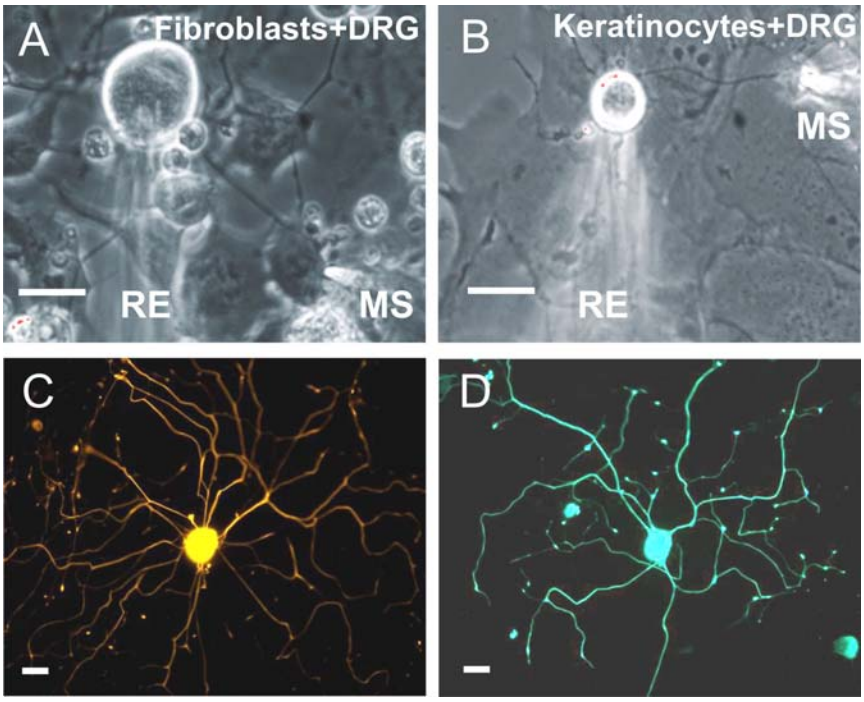

Figure 18. Sensory neuron neurite outgrowth on fibroblasts and keratinocyte monolayer
A. Light micrograph of sensory neuron cultured on fibroblast monolayer. **B.** Light micrograph of sensory neuron cultured on keratinocyte monolayer. **C.** Immunostaining (nf-200) of neuron cultured on fibroblast monolayer showing good neurite growth. **D.** Immunostaining (nf-200) of neuron cultured on keratinocyte monolayer showing good neurite growth. RE denotes recording pipette and MS denotes mechanical stimuli. Scale bar is 20 μm.

3.2.2 Modulation of mechanically activated currents on keratinocytes matrix

Neurons on the keratinocytes and fibroblasts substrates were randomly selected and recorded. Neurites that had grown on top of the keratinocyte monolayer were mechanically stimulated and sensory neurons of all sizes were recorded. For sensory neurons grown on keratinocytes there was a dramatic increase in the number of cells that displayed no response to the standard mechanical stimulation (Fig. 19), thus more than 43% of cells (19/43) showed no current response compared to 7.8% (10/126) on the control PLL/laminin substrate ($p<0.01$; Chi-square test). In contrast, neurons grown on a fibroblast monolayer showed very robust mechanically activated currents with only 2.2% (1/45) of the cells showing no current. Interestingly, the proportion of cells that exhibited SA and IA currents in these keratinocytes and fibroblast co-cultures was unaltered compared to controls. In the keratinocyte co-culture experiments there was a dramatic loss of cells with an RA current. Despite the major loss of mechanically gated currents in almost half of the cells cultured on a keratinocytes substrate the remaining cells displayed mechanically gated currents with peak amplitudes that were indistinguishable from those found in control cultures. Thus co-culture of sensory neurons with keratinocyte monolayers dramatically affected the incidence of mechanically activated currents. Although the sensory neurons were cultured together with keratinocytes for relatively short periods (24 hours) it is possible that secreted factors from keratinocytes affect the differentiation of the neurons and thereby bring about the changes in mechanosensitivity described above. To address this issue, two types of control experiment were conducted. In the first experiment, freshly cultivated sensory neurons were incubated with

conditioned medium from keratinocytes overnight. Keratinocyte-conditioned media was obtained from frozen stocks (-20°C) or taken directly from cultivated keratinocytes monolayer. Recordings were then made of mechanically gated currents evoked by neurite stimulation. Sensory neurons displayed mechanically evoked currents that were essentially indistinguishable from those found in control cultures. This experiment suggests that secreted soluble factors from keratinocytes cannot by themselves negatively modulate mechanically gated currents in cultured sensory neurons. With the second control experiment it was asked whether a cell-free matrix secreted by keratinocytes might be sufficient to produce similar changes in sensory neuron mechanically gated conductances as does co-culture with keratinocytes. To answer this question, coverslips coated with keratinocyte-derived matrix by first establishing keratinocyte monolayer and then removing the cells by treating the monolayer with a diluted detergent solution were obtained. These cover slips were then used to culture freshly dissociated adult mouse sensory neurons. Sensory neurons grow well on the keratinocyte-derived substrate. Interestingly, when the cells were stimulated with the standard mechanical stimulus on the neurite most recorded cells did not respond with inward currents. The neurites of single cells were stimulated several times at different locations to be sure that no false negative results were obtained. In cells in which a mechanically gated current was observed the current was always slowly adapting. The loss of RA current on the keratinocyte-derived matrix is even more dramatic than the keratinocyte co-culture experiment. It thus appears that sensory neuron neurite contact with surface bound material conditioned by keratinocytes is sufficient to dramatically alter the properties of

mechanically gated currents in the sensory neuron (Fig. 19A) (experiment carried out by Dr. Jing Hu).

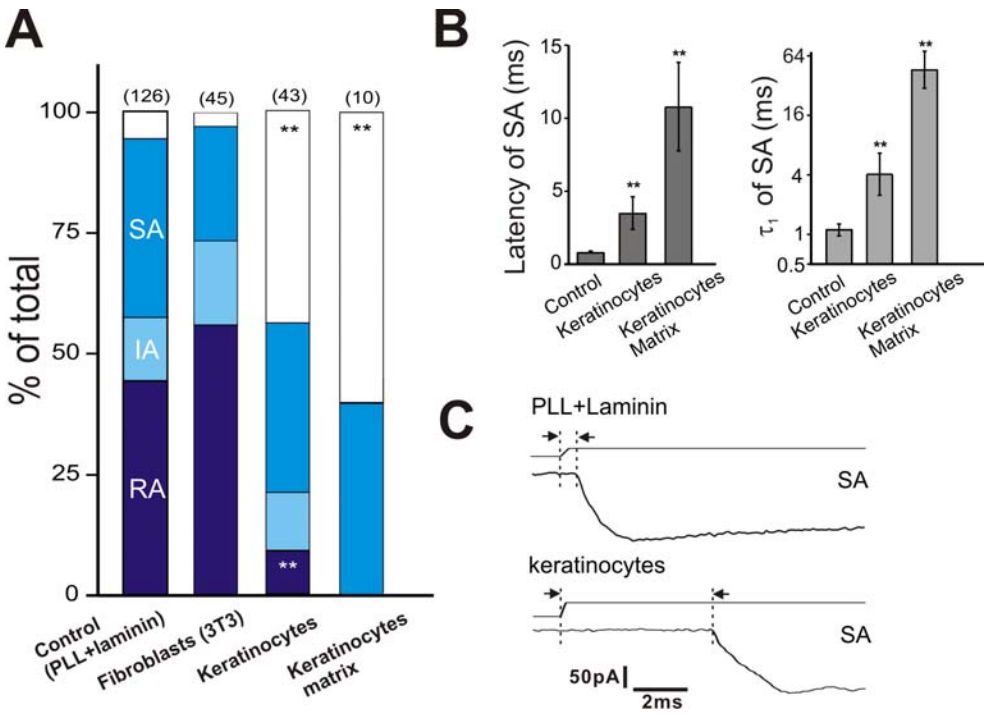

Figure 19. Proportion of mechanically activated currents and gating kinetics of SA current on a keratinocyte monolayer, fibroblast monolayer and keratinocyte-derived matrix. A. It is clear that a keratinocyte monolayer does not support RA current. On a cell-free keratinocyte matrix, this negative effect is even more dramatic. Fibroblasts do not alter the gating of mechanotransduction. Numbers on top of histogram represent for cell number recorded in each group (Chi-square test; $P<0.01$). **B.** A comparison of the latency and activation time constant of neurons cultured on PLL/laminin, keratinocytes and keratinocyte-derived matrix. The latency of SA in keratinocytes co-culture is significantly longer than on control laminin. The time constant for SA current activation (τ_1) on a keratinocyte monolayer was also significantly longer than on the control PLL/laminin substrate ($P<0.01$ Mann Whitney U-test). **C.** Example traces show typical measurements of current latency for different culture condition. Note the very long latency and relatively slow activation for inward currents evoked on a keratinocyte monolayer (experiment carried out by Dr. Jing Hu).

The latency for channel gating as well as the speed of channel opening (τ_1) on keratinocytes and the keratinocyte-derived matrix were measure. Surprisingly,

both the latency and the activation time of SA currents measured in keratinocyte co-cultures and keratinocyte-derived matrix were dramatically and significantly increased. Thus the mean latency for channel gating jumped several fold from ~600 μs to between 3 and 6 ms for SA currents (Table 5). The time constant for activation τ_1 was slowed from around 1ms to 4ms for SA neurons (Mann Whitney U-test; $P<0.01$) (Fig. 19B & 19C & Table 5) (experiment carried out by Dr. Jing Hu). To summarize, these data show that keratinocytes have a negative effect on mechanosensitivity of cultured sensory neurons, specifically on the expression of RA current and can significantly alter the gating kinetics of the SA current. This negative effect of the keratinocyte-derived matrix is even more dramatic, strongly suggesting that molecules secreted by keratinocytes might play an important role in loss of RA current.

3.2 Summary

The ECM is very important for cell migration, adhesion, proliferation and survival. Genetic screens carried out in *C. elegans* and *D. melanogaster* have suggested that extracellular proteins are necessary for the transducton of body touch and fly bristle movement but there is no direct evidence that extracellular factors are crucial for the gating of somatic mechanotransduction complex in vertebrates and little is know about the role of ECM in sensory mechanotransduction. To investigate this, co-cultures of sensory neurons and skin-derived keratinocytes or sensory neurons and fibroblasts were established to simulate the skin innervated by sensory nerve endings *in vitro* due to the inaccessibility nerve endings at the cutaneous layer *in vivo*. In this chapter it was found that keratinocytes have the

ability to profoundly alter the mechanically activated channel gating. These data show that keratinocytes do not support the mechanically evoked RA current and can alter the gating kinetics of the mechanically activated SA current by delaying the latency and activation time constant. The keratinocyte-derived matrix was then produced by washing away keratinocytes and leaving keratinocyte-derived matrix intact. The negative effect on mechanosensitivity of sensory neurons on keratinocyte-derived matrix was even more dramatic. This suggests that ECM components can modulate mechanically activated channel gating.

3.3 Identification of Laminin-332 for mechanosensitivity modulation

3.3.1 Screening for keratinocyte-derived ECM proteins, which account for the mechanosensitivity modulation

It was found that keratinocytes and keratinocyte-derived ECM can profoundly alter mechanically activated channel gating. I next asked which molecule has caused the loss of RA current on epidermal keratinocyte monolayer and keratinocyte-derived matrix but neither on fibroblasts nor on a laminin substrate. To address this question, a series of screening experiments were donducted. The commercially available laminin used for control was a mixture of various laminin proteins purified from the Engelbreth-Holm-Swarm (EHS) sarcoma (see Materials). To compare the proteomic composition of laminin with ECM proteins from fibroblasts and keratinocytes, ECM molecules from keratinocytes and 3T3 cells were isolated by removing the confluent cell monolayer and collecting the remaining ECM molecules in the presence of RIPA buffer (see Methods). Using electrophoresis and silver staining techniques, one could clearly see that the ECM proteins secreted by cultured keratinocytes and 3T3 cells as well as the control laminin (EHS-derived matrix; commercially available) are all highly diverse in their contents. These data show that the isolated ECM extracts and the commercial laminin, which is also an ECM extract from EHS sarcoma contain at least dozens of bands, suggesting each cell type secretes a wide range of different proteins to form an ECM (Fig. 20).

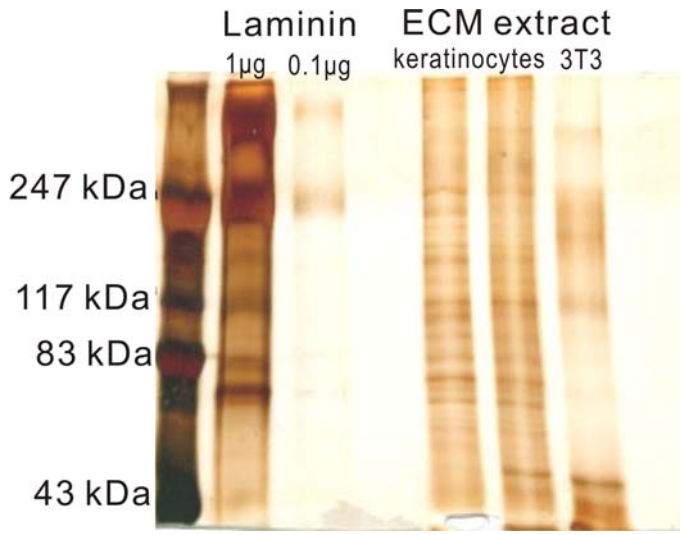

Figure 20. Silver staining of electrophoresis SDS-PAGE of laminins vs. keratinocyte-derived ECM vs. fibroblast-derived ECM. Note number of bands showing the diversity of laminins, keratinocytes ECM extract and fibroblast ECM extract. Gel was run at 160mV; room temperature.

I hypothesized that if any molecule causes loss of mechanosensitivity on keratinocytes but not on fibroblasts in comparison with laminin, then it must be expressed by keratinocytes, but not by fibroblast and should be absent in EHS-derived laminins. It was previously found by other groups using proteomics techniques that several molecules including plectin, fibronectin and laminin-332 (also known as laminin-5/Kalinin/nicein/epiligrin/ladsin/BM600) (Masunaga et al. 1996; Aumailley and Yurchencho 2005; Marinkovich 2007) are keratinocyte markers (Kim Bak Jensen 2003). To verify which molecule contributes to the loss of mechanosensitivity, Western-blotting experiments were conducted and the results showed that laminin-332 was expressed by keratinocytes, but not present in fibroblast-derived ECM nor in laminin (EHS-derived matrix), suggesting that laminin-332 is a promising candidate molecule to account for the loss of RA

mechanosensitive current (Fig. 21) (laminin-332 monoclonal Ab provided by Manuel Koch) (experiment.carried out by Dr. Regina Bönsch)

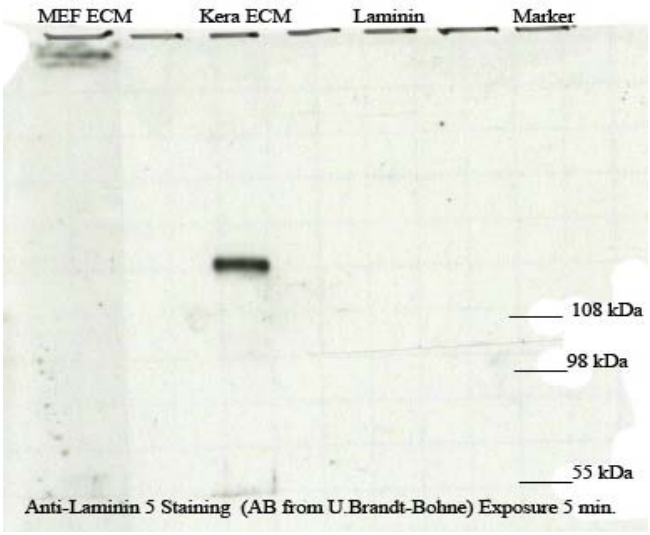

Figure 21. Western blotting result from laminin, keratinocyte-derived ECM and fibroblast-derived ECM. Result shows that laminin-332 is present in keratinocytes ECM but not in fibroblast ECM nor in laminin (commercial EHS-derived matrix; see Materials). Kera denotes keratinocytes. MEF denotes mouse embryonic fibroblast.

3.3.2 Laminin-332 can partially reproduce keratinocyte mechanosensitivity modulation

The silver staining and Western blotting results showed that laminin-332 is a promising candidate as the mechanosensitivity inhibitory factor of keratinocytes. Laminins are large extracellular glycoproteins that are important components of all basement membrane zones (BMZs), and are involved in several important biological processes (Sasaki et al. 2004) including tissue development, wound healing, and tumorigenesis (Marinkovich 2007). All laminin molecules are trimeric

glycoproteins consisting of α, β and γ chains. Five α chains, three β chains and three γ chains have been identified and localization of distinct chain combinations in various tissues leads to the formation of as many as 16 different laminin isoforms with tissue-specific functions. All the protein isoforms in the laminin family have a cross-like structure as viewed by rotary shadowing electron microscopy (Fig. 22 modified from Marinkovich 2007) (Martin and Timpl 1987). Laminin-111 (the trimeric protein which consists of α1, β1 and γ1 chains) was the first laminin molecule to be studied (Timpl 1979). It was originally purified from EHS sarcoma in the late 1970s. Laminin-111 is the major component of EHS sarcoma ECM proteins, which were used in this study as control laminin. It has been traditionally viewed as the prototypic laminin molecule, even though recent evidence suggests that the actual tissue distribution of laminin-111 in mature tissues is quite limited, and it is mainly expressed during embryonic and fetal development (Ekblom et al. 2003). The main role of laminin-332 (a trimeric protein which consists of α3, β3 and γ2 chains) in normal tissues is in the maintenance of epithelial- mesenchymal cohesion in tissues exposed to external disruptive forces (Ryan 1996). Laminin-332 plays a crucial role in epidermal adhesion (Aberdam 1994; Pulkkinen 1994) and gene mutations or impairment of laminin-332 leads to a severe and lethal blistering disease: Herlitz's junctional epidermolysis bullosa (JEB) (Meneguzzi 1992; Marinkovich 1993). To compare laminin-332 with laminin-111, it was found that the long arm of the cross consists of domains I and II, which function primarily in the intramolecular assembly of laminin trimers (Fig. 22) (Carter et al. 1991; Patricia Rousselle 1995). At the base of the long arm is a globular structure termed the G domain, which contains five epidermal growth factor (EGF)-based repeats. Laminin-332 is a highly specialized

molecule. Although the long arm and G domain of laminin-332 and laminin-111 are roughly the same size, the short arms of laminin-332 are very short. Laminin-332 interacts with at least two major epithelial integrin receptors: $\alpha_3\beta_1$ and $\alpha_6\beta_4$ through its G-domain on the α chain and promotes formation of focal adhesions and stable anchoring contacts (SACs), which form hemidesmosomes *in vivo* (Carter et al. 1991; Patricia Rousselle 1995).

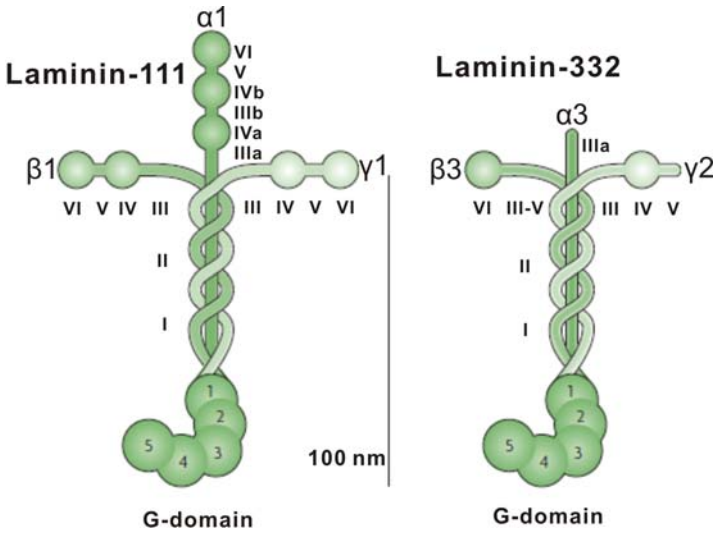

Figure 22. Diagram of the structure of laminin-111 and laminin-332 as modified from (Marinkovich 2007). Cross-like structures are viewed by rotary shadowing electron microscopy. The first three repeats of G-domain in α chain contain binding sites for integrin receptors. Laminin-332 as compared to laminin-111 contains significantly truncated globular domains on the α3, β3 and γ2 chains that comprise the short arms of the laminin molecule. These chains differ significantly in their abilities to interact with other ECM molecules.

I next asked if laminin-332 can reproduce the keratinocytes inhibitory effect. To answer this question, I obtained purified rat laminin-332 (Cat # CC145 Chemicon Ltd; see Materials) and coated coverslips with the purified protein, which were pre-coated with PLL as previously described (see Methods). After 24 hours, I

could confirm that laminin-332 sustains neurite outgrowth (Culleya et al. 2001) (Fig. 23A).

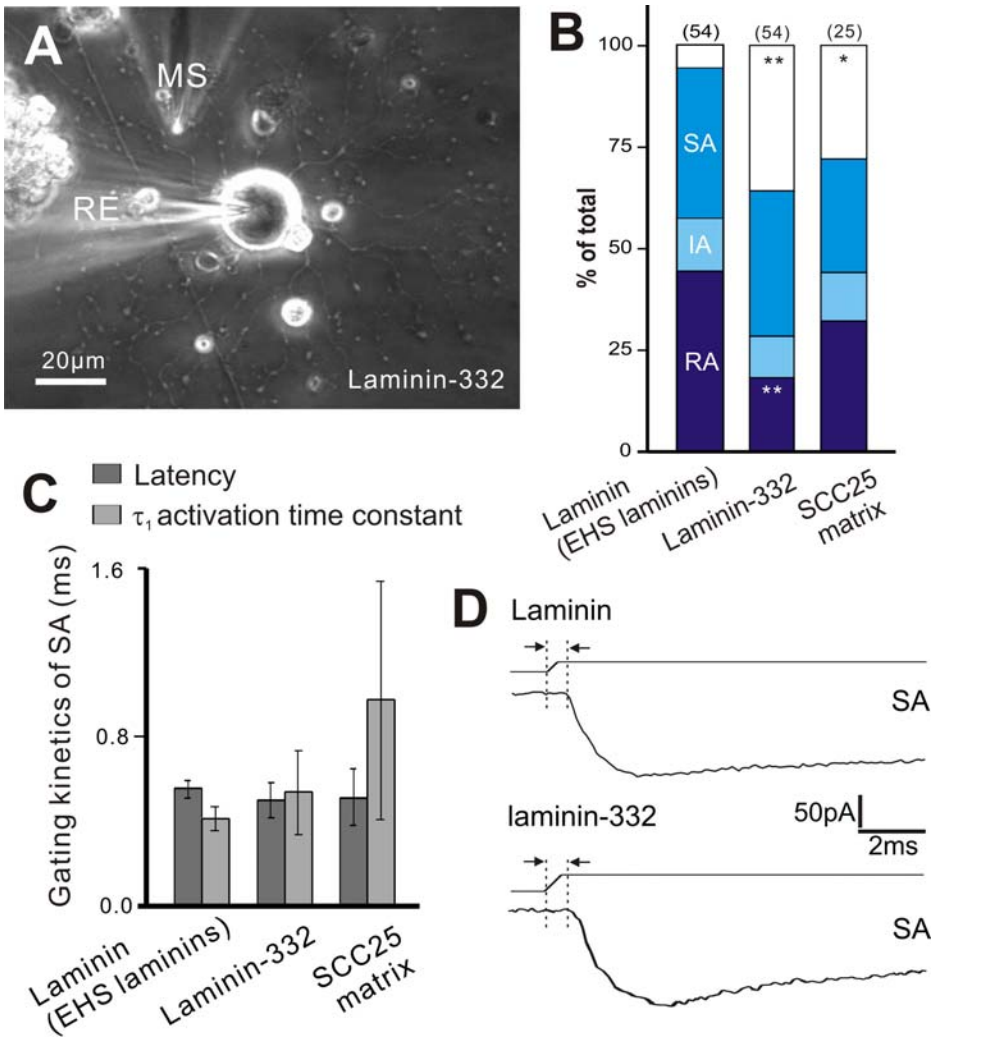

Figure 23. Laminin-332 substrate is inhibitory for mechanosensitive-RA current but not for the gating kinetics of mechanosensitive-SA current. A. Laminin-332 substrate supports robust neurite outgrowth. **B.** Laminin-332 can reproduce mechanosensitivity inhibition of keratinocytes for RA current expression. SCC25, which secret a significant amount of laminin-332 can reproduce RA current inhibition, suggesting an inhibitory role of laminin-332. Number on top of each histogram is number of recorded cells (*P<0.05; **P<0.01; Chi-square test). **C.** Latency and activation time constant for SA current expression is intact for cultured neurons on a laminin-332. SCC25 matrix slightly delays the activation time constant but the alteration does not reach significance (Mann Whitney U-test). **D.** SA current trace on a laminin-332 substrate.

Using sensory neurons cultured on purified rat laminin-332, I performed a series of experiments to examine the effects of laminin-332 on the mechanosensitive current and the gating kinetics. I recorded from sensory neurons of all sizes and mechanically stimulated neurites that had grown on a laminin-332 substrate. For sensory neurons grown on a laminin-332 substrate, there was a dramatic increase in the number of cells that displayed no response to the standard mechanical stimulation (Fig. 23B). Thus more than 33% of cells (18/54) showed no current response compared to 7.4% (4/54) on the control PLL/laminin substrate ($p<0.01$ Chi-square test). I then measured the gating kinetics of mechanically activated SA current and found that the latency for channel gating and the current activation time constant both remained intact in comparison with neurons on a laminin substrate (Mann Whitney U-test) (Fig. 23C, 23D & Table 5).

The electrophysiology results show that laminin-332 can reproduce the inhibitory effect on the mechanosensitive-RA current (Fi. 19A & Fig. 23B). However, unlike the keratinocyte-derived matrix, laminin-332 does not alter the gating properties of mechanosensitive-SA current expression (Fig. 19B, 19C, 23C, 23D & Table 5). I next hypothesized that if laminin-332 plays an important role in altering mechanically evoked current expression, then I must see a similar effect when I mechanically stimulate neurons cultured on matrix produced by SCC25, which secret a significant amount of laminin-332 (Patricia Rousselle 1995). Not surprisingly, I could confirm that on SCC25 matrix, the number of cultured sensory neurons having no current response to mechanical stimulation was significantly increased from 7.4% (4/54) on the control PLL/laminin substrate to 32% (8/25) ($p<0.05$ Chi-square test) (Fig 23B). In addition, like neurons on a

laminin-332 substrate, SCC25-derived matrix does not have the ability to modify latency for channel gating of mechanically activated SA current. However, SCC25-derived matrix slightly delays the SA current activation time constant, although the alteration does not reach statistical significance (Mann Whitney U-test) (Fig. 23C, 23D & Table 5). .

3.3.3 Laminin-332 is potent for mechanosensitivity modulation

I next asked how potent is laminin-332 inhibition of the RA current expression? To answer this question, I have designed a functional assay and have carried out a series of experiments by recording the mechanosensitivity of neurons cultured on a mixture of laminin/laminin-332 substrate with unaltered laminin concentration and a series of decreasing laminin-332 concentrations. The coating concentration of laminin is maintained at 20μg/ml as suggested by the product data sheet (see Materials). I used 1.33 μg/ml as the initial laminin-332 coating concentration as suggested by the product sheet (see Materials). I added laminin-332 to the control laminin (EHS-derived laminins) according to the above suggested working concentrations so the ratio of laminin/laminin-332 is 15/1. Interestingly, the number of neurons exhibiting the RA-type current was significantly reduced from 42% (23/54) on laminin to 11% (2/18) on laminin/laminin-332 mixture (laminin/laminin=15/1) (Fig. 24) ($p<0.01$ Chi-square test). Mechanically unresponsive neurons have dramatically increased from 7.4% (4/54) on laminin substrate to 38.8% (7/18) on the mixture of 1/15 laminin-332 with laminin substrate (Fig. 24) ($P<0.01$ Chi-square test). Thus this laminin/laminin-332

mixture substrate has the same potency on RA current reduction as does laminin-332 alone.

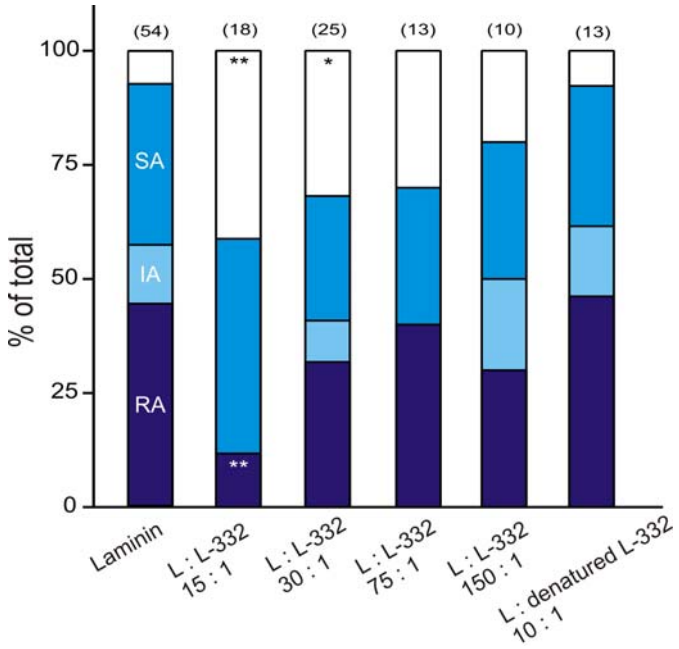

Figure 24. Functional assay: laminin-332 potently inhibits mechanosensitivity

Stacked histogram shows the proportion of different mechanically activated currents. Here I dilute laminin-332 concentration by gradiently decreasing Laminin-332 amount in laminin while laminin concentration remains unaltered. Result shows that laminin-332 takes effect at very low concentration. (Number on tope of each histogram denotes the number of recorded neurons. (*P<0.05; **P<0.01; Chi-square test)

I further depleted laminin-332 concentration in laminin/laminin-332 mixture to 30/1. In this group I could observe a significant increase of mechanically silent neurons to 40% (10/25) in contrast to only 7.4% (4/54) on laminin substrate (Fig. 24) (P<0.05; Chi-square test). I next depleted the laminin-332 concentration in the laminin/laminin-332 mixture to 75/1 and 150/1 level and tested the mechanosensitivity of sensory neurons. It is clear that the number of mechanically unresponsive neurons has increased from 7.4% (4/54) on the

control PLL/laminin substrate to 31% (4/13) on laminin/laminin-332=75/1 group and 30% (3/10) on laminin/laminin-332=150/1 group, although these groups were not significantly different probably due to the relatively small sample (Fig. 24) (Chi-square test). To test whether laminin-332 is necessary for suppressing mechanosensitivity, laminin-332 was boiled for 10 minutes to denature it and then mixed laminin. Strikingly, I found that the mechanosensitivity and proportion of different mechanically activated currents of neurons grown on laminin/denatured laminin-332 mixture is almost identical to neurons grown on laminin, suggesting that laminin-332 is necessary for inhibition mechanosensitivity of cultured sensory neurons (Fig 24).

3.3.4 Laminin-332 selectively inhibits RA current expression in both mechanoreceptors and nociceptors

I next asked how specific is laminin-332 mechanosensitivity suppression? From previous experiments, I noticed that when neurons were grown on a laminin-332 substrate or on a laminin/laminin-332 = 15/1 mixture substrate, that the increase of mechanically unresponsive neurons was coupled with the decrease of RA currents (Fig. 23B & Fig. 24). One question that arose was: does laminin-332 have an overall inhibitory effect on all cultured neurons or does it specifically inhibit mechanosensitivity of a sub-population of neurons in culture? It was previously described that putative mechanoreceptor usually have narrow AP spikes without humps and nociceptors usually have wide AP with humped AP spikes, in which the first derivative of each humped spikes (dV/dt) exhibits two

relative minima as compared to one minimum in mechanoreceptors (Fig. 8) (Koerber et al. 1988; Djouhri et al. 1998; Lawson 2002). Using this criterium, I could classify all recorded neurons into two groups: low-threshold mechanoreceptors and high-threshold nociceptors. I could then analyze the specificity of laminin-332 mechanosensitivity inhibition for each sub-group.

It was generalized from the data and confirmed that in the mechanoreceptors group, all mechanoreceptors respond to mechanical stimulation and nearly all (~80%; 15/19) mechanoreceptors possess RA currents on a laminin substrate (Fig. 25A). Laminin-332 substrate significantly reduces RA current expression to 36.8% (7/19) ($P<0.01$; Chi-sruare test) and dramatically increases the number of mechanically unresponsive neurons (21.1%; 4/19) in the mechanoreceptor group compared to a laminin substrate (Fig. 25A) ($P<0.01$; Chi-square test). I also observed a slight increase of of IA and SA current expression on laminin-332 although this was not significant. I then analyzed the mechanosensitivity of nociceptors on laminin-332 compared to laminin. It was found that laminin-332 selectively suppressed the RA current expression. Nociceptive RA current expression on laminin was significantly reduced from 27% (10/37) to only 4% (1/26) on a laminin-332 substrate ($P<0.01$ Chi-square test) (Fig. 25B). The reduction in the number of neurons with a RA current is coupled to a significant increase in the number of unresponsive neurons from 16.2% (6/37) on laminin substrate to 46.1% (12/16) on a laminin-332 substrate ($P<0.01$ Chi-square test) (Fig. 25B). It can be concluded from these results that laminin-332 selectively inhibits the RA current expression in both sensory neuron sub-types: mechanoreceptors and nociceptors.

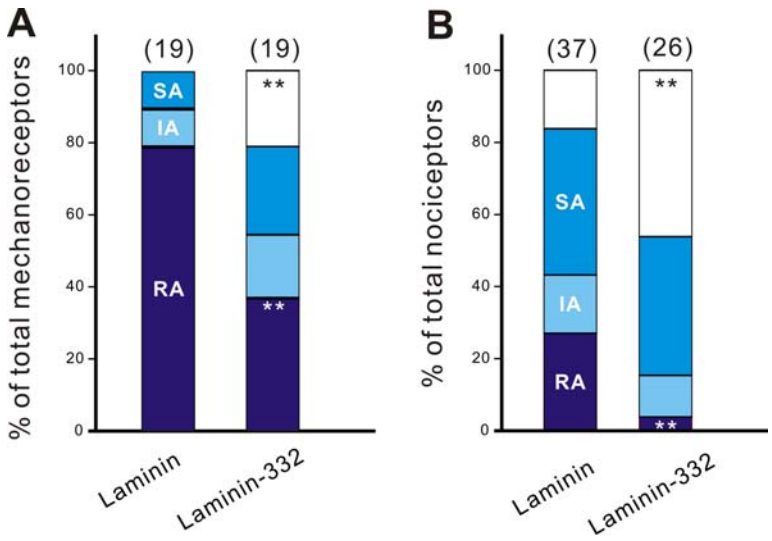

Figure 25. Laminin-332 has a mechanosensitivity inhibitory effect selectively on RA current expression. A. In mechanoreceptors group (neuron with narrow, non-humped AP spikes), RA current expression is significantly suppressed by a laminin-332 substrate as compared to laminin ($P<0.01$, Fisher's exact test). A slight increase of IA and SA current expression is also observed on laminin-332 substrate. **B.** In the nociceptor group (neurons with wide, humped AP spikes), RA current expression is significantly suppressed by a laminin-332 substrate as compared to laminin ($P<0.01$, Fisher's exact test).

3.3 Summary

Screening experiments were conducted to identify molecules that may lead to sensory neuron mechanosensitivity inhibition on keratinocytes matrix. It was hypothesized that if any molecule causes loss of mechanosensitivity on keratinocyte-derived matrix but not on fibroblast-derived matrix in comparison with neuron mechanosensitivity on laminin (ECM extract from Engelbreth-Holm-Swarm sarcoma), then it must be expressed by keratinocytes but not by fibroblasts and should be absent in laminin. The molecular composition of ECM proteins from laminin, fibroblast, and keratinocytes groups were analyzed. The

results showed that laminin-332 is exclusively expressed by keratinocytes in contrast to laminin and fibroblasts. I next obtained purified rat laminin-332 and then cultured neurons on a laminin-332 substrate. These data show that laminin-332 can potently reproduce the inhibitory effect of keratinocytes selectively on mechanically evoked RA current expression but not on mechanically evoked SA current. Further analysis shows that laminin-332 selectively inhibits the RA current expression but its inhibition is not selective for neuron subtypes, ie. low-threshold mechanoreceptors and high-threshold nociceptors.

3.4 Characterization of laminin-332 mechanosensitivity modulation

3.4.1 Mechanosensitivity modulation is not attributable to the absence of putative mechanoreceptors or nociceptors

What is the cause of laminin-332 inhibition of mechanosensitivity? To answer this question, I performed a series of experiments to characterize the laminin-332 inhibition mechanism. The previous biophysical data suggested that laminin-332 selectively inhibits the RA current expression in both mechanoreceptors and nociceptors (Fig. 25). Thus I could make a null hypothesis that if laminin-332 selectively inhibits RA current expression but not a neuron subtype expression, I must not see an alteration in the proportion of mechanoreceptors or nociceptors in total cultured sensory neurons. To address this hypothesis, I obtained antibodies against neurofilament-200 (nf200 Ab) and transient receptor potential channel, subfamily V type 1 (TRPV1 Ab; also known as capsaicin receptor or vanilloid receptor 1) and used them to label putative myelinated A-fibers and C-fiber nociceptors respectively and then conducted an immunocytochemistry experiment (see Materials). Neurofilament is an intermediate filament that represent the most abundant cytoskeletal element in large, myelinated axons, making it an ideal marker for putative mechanoreceptors (Ohara O 1993; Draberova et al. 1999; Kumar et al. 2002). TRPV1 is used as a marker for a subtype nociceptors because it is expressed on a subset of peptidergic nociceptors (Jasmin and Ohara 2004). Using fluorescence microscopy, I could observe neurons which were either nf200-positive or TRPV1-positive. There were

also some neurons expressing both nf200 and TRPV1, suggesting that these might be A-fiber nociceptors and a small neuron population that are negative in both nf200 and TRPV1 expression. From the immunocytochemistry micrograph, I could see that laminin and laminin-332 both support robust neurite outgrowth of putative mechanoreceptors (nf200-positive) and nociceptors (TRPV1-positive) in culture and the neurite branching of putative mechanoreceptors on laminin-332 substrate is morphologically similar to those grown on laminin (Fig. 26A & Fig. 26B). In addition, the immunocytochemistry micrograph shows that the arborization of both nf200-positive and TRPV1-positive neurons is qualitatively similar on the laminin and laminin-332 substrate.

I then quantified the immunocytochemistry data and calculated the proportion of nf200-positive neurons (putative mechanoreceptors) and TRPV1-positive neurons (putative nociceptors) in total cultured neurons on laminin or laminin-332 substrate. It was found that among all observed cultured neurons on laminin substrate, 51.8% (71/137) were nf200-positive and on laminin-332 substrate, nf200-positive neurons accounted for 48.7% (60/123) of all cultured neurons, which is almost identical to the laminin substrate (Fisher's exact test) (Fig. 26C). It was also found that among total neurons in culture, 38.6% (53/137) were TRPV1-positive on laminin and on laminin-332 substrate, TRPV1-positive neurons accounted for 42.2% (53/123) of all cultured neurons, which is almost identical to the laminin substrate (Fisher's exact test) (Fig. 26D). These data showed that laminin-332 substrate did not change the proportion of putative mechanoreceptors or nociceptors in culture. The immunocytochemistry results

could confirm the biophysical data that laminin-332 does not selectively support the survival of mechanoreceptive or nociceptive neuron subtypes (Fig. 25 & 26).

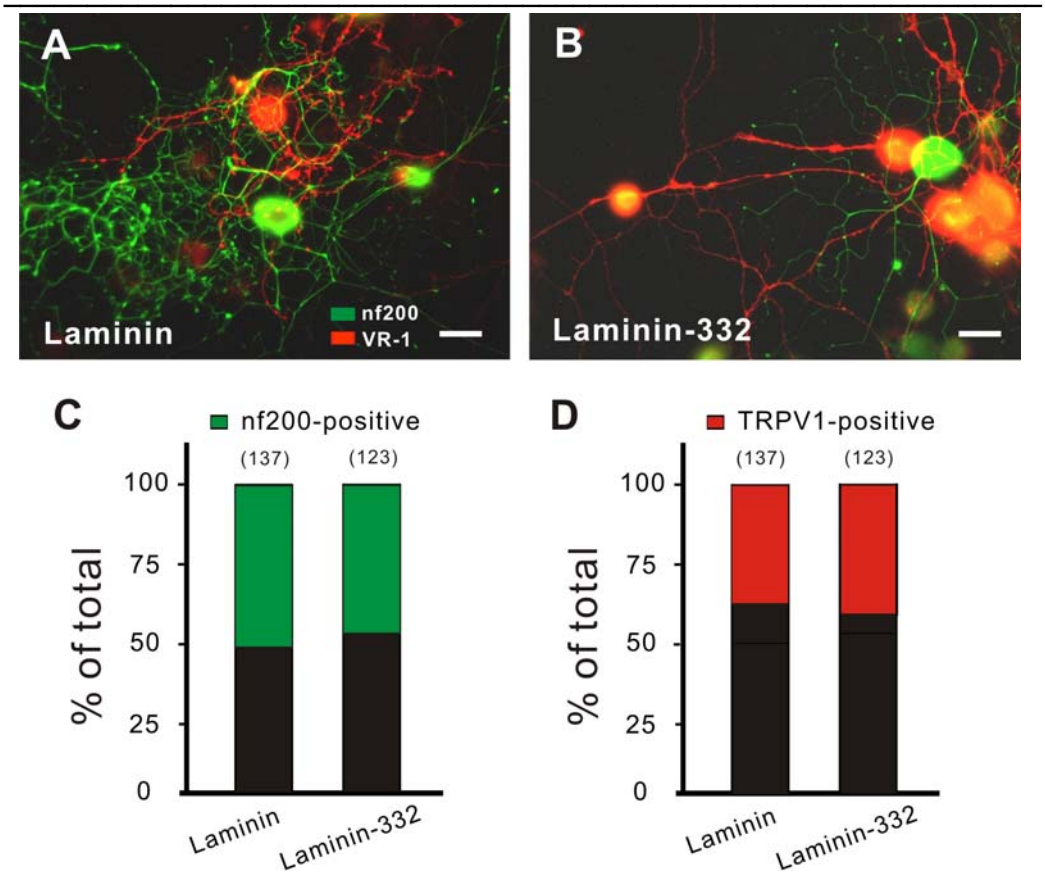

Figure 26. Immunostaining micrograph of sensory neurons cultured on laminin or laminin-332 substrate. A. B. Immunostaining micrograph of sensory neurons cultured on laminin and laminin-332. Antibodies were used to localize nerofilament (nf200; marker for putative A-fiber mechanoreceptors) and vanilloid receptor1 (TRPV1; marker for a subtype of nociceptors), which were labeled green and red respectively. I could see that laminin and laminin-332 both supported robust neurite outgrowth for mechanoreceptors and nociceptors in culture and the neurite branching of putative A-fiber neurons cultured on laminin-332 substrate looks identical to those grown on laminin substrate. Scale bar is 20μm. **C. D.** Proportion of nf200-positive neurons (putative mechanoreceptors) and TRPV1-positive (putative nociceptors) was quantified. Data showed that each neuron subtype was not altered on laminin-332 in comparison to laminin.The number of recorded neurons is indicated at the top of each stacked histogram (Fisher's exact test).

3.4.2 An extracellular tether required for mechanosensitive channel gating is absent on a laminin-332 substrate

I next asked whether laminin-332 is inhibitory for the extracellular tether, that is required for mechanically activated RA-type current? To answer this question, I cultured neurons on laminin-332 and carried out a detailed TEM study on the ultrastructure of the interface between cultured sensory neurite and the underlying laminin-332 substrate. I fixed and stained the culture on laminin-332 using the method optimized to enhance the electron density of extracellular structure as previously described (see Methods). Ultrathin micrographs were randomly photographed and observed using TEM (Fig. 27 A, B, C, D).

I then made a quantitative TEM analysis comparing electron dense attachments between the neurite membrane and the laminin-332 substrate. I quantified this data by randomly photographing microscopic fields in 116 ultrathin sections (thickness 50nm) from 3 cultures. The total area of measured membrane contact was 9.2 μm^2 (Table 4). The longest connecting objects were similar in length (~100nm) and shape to those observed in TEM of sensory neuron on laminin, however the longest protein tethers were rarely observed on laminin-332 substrate. The length of each object was then randomly plotted in a 2-dimensional space (Fig. 27e). It is clear from this representation of the raw data that links with a length of between 5 and 75 nm were largely unaffected on laminin-332. However, electron dense objects >75 nm in length, presumably corresponding to protein filaments required for RA current expression are significantly reduced in presence of laminin-332 (Table 4) (unpaired t-test). Thus

it could be concluded from the TEM data that the laminin-332 inhibition of mechanosensitivity is due to the absence of an extracellular protein filament required for the gating of RA mechanosensitive current.

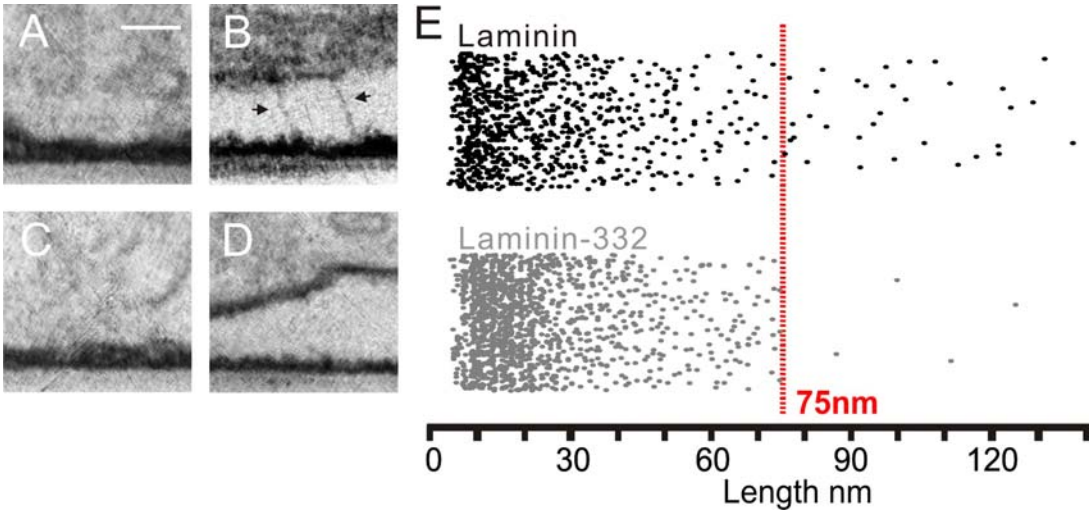

Figure 27. TEM shows that laminin-332 is inhibibitory for a protein filament necessary for RA current A.B. Sample electron micrographs of the neurite/matrix interface in control **C.D.** sample electronmicrographs from neurons grown on laminin-332 substrate where no long tethers were observed. **E.** Quantification of the electron dense attachments in many sections from neurons cultured on laminin and on laminin-332. The length of each measured attachment is plotted in random 2D space to illustrate the range of attachment lengths observed. Each dot represents for measured length of each linking object. Note absence of long tether like proteins greater than 75 nm on laminin-332. Means are shown ± s.e.m. Scale bar is 100 nm.

It could be concluded from above data that laminin-332 is likely to inhibit the RA current expression by suppressing an extracellular protein tether required for mechanosensitivity. One question arises: does laminin-332 inhibit the systemic expression profile of the tether required for mechanosensitivity as a signaling factor or does laminin-332 locally abolish assembly of the tether binding to the

ECM? A novel microcontact printing technique was introduced and developed to address this question.

	Total Measured Area	Density of attachments <75nm ($1/\mu m^2$)	Density of attachments >75nm ($1/\mu m^2$)	Average distance of attachment <75nm(nm)	Average distance of attachment >75nm(nm)
Laminin (n=4)	7.5 μm^2	150.3 ± 7.0 (N=1030)	4.9 ± 1.3 (N=31)	22.6 ± 0.5 (N=1030)	100.0 ± 3.1 (N=31)
Laminin-332 (n=3)	9.2 μm^2	151.9 ± 5.1 (N=1372)	0.4 ± 0.2** (N=4)	21.3 ± 0.4 (N=1372)	99.4 ± 8.7 (N=4)

Table 4. Quantification of TEM data on a laminin-332 substrate

Data shows results from control experiments (prep=4) and from experiments where neurons were cultured on laminin-332 (prep=3). The total measured area is summed up. Density and average distance of short and long links respectively are calculated. No significant differences in density of short attachments were noted between control neurons and laminin-332 groups. However, the long links are significantly decreased on laminin-332. The average distances of short and long links are conserved across different experiments. N=number of identified attachments (**P<0.01 Unpaired t-test).

3.4.3 Laminin-332 locally modulates mechanosensitivity

I proposed two models to account for absence of the tether on a laminin-332 substrate (Fig. 28 & Fig. 29). In the first model, laminin-332 acts as a signaling factor and after sensory neurons have received a signal through activation of integrin receptors such as integrin $\alpha_3\beta_1$ and $\alpha_6\beta_4$, a downstream signaling cascade is activated, which in turn leads to a global suppression of tether expression. In this case, laminin-332 acts globally and has inhibitory effect on the tether expression.

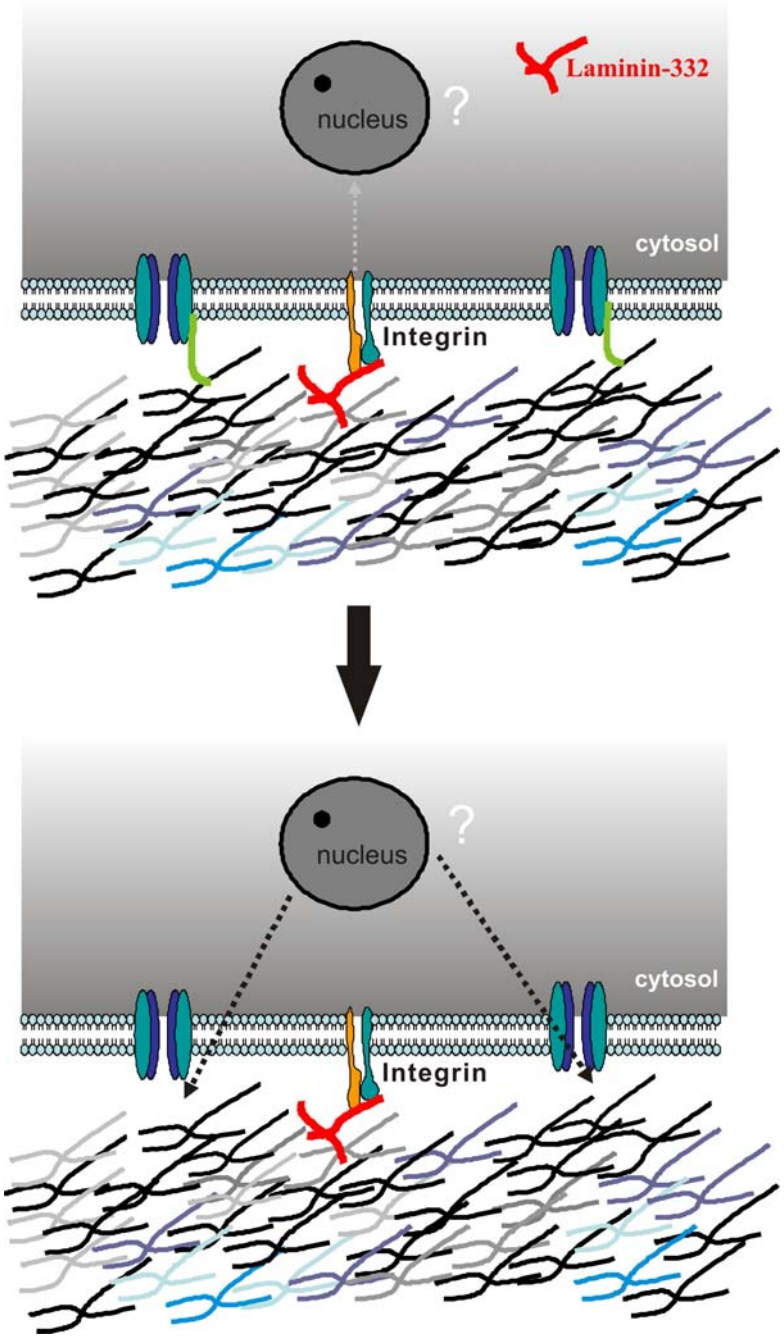

Figure 28. Model 1: laminin-332 as a signaling factor, which globally inhibits tether expression In this case, laminin-332 acts as a signaling factor and after sensory neurons have received its signal through the integrin receptors on membrane surface, a downstream signaling cascade is activated, which eventually leads to a global suppression for the tether expression profile. Laminin-332 acts globally and takes effect on the whole cell.

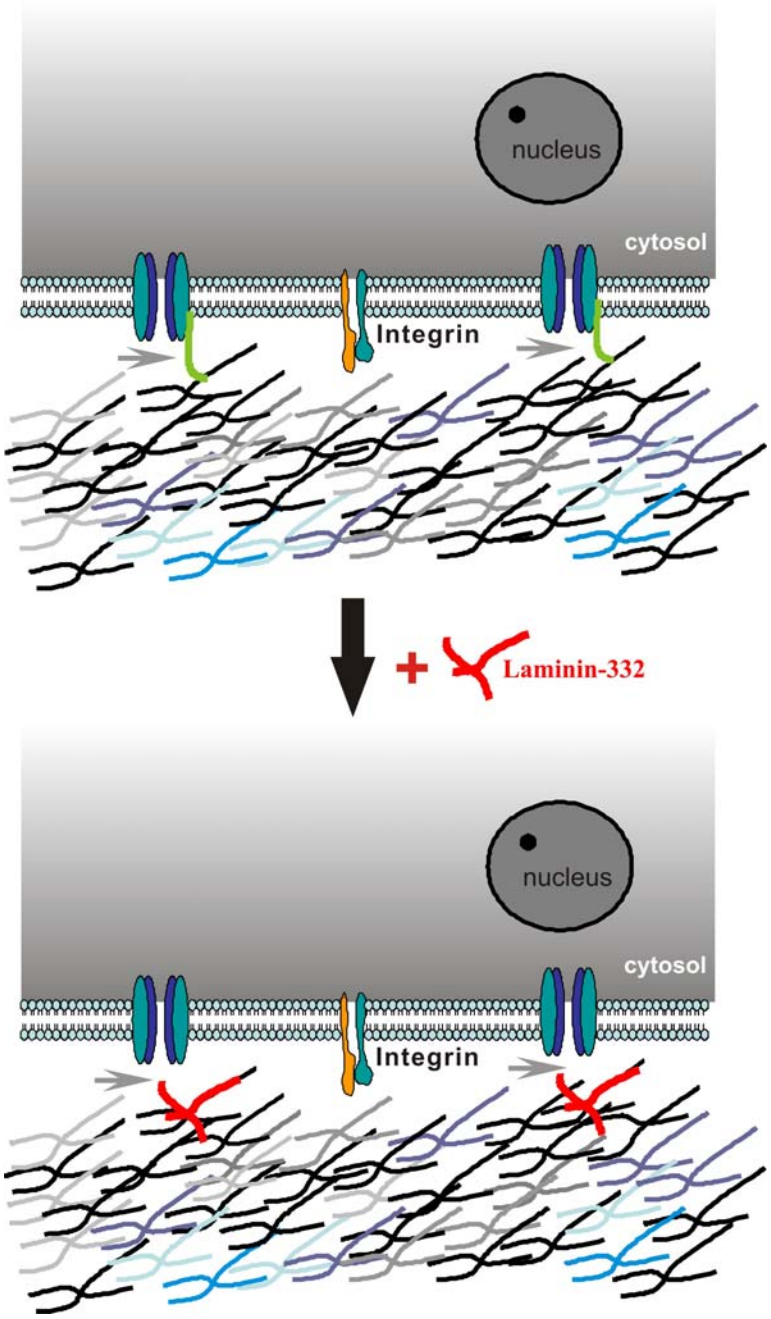

Figure 29. Model 2: laminin-332 as a local inhibitory factor for tether binding

In this case, laminin-332 acts as an inhibitory factor by locally covering the binding site of the extracellular protein filament, which eventually prevents the tether from binding to its ECM partner. Mechanosensitivity inhibition takes place locally where sensory neurite has contact with the ECM substrate. Integrin-mediated cascade is not involved.

In the second model, laminin-332 acts as an inhibitory factor by locally competing with laminin proteins for the binding site of the extracellular protein filament, which eventually prevents the tether from binding to its binding partner: laminin-111 (supplementary paper; Hu, Chiang et al 2009). In this case, mechanosensitivity inhibition only takes place locally where sensory neurite has contact with laminin-332 substrate. To test the plausibility of the above two scenarios, a unique technique was introduced to physically guide axon growth on specific patterns(von Philipsborn et al. 2006). This technique was modified and optimized for testing the plausibility of the proposed models (see Methods). Using this technique, I could prepare coverslips with different laminin stripes and guide neurite outgrowth of cultured neurons. To prepare coverslips with striped laminin substrates, I first covered the microcontact printing stamps, which were made of an elastomer PDMS with laminin proteins in presence of fluorescence dyes such as Alexa 488 or Alexa 555 as markers for subsequent microscopic observation. After incubation, stamps were rinsed and dried then placed onto a glass coverslip for printing. After this step, laminin proteins on PDMS stamps were transferred onto coverslips. Previously described steps were repeated and proteins labelled with a different fluorescence dye were then printed in next step perpendicularly to the previously stamped stripes then the coverslips with cross-patterned substrates were ready for use (Fig. 30). Each coverslip with cross-patterned substrates allowed guided neurite outgrowth on different substrates along with the examination of the impact of different substrates on mechanosensitivity as well as on morphology of neurites which derive from same soma.

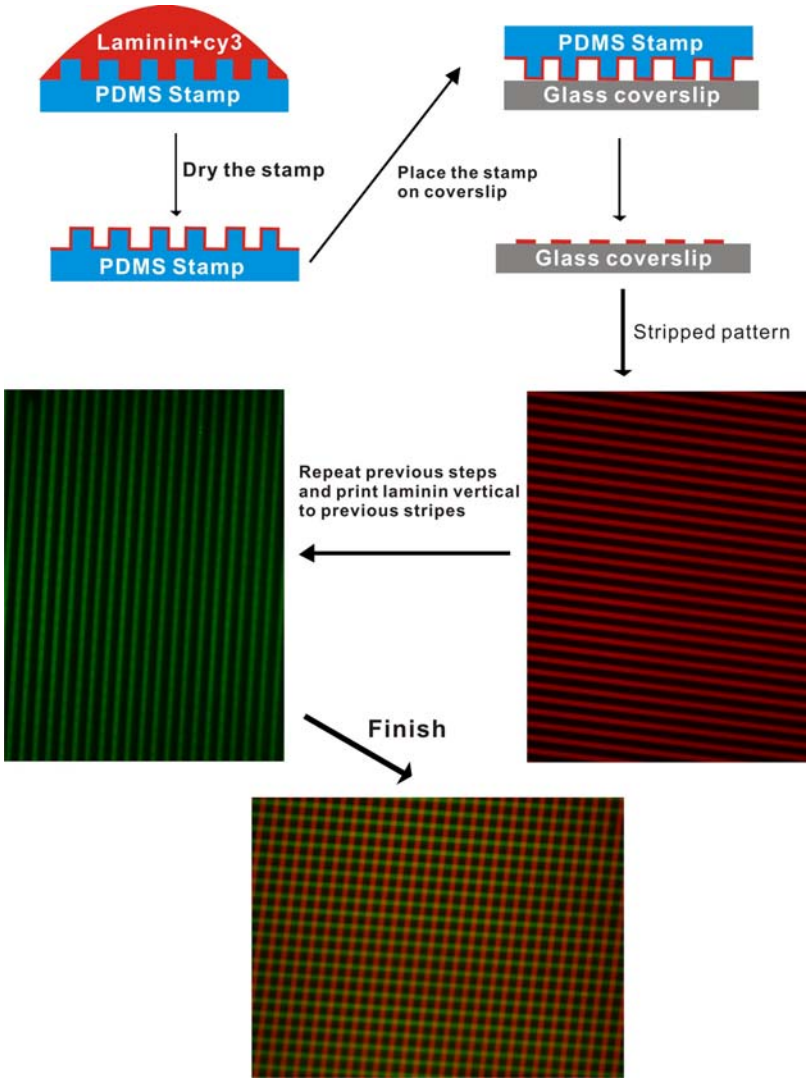

Figure 30. Schematic diagram of microcontact printing technique to generate striped laminin patterns. Laminin was incubated with a PDMS stamp in the presence of a fluorescence dye as marker for observation. After incubation, the PDMS stamp was dried and placed on coverslips then laminin stripes were printed onto the coverslip. To prepare cross-patterned laminin, previous steps were repeated and laminin was printed vertically to previous stripes.

To test the feasibility of the proposed two models, I obtained PDMS stamps with a 25 μm gap between adjacent stripes and carried out a series of experiments to characterize laminin-332 inhibition mechanism. I manually cross printed stripes of laminin and laminin-332, which were labeled with different fluorescence dyes

(Alexa 488; Alexa 555) onto glass coverslips (Fig. 31A). A 25 μm gap is wide enough to avoid signal interference from other stripes and good for discreet mechanical stimulation. I subsequently cultured neurons on the pattern. After 24 hours, I observed that patterned laminin proteins indeed guided neurite outgrowth (Fig. 31B). In most cases the neurons were loaded with lucifer yellow delivered through the patch pipette so that neurites belonging to the recorded neuron could be unequivocally identified (Fig. 31C).

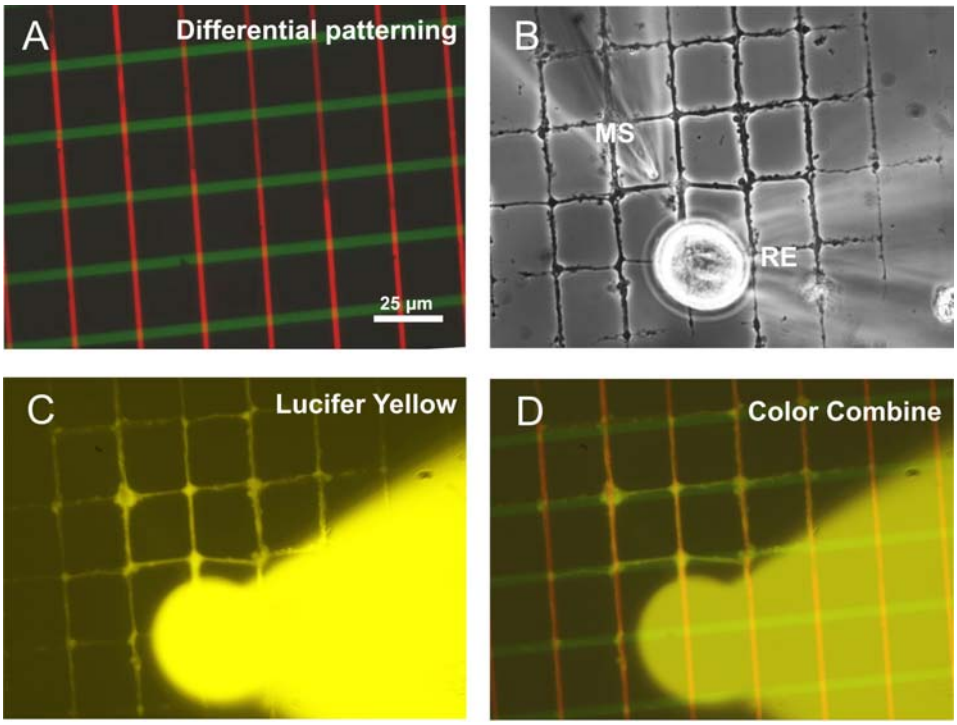

Figure 31. Microcontact printing experiments - a good tool to verify signaling model.
A. Two distinctive laminin proteins, respectively labeled with different color (green-cy2; red-cy3) were deliberately stamped on colorslip. Stripe gap is 25 μm. **B.** Light micrograph shows that neurite outgrowth is guided by protein patterns. Stripe gap is wide enough to allow discreet mechanical stimulation. **C.** Lucifer yellow shows that neurites belonging to the same soma. **D.** Color combine of **A** and **C**, showing neurite growth does not exceed protein stripes.

Neurite processes grew only on laminin substrates and did not exceed the boundaries of stripes that can be tracked by labeled fluorescence dyes (Fig.

31D). I next stamped cross-patterned protein stripes with distinct laminin proteins on the coverslips to examine whether mechanosensitivity or growth morphology of sensory neurites is dependent on the protein substrate in contact with it. In laminin vs. laminin group, the neurite outgrowth is basically identical on both stripes directions. However, in laminin vs. laminin-332 group I found that amongst all observed cultured neurons of various soma sizes, neurites growth/thickness on a laminin-332 substrate originating from one soma was altered by the laminin-332 substrate while the neurite morphology on laminin remained identical to those in laminin vs. laminin group (Fig. 32).

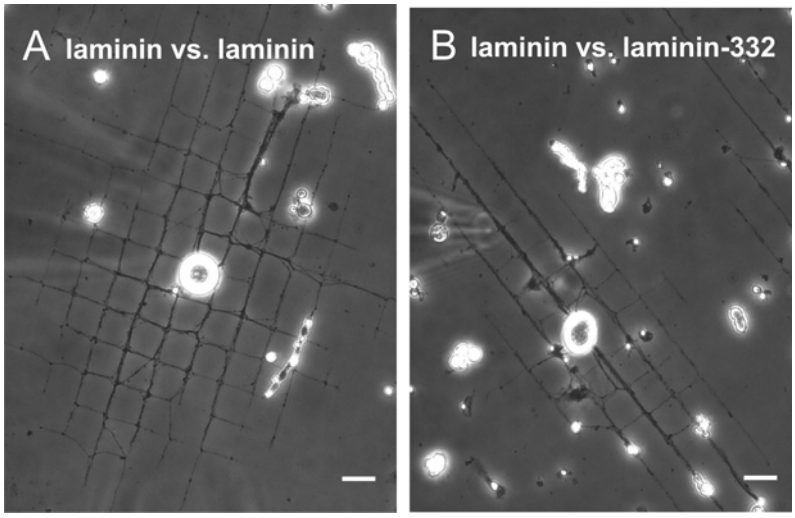

Figure 32. Laminin-332 locally altered neurite growth/thickness. A. In laminin vs. laminin group, neurite growth on both patterned laminin substrate, regardless of being labeled with green and red respectively is basically identical to each other. **B.** In laminin vs. laminin-332, laminin-332 significantly alters neurite growth. Neurite on laminin-332 looks thinner. Scale bar is 25 μm.

I then made a quantitative analysis comparing neurite thickness on two stripe directions which derived from one soma in each group. I quantified this data by randomly measuring the neurite thickness in 120 sections from at least 30 cells in

each group. In laminin vs. laminin group, the neurite thickness is 1.09±0.08 μm and 1.13±0.05 μm, respectively on each direction. In laminin vs. laminin-332 group, the neurite thickness on laminin is 1.11±0.07 μm, almost identical to those in laminin vs. laminin group. However, the neurite thickness on laminin-332 is significantly reduced to 0.52±0.05 μm (P<0.001, Unpaired t-test), suggesting that laminin-332 locally inhibits the neurite growth/thickness in contrast to neurite on laminin originating from same soma (Fig. 33A).

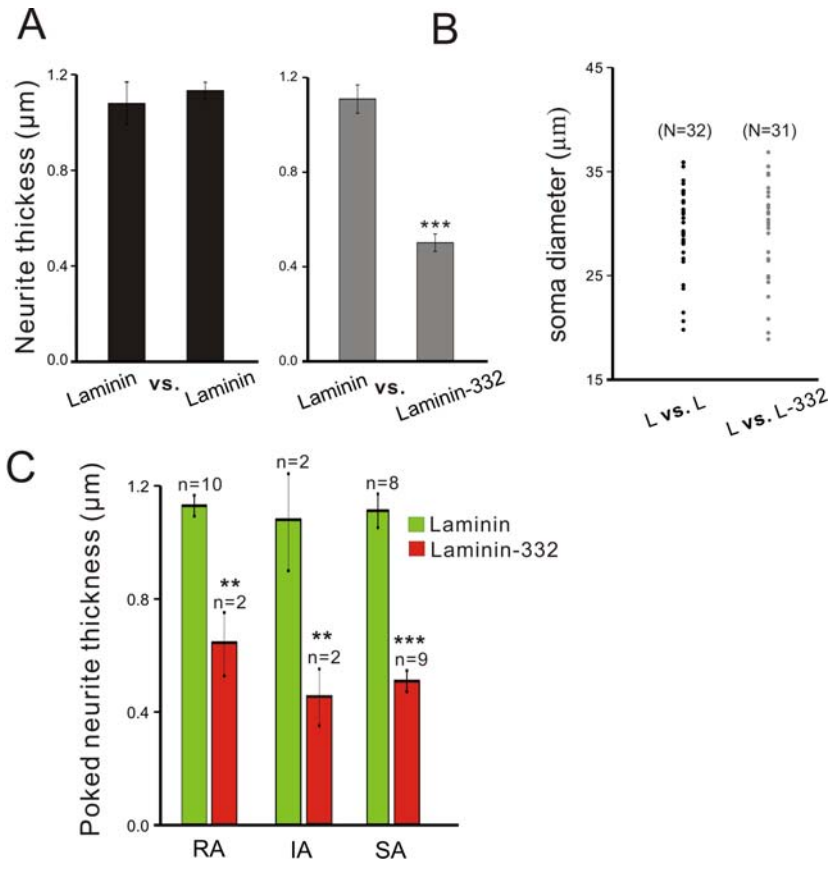

Figure 33. Quantification of laminin-332 local inhibition of neurite outgrowth. A. In laminin vs. laminin group, the neurite thickness is 1.09±0.08 μm and 1.13±0.05 μm, respectively on each direction. In laminin vs. laminin-332 group, the neurite thickness on laminin is 1.11±0.07. Laminin-332 significantly reduces neurite thickness to 0.52±0.05 (P<0.001, Unpaired t-test). **B.** In L vs. L-332 group, neurons of all sizes are ubiquitously affected by a laminin-332 substrate in terms of neurite morphology (growth/thickness). **C.** Thick neurites are not necessary for evoking mechanically activated currents (**P<0.01;***P<0.001; unpaired t-test).

It was observed that in the laminin vs. laminin-332 group, the laminin-332 substrate locally inhibits neurite growth/thickness of all observed neurons of all sizes with no exception, suggesting a ubiquitous effect of laminin-332 on neurite morphology (Fig. 33B). I then asked whether a thick neurite is necessary for evoking mechanically activated currents. Thus I quantified the thickness of mechanically stimulated neurites that evoked RA, IA and SA type currents respectively and found that all three types of mechanically activated currents are evoked from neurites with dramatically reduced thickness on the laminin-332 stripes, suggesting that thick neurites are not necessary for evoking mechanically activated currents (Fig. 33C). In the laminin vs. laminin-332 group, neurite growth/thickness on the laminin stripes was identical to neurite morphology on either laminin stripes in laminin vs. laminin group, suggesting that presence of laminin-332 in laminin vs. laminin-332 group did not inhibit the morphology of neurite originating from same soma on the laminin substrate. From the above morphological observations, I could conclude that laminin-332 has the ability to locally alter the neurite growth/thickness, making it thinner in contrast to laminin.

I next asked whether laminin-332 has a local inhibitory effect on mechanosensitivity? To answer this question, I made recording from sensory neurons grown on patterned stripes and examined the mechanosensitivity of neurites on different substrates. In laminin vs laminin group, neurons with neurite outgrowth on both stripe directions were recorded. Stripes could be tracked by labeled colors green and red. The results showed that in laminin vs. laminin group, the mechanosensitivity of neurites on one direction of laminin substrate is identical to the other direction, which was labeled with a different fluorescence

dye, suggesting that different fluorescence dyes for labeling laminin protein stripes did not alter the mechanosensitivity of neurites which grew on it. Interestingly, in the laminin vs. laminin group, most neurons responded to mechanical stimulation of the neurites growing on either direction of laminin stripes. However, in the laminin vs. laminin-332 group, some cells which responded to mechanical stimulation of neurites on laminin stripe did not respond to mechanical stimulation of neurites on the laminin-332 substrate, suggesting that mechanically activated current was locally inhibited by laminin-332 in contrast to laminin substrate in the other direction (Fig. 34).

Figure 34. Laminin-332 substrate locally inhibits expression of mechanosensitive RA-type current. In some cells, neurites on laminin stripe respond to mechanical stimuli while neurite on laminin-332 stripe does not.

Quantitative analysis showed that in the laminin vs. laminin group, among all 32 recorded neurons, RA currents accounted for 43.8% (14/32) of all recorded neurons on the Alexa 488-labeled laminin stripes; 15.6% (5/32) had IA currents; 28.1% (9/32) had SA currents and only 12.5% (4/32) had no response to

mechanical displacement. On the Alexa 555-labeled laminin stripes, RA current accounted for 43.8% (14/32) of all recorded neurons; 12.8% (4/32) had IA currents; 31.3% (10/32) had SA currents and only 12.5% (4/32) had no response to mechanical displacement (Fig. 35A). Stacked histogram of laminin vs. laminin group showed that the mechanosensitivity was not altered by different fluorescence dyes. The proportion of mechanosensitive currents of neurites on the laminin stripes is almost identical to neurites on a globally coated laminin substrate on a coverslip (Fig. 7 & 35).

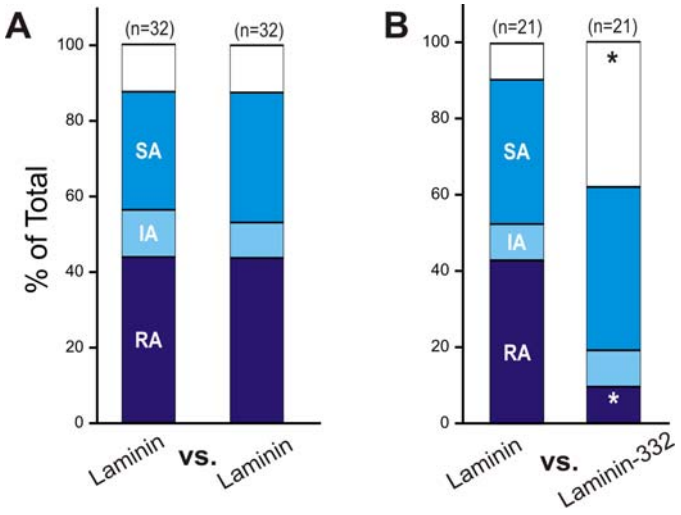

Figure 35. Quantification of mechanosensitivity on patterned laminin vs. laminin-332 substrate. A. Stacked histogram of the laminin vs. laminin group shows that, the mechano-sensitivity was not altered by laminin labeled with different secondary antibody cy2 and cy3 in comparison with laminin global coating on coverslip. **B.** Stacked histogram of the laminin vs. laminin-332 group shows that, the RA current expression was significantly altered by laminin-332. NThe number of recorded neurons is indicated at top of histograms. (*P<0.05, Chi-square test)

I next examined and quantified the mechanosensitivity of neurites on the laminin vs. laminin-332 stripes, 21 neurons with neurite outgrowth on both stripe

directions were recorded. On laminin stripes, RA currents accounted for 42.8% (9/21) of all recorded neurons; 9.5% (2/21) had IA currents; 38.1% (8/21) had SA currents and only 9.6% (2/21) had no response to mechanical displacement. On laminin-332 stripes, RA current expression was significantly reduced to 9.5% (2/21) of all recorded neurons; 9.5% (2/21) had IA-type current; 42.9% (9/21) had SA currents and mechanically unresponsive neurons had significantly increased to 38.1% (8/21) (Fig. 35B) ($P<0.05$, Chi-square test). These data suggested that laminin-332 substrate locally inhibited mechanically activated RA current conductance of sensory neurite in contact with a laminin-332 substrate as opposed to neurite derived from same soma on a laminin substrate.

3.4.4 Laminin-332 does not act through an integrin-mediated pathway

I next carried out a series of biochemical and biophysical experiments to determine whether an integrin-activated singnaling cascade is involved in laminin-332 inhibition of mechanosensitive RA current conductance. Laminin-332 plays an important role in cell adhesion, metastasis, signal transduction and keratinocytes differentiation through anchorage mediated by integrin receptors $\alpha_3\beta_1$ and $\alpha_6\beta_4$ to the α_3 domain of laminin-332 (Xia 1996; Aumailley et al. 2003; Tsuruta et al. 2003; Kariya and Miyazaki 2004; Kunneken et al. 2004). During the course of this study, I obtained a monoclonal antibody CM6 (#sc-32794 L, Santa Cruz Biotechnology, Ltd.) and a monoclonal antibody BM2 (also termed BM165, provided by Manuel Koch), which localizes to the globular or integrin-binding G-domain of rat laminin-332 and human laminin-332 heterodimers respectively.

The CM6 and BM2 antibodies were used to block integrin-mediated interaction of rat laminin-332 (Cate et al. 1995; Baker et al. 1996; Falk-Marzillier et al. 1998) and human laminin-332 (Zhang and Randall 1996; Lotz et al. 1997) respectively. I could confirm that integrin-mediated adhesion was completely blocked by the CM6 antibody on rat laminin-332 substrate and neurons did not attach to rat laminin-332 substrate in the event when laminin-332 was pre-incubated with the CM6 antibody (Fig. 36A upper panel). However, the BM2 antibody (against integrin binding of human laminin-332) did not block neurite outgrowth on the rat laminin-332 susbtrate as expected due to species specificity (data not shown). I then incubated rat laminin-332 and the CM6 antibody in presence of laminin and cultivated neurons on this substrate to see if neuron attachment and neurite outgrowth was recovered in the presence of laminin. After 24 hours it was observed that neurons attached well and normal neurite outgrowth was present (Fig. 36A lower panel). I next examined the mechanically activated currents of cells cultured on mixture of laminin and laminin-332, which was pre-incubated with the CM6 antibody. Interestingly, it was found that CM6 does not rescue laminin-332 inhibition of the RA mechanosensitive current. Mechanically unresponsive neurons were significantly increased from 7.4% (4/54) on laminin to 25.9% (7/27) on laminin+laminin-332 substrate in presence of the CM6 antibody ($P<0.05$, Chi-square test). Mechanically activated RA currents were significantly reduced from 42% (23/54) on laminin to 18.5% (5/27) on laminin+laminin-332 substrate in presence of the CM6 antibody (Fig. 36B) ($P<0.05$, Chi-square test). It could be concluded from the CM6 antibody experiments that laminin-332 inhibition for mechanosensitivity was not rescued by blocking laminin-332

integrin-binding domain, suggesting that integrin-mediated signaling cascade is not involved in the mechanism for inhibition of the RA current expression.

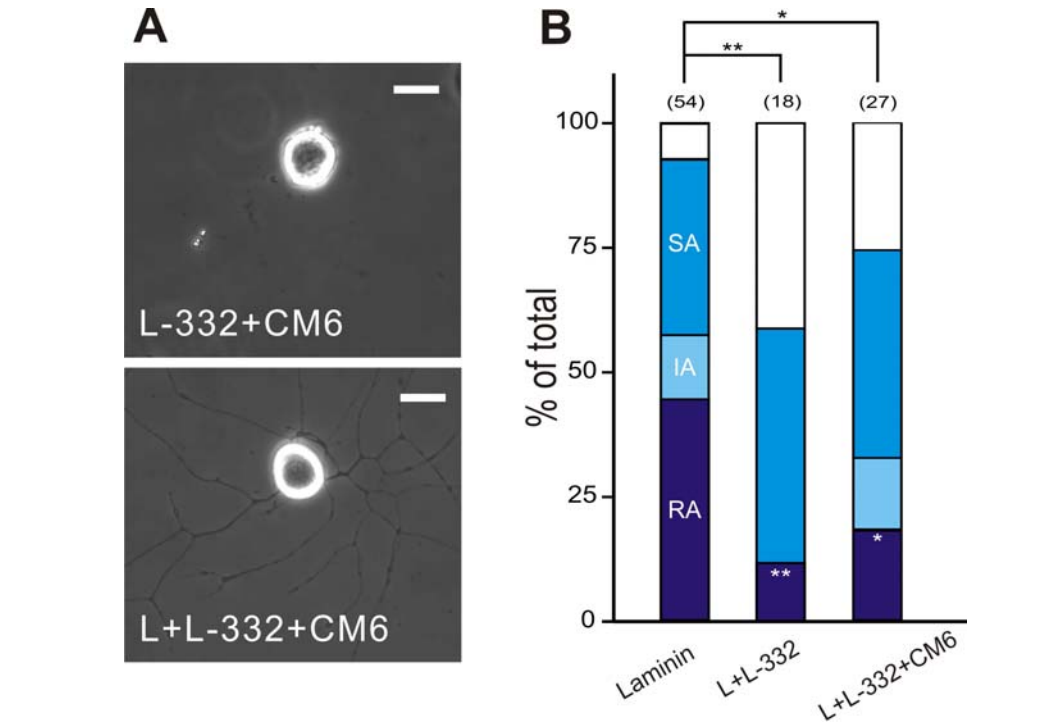

Figure 36. CM6 (antibody which blocks integrin binding of laminin-332) does not rescue laminin-332 inhibition of RA current expression.

A. In upper panel, neurite outgrowth induced by integrin binding was totally blocked by the CM6 antibody on the laminin-332 substrate. In lower panel, normal neurite outgrowth was observed on mixture of laminin, laminin-332 and the CM6 antibody. **B.** Mechanosensitivity of neurons on laminin+laminin-332 was not rescued by the CM6 antibody (*P<0.05, **P<0.01, Chi square test). Scale bar is 20 μm.

I also used the CM6 antibody to ask whether laminin-332 inhibition of neurite growth/thickness was attributable to integrin receptor binding. Neurons were cultivated on cross pattern stripes, which in one direction was laminin and in the other direction was laminin+laminin-332. After 24 hours, I could observe that neurite outgrowth was indeed guided by patterned laminin protein. However, neurite outgrowth from the same neuron was distinctly different on

laminin+laminin-332 compared to the control laminin substrate. I observed that neurite branching off from the same neuron was altered by the laminin-332 substrate even in presence of laminin (Fig. 37A). I next added the CM6 antibody to the mixture of laminin/laminin-332 on the converslip to examine whether laminin332-induced alteration of neurite branching and thickness could be rescued. The results showed that CM6 did not rescue neurite morphology to the laminin state. Neurite outgrowth on laminin+laminin-332 substrate was still distinctly different in presence of CM6, suggesting that the influence of laminin-332 on neurite growth/thickness is not regulated through the integrin-mediated pathway (Fig. 37B).

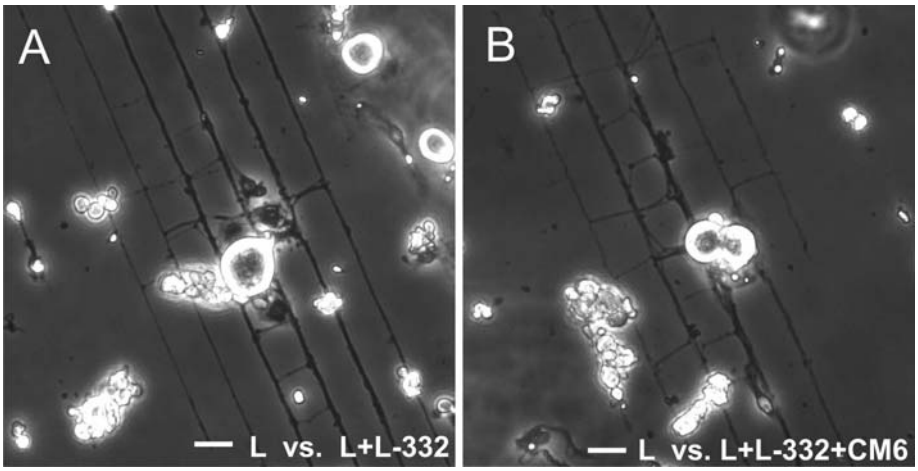

Figure 37. CM6 (antibody which blocks integrin binding to laminin-332) does not rescue laminin-332 inhibition of the neurite outgrowth A. Neurite outgrowth on laminin+laminin-332 was distinguishably altered. **B.** L+Laminin substrate still altered neurite morphology in presence of CM6, suggesting that CM6 did not rescue laminin-332 inhibition of neurite outgrowth. Scale bar is 25 μm.

Previous experimental results suggest that secreted soluble factors from cultured keratinocytes cannot by themselves negatively modulate mechanically gated currents in cultured sensory neurons as does the keratinocytes substrate or the

keratinocyte-derived matrix substrate. This prompted us to ask whether soluble laminin-332 could inhibit RA current expression similarly to a laminin-332 substrate. To answer this question, recordings were made from sensory neurons cultured in a medium containing soluble laminin-332 at the same concentration as used for coating. It was found that mechanically stimulated neurites displayed mechanically evoked currents that were essentially indistinguishable from those found on laminin (Fig. 38A) (n=21; Chi-square teat), suggesting that laminin-332 in a soluble form does not by itself reproduce laminin-332 inhibition of RA type current expression. From the CM6 antibody experiments, it is shown that the α-chain of laminin-332, which contains the integrin-binding G domain is not involved in laminin-332 inhibition. I next asked whether the other two subunits of laminin-332, e.g. β_3 domain or γ_2 domain contribute to mechanosensitivity modulation of laminin-332. To address this question, I carried out experiments to examine whether mixtures of laminin with either β_3 or γ_2 domain could alter sensory mechanotransduction of neurites in culture. These two short arm laminins (β_3: NM_001127641; AA: 18 - 576 and γ_2: BC113378; AA: 22 - 631) were amplified by PCR and subcloned into a modified episomal expression vector. The expression vectors were transfected into 293-EBNA cells and selected clones with the highest protein expression were expanded for large scale production. The purification of the secreted proteins was performed as previously described (Gara et al. 2008). Sensory neurons were cultured on laminin+β_3 domain substrate and neurites grown on the substrate were mechanically stimulated. In contrast to the laminin+laminin-332 substrate, which significantly inhibits neurite mechanosensitivity, no mechanosensitivity alteration of neurites was observed on a laminin+β_3 substrate (n=18; Chi-square test) (Fig. 38A).

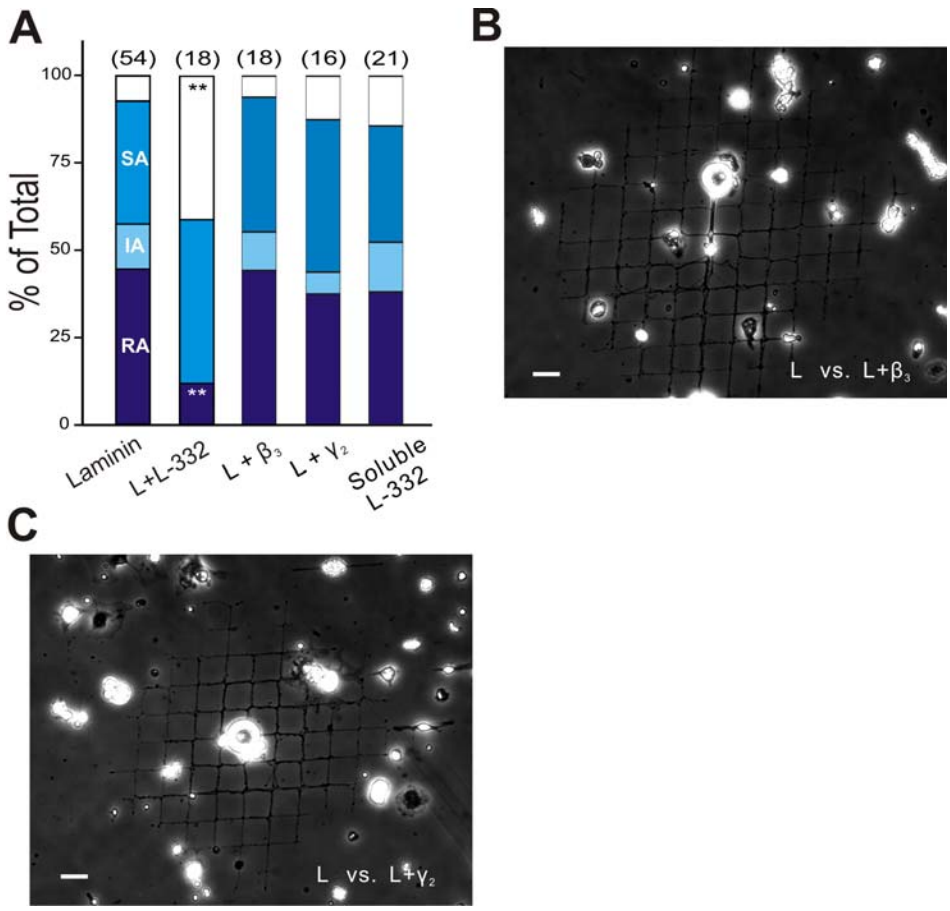

Figure 38. Neither β_3 nor γ_2 domain of laminin-332 can reproduce laminin-332 inhibition of mechanosensitivity and neurite outgrowth

A. Stacked histograms show that the proportion of mechanically activated currents were unaltered by a laminin+β_3 (abbreviated L+β_3) or a laminin+γ_2 (abbreviated L+γ_2) substrate in contrast to laminin+laminin-332 substrate (abbreviated L+L-332) (Number of measured neurons is shown on top of each group) (Chi-square test) **B.** Laminin+β_3 does not locally alter neurite morphology in comparison with laminin substrate. **C.** Laminin+γ_2 does not locally alter neurite morphology in comparison with laminin substrate. Scale bar is 20 μm.

I then cultured neurons on a laminin+γ_2 substrate and measured the mechanically activated currents of neurites. In this group, I also did not observe a significant alteration of mechanosensitivity (n=16; Chi-square test) (Fig. 38A). These electrophysiology experimental data suggests that a properly folded laminin-332

protein is necessary for the suppression of the RA current expression. In addition to mechanosensitivity test, I also examined whether either β_3 or γ_2 domain of laminin-332 could reproduce laminin-332 local morphological inhibition of neurite growth/thickness as does laminin-332. I prepared patterned substrates, which in one direction was printed with laminin and in the other direction was printed with laminin+β_3 or laminin+γ_2 mixtures and then cultivated neurons on the cross-patterned substrates. The results showed that neurite outgrowth on laminin+β_3 substrate and on laminin+γ_2 was almost identical to the neurite morphology as on a laminin substrate. It could be implied from the data that neither laminin+β_3 substrate nor laminin+γ_2 substrate could locally inhibit neurite morphology as does the laminin+laminin-332 mixture substrate, indicating that these two laminin-332 subunits did not possess the morphological inhibition ability of laminin-332 molecule as a whole. These data suggest that a properly folded laminin-332 molecule is necessary for the alteration in neurite outgrowth (Fig. 38B & 38C).

3.4 Summary

I have shown that laminin-332 suppression of the RA current expression is not attributable to a loss of neuron subtypes: low-threshold mechanoreceptors and high-threshold nociceptors. The TEM data show that a protein tether required for RA current conductance is absent on a laminin-332 substrate, suggesting that laminin-332 plays a role in lack of binding of the tether to the extracellular substrate. The microcontact printing experimental data support a model, in which

laminin-332 acts as a local inhibitory factor by competing with the tether binding partner: laminin-111 for a binding site on the ECM but integrin receptor activation is not required. In addition to mechanosensitivity inhibition, morphological study reveals that laminin-332 inhibits neurite growth/thickness. The data show that the effects of laminin-332 on mechanosensitivity and on neurite thickness/growth are two scenarios, which might be independent of each other. In both scenarios, laminin-332 acts as an inhibitory factor only if it is a properly folded whole molecule on the substrate.

Substrates	**Laminin (EHS-derived matrix)**	**Keratinocytes**	**Keratinocyte-derived matrix**	**Keratinocyte-conditioned medium**
	n=56	**n=43**	**Nn=10**	**n=14**
RA cells	n=25	n=4	n=0	n=6
RMP	-59.9 ± 1.0	-63.67±1.33		-59.17±2.23
mean soma size	31.8 ± 1.1 (24-41µm)	24,75±4,27 (16-36µm)		29,34±2,27 (32-48µm)
latency (ms)	0.5 ± 0.04	0.35±0.22		0.78±0.08
mean current amplitude (pA)	369.4 ± 73.7	283,75±80,82		528,46±311,55
activation τ_1 (ms)	0.43 ± 0.06	0,58±0,03		0,73±0,25
inactivation τ_2 (ms)	2.11 ± 0.25	2,33±0,44		1,2±0,23
SA cells	n=18	n=15	n=4	n=6
RMP	-58.2 ± 0.9	-71.25±1.87	-63.25±4.17	-55.83±3.36
mean soma size	27.8 ± 1.2 (18-35µm)	22,27±1,29 (16-32 µm)	28.85±0.93 (28-32µm)	23,07±4,89 (20-31µm)
latency (ms)	0.54 ± 0.03	3.41±1.15***	10.72±3.07***	0.63±0.15
mean current amplitude (pA)	161.9 ± 26.9	329,68±146,48	47,97±6,99	286,88±71,09
activation τ_1 (ms)	1.3 ± 0.17	4,03±2,56**	46,01±25,15***	0,99±0,23
IA cells	n=7	n=5	n=0	n=2
RMP	-59.4 ± 1.5	-65.67±3.62		-49.00±16.00
mean soma size	28.5 ± 2.1 (24-36µm)	24,4±1,86 (20-30µm)		27,05±10,25 (20-34µm)
latency (ms)	0.6 ± 0.13	4.40±1.48		7.30±2.55
mean current amplitude (pA)	98.1 ± 24.1	474,31±274,37		335,65±3,35
activation τ_1 (ms)	1.01 ± 0.17	1,69±0,82		1,32±1,07
inactivation τ_2 (ms)	18.76 ± 4.06	47,73±21,96		15,55±5,25
No response	n=6	n=19	n=6	n=0
RMP	-53.2 ± 9.3	-64.05±1.72	-52.83±4.87	
mean soma size	22.4 ± 3.3 (16-31µm)	22,05±1,45 (16-40µm)	29.17±1.40 (25-35µm)	

Substrates	**Laminin-332**	**SCC25**	**L : L-332 15 : 1**	**L : L-332 30 : 1**	**L : L-332 75 : 1**
	n=45	**n=27**	**n=18**	**n=25**	**n=13**
RA cells	n=8	n=8	n=2	n=8	n=5
RMP	-64.6 ± 2.9	-57.25 ± 1.9	-55 ± 5	-64.3 ± 1.1	-64.5 ± 2.02
mean soma size	27.9 ± 1.2 (22-34μm)	26.0 ± 1.2 (23-32μm)	26.1 ± 0.8 (25-27μm)	30.9 ± 1.1 (26-33μm)	28.9 ± 0.43 (28-32μm)
latency (ms)	0.76 ± 0.31	0.98 ± 0.56	0.3 ± 0.1	0.56 ± 0.21	0.56 ± 0.06
mean current amplitude (pA)	345.5 ± 57.6	126.8 ± 49.3	311.85 ± 14.4	485.5 ± 178.1	186.7 ± 68.6
activation τ_1 (ms)	0.72 ± 0.15	0.77 ± 0.36	0.61 ± 0.17	0.56 ± 0.14	0.42 ± 0.09
inactivation τ_2 (ms)	2.44 ± 0.67	1.95 ± 0.61	1.82 ± 0.41	1.93 ± 0.44	2.33 ± 0.92
SA cells	n=16	n=7	n=9	n=6	n=4
RMP	-59.6 ± 1.4	-57.5 ± 1.7	-65 ± 1.03	-65 ± 1.03	-59.7 ± 0.9
mean soma size	26.3 ± 1.2 (17-33 μm)	23.5 ± 1.5 (16-28μm)	27.8 ± 0.9 (23-31μm)	26.9 ± 0.9 (19-32μm)	28.1 ± 2.9 (23-34 μm)
latency (ms)	0.48± 0.06	0.5± 0.11	0.54± 0.06	0.48± 0.05	0.56± 0.09
mean current amplitude (pA)	94.18 ± 16.93	82.29 ± 11.29	219.66 ± 41.9	89.1 ± 13.1	104.3 ± 61.6
activation τ_1 (ms)	1.48 ± 0.24	0.99 ± 0.18	0.96 ± 0.14	1.01 ± 0.18	0.94 ± 0.46
IA cells	n=5	n=3	n=0	n=2	n=0
RMP	-59 ± 2.9	-53.7 ± 2.2		-54.5 ± 1.5	
mean soma size	27.7 ± 2.2 (22-35 μm)	24.5 ± 0.8 (23-26 μm)		26.1 ± 1 (25-28 μm)	
latency (ms)	0.32± 0.07	0.92 ± 0.29		0.39 ± 0.02	
mean current amplitude (pA)	150.4 ± 39.1	70.2 ± 11.6		262.3 ± 71.2	
activation τ_1 (ms)	0.76 ± 0.18	0.94 ± 0.07		0.53± 0.28	
inactivation τ_2 (ms)	17.53 ± 5.44	14.12 ± 5.17		27.5 ± 21.2	
No response	n=16	n=7	n=7	n=9	n=4
RMP	-59.9 ± 1.3	-51.8 ± 2.6	-51.8 ± 2.6	-55.4 ± 2.6	-59.9 ± 1.3
mean soma size	29.7 ± 1.6 (19-40μm)	21.9 ± 2 (16-31μm)	25.6 ± 1.7 (22-38μm)	24.2 ± 1.9 (16-31μm)	23.3 ± 0.15 (23-24μm)

Substrates	**L : L-332** **150 : 1** **n=10**	**L : denatured L-332** **10 : 1** **n=13**	**L : L-332:CM6** **15 : 1 : 2** **n= 27**	**L :β3** **10:1** **n=18**
RA cells	n=3	n=6	n=6	n=9
RMP	-63.3 ± 3.71	-60.3 ± 1.23	-67.2 ± 1.38	-62.3 ± 1.9
mean soma size	35.3 ± 0.32 (34-36μm)	31.1 ± 1.5 (25-36μm)	32.5 ± 1.32 (28-37μm)	33.5 ± 1.44 (27-38μm)
latency (ms)	0.39 ± 0.13	0.31 ± 0.01	0.3 ± 0.06	0.35 ± 0.04
mean current amplitude (pA)	256.5 ± 46.7	210.9 ± 26.3	218.1 ± 67.3	616.2 ± 429.2
activation τ_1 (ms)	0.66 ± 0.06	0.53 ± 0.11	0.82 ± 0.16	0.34 ± 0.06
inactivation τ_2 (ms)	2.07 ± 0.54	3.67 ± 0.77	1.5 ± 0.3	1.8 ± 0.8
SA cells	n=3	n=4	n=11	n=6
RMP	-60.3 ± 2.3	-57.8 ± 1.7	-63.1 ± 2	-61.2 ± 2.6
mean soma size (μm)	27.2 ± 2.04 (23-30 μm)	26.2 ± 3.5 (22-36 μm)	28.7 ± 1.4 (19-34 μm)	26.8 ± 1.6 (21-32 μm)
latency (ms)	0.46± 0.08	0.56± 0.16	0.35± 0.05	0.3± 0.04
mean current amplitude (pA)	201.2 ± 120	68.9 ± 20.5	198.2 ± 50.5	193.6 ± 123.1
activation τ_1 (ms)	1.8 ± 1	1.42 ± 0.32	0.9 ± 0.1	1.05 ± 0.2
IA cells	n=2	n=2	n=3	n=2
RMP	-56.6 ± 5.5	-62 ± 2	-66 ± 2.5	-57 ± 3
mean soma size	23.4 ± 5.2 (18-29 μm)	25.95 ± 1.6 (24-27 μm)	27.4 ± 2.2 (23-31 μm)	26.4 ± 1 (25-27 μm)
latency (ms)	0.33± 0.04	0.34± 0.07	0.38± 0.1	0.38± 0.05
mean current amplitude (pA)	490.1 ± 355.2	84.7 ± 13.6	529.6 ± 204.6	354.7 ± 72.2
activation τ_1 (ms)	0.24 ± 0.01	0.68 ± 0.03	0.26 ± 0. 1	0.35 ± 0.2
inactivation τ_2 (ms)	29.4 ± 17	25.9 ± 13.8	15.9 ± 3.5	9.12 ± 1.6
No response	n=2	n=1	n=7	n=1
RMP	-61 ± 1	-57	-61.4 ± 3.2	-59
mean soma size	28.5 ± 5.35 (23-34μm)	21.2μm	30.5 ± 3.1 (20-38μm)	23.1 μm

Substrates	**L : γ2 10:1** **n=16**	**Soluble laminin-332** **n=21**	**Pattern L vs L On cy3-Laminin** **n=32**	**Pattern L vs L On cy2-laminin** **n=32**
RA cells	n=6	n=8	n=14	n=14
RMP	-63.5 ± 2.1	-61.3 ± 1.9	-63.8 ± 0.87	-64 ± 0.92
mean soma size	29.9 ± 1.8 (24-38μm)	30.6 ± 1.22 (23-36μm)	30.8 ± 0.72 (26-36μm)	31.3 ± 0.78 (26-36μm)
latency (ms)	0.33 ± 0.03	0.33 ± 0.06	0.33 ± 0.05	0.38 ± 0.05
mean current amplitude (pA)	191.4 ± 61.6	193.2 ± 63.5	286.5 ± 53.8	257.6 ± 77.1
activation τ_1 (ms)	0.85 ± 0.25	0.76 ± 0.15	0.54 ± 0.08	0.4 ± 0.1
inactivation τ_2 (ms)	1.25 ± 0.47	2.2 ± 0.5	1.92 ± 0.32	1.61 ± 0.24
SA cells	n=7	n=7	n=11	n=10
RMP	-58.2 ± 0.9	-61.4 ± 2.4	-65.3 ± 0.9	-65.7 ± 0.9
mean soma size	27.8 ± 1.2 (18-35μm)	25.3 ± 1.9 (16-31 μm)	30.5 ± 1.4 (21-36 μm)	30 ± 1.4 (21-36 μm)
latency (ms)	0.54 ± 0.03	0.4± 0.06	0.38± 0.04	0.49± 0.1
mean current amplitude (pA)	161.9 ± 26.9	105.9 ± 22.5	60.1 ± 15.7	111.6 ± 27
activation τ_1 (ms)	1.25 ± 0.47	1.23 ± 0.22	1.38 ± 0.24	1.1 ± 0.24
IA cells	n=1	n=3	n=3	n=4
RMP	-65	-63.6 ± 7.9	-66.7 ± 1.3	-64.5 ± 1.4
mean soma size	31.3 μm	25.7 ± 2.2 (21-29 μm)	28.3 ± 2.7 (23-33 μm)	28.9 ± 2.2 (23-33 μm)
latency (ms)	0.47	0.36± 0.04	0.26± 0.04	0.41± 0.14
mean current amplitude (pA)	559.5	99.7 ± 33.4	93.9 ± 12.4	114.3 ± 67.3
activation τ_1 (ms)	0.424	1.15 ± 0.3	0.65 ± 0.1	0.8 ± 0.16
inactivation τ_2 (ms)	15.6	25.8 ± 9.39	25.9 ± 7.3	13.6 ± 3.5
No response	n=2	n=3	n=4	n=4
RMP	-66.5 ± 4.5	-59 ± 5.5	-62.5 ± 2.7	-62.5 ± 2.7
mean soma size	27.3 ± 3.3 (23-30μm)	25.3 ± 1.1 (23-27μm)	23.9 ± 2.2 (19-28μm)	23.9 ± 2.2 (19-28μm)

Substrates	**Pattern L vs L-332 On laminin** **n=21**	**Pattern L vs L-332 On laminin-332** **n=21**
RA cells	n=10	n=2
RMP	-62.8 ± 0.78	-63 ± 0.82
mean soma size	31.3 ± 1.5 (24-38μm)	33.2 ± 2.3 (30-35μm)
latency (ms)	0.33 ± 0.06	0.48 ± 0.23
mean current amplitude (pA)	272.5 ± 80.3	98.7 ± 39.6
activation τ_1 (ms)	0.64 ± 0.16	0.4 ± 0.17
inactivation τ_2 (ms)	1.6 ± 0.4	0.8 ± 0.4
SA cells	n=8	n=9
RMP	-64.5 ± 0.7	-63.2 ± 0.8
mean soma size (μm)	30.1 ± 2.04 (16-34 μm)	31.5 ± 1.3 (24-35 μm)
latency (ms)	0.4 ± 0.05	0.44 ± 0.06
mean current amplitude (pA)	143.4 ± 32.1	73.9 ± 13.6
activation τ_1 (ms)	1.41 ± 0.3	1 ± 0.16
IA cells	n=1	n=1
RMP	-65.4	-64.5
mean soma size	30.3 μm	31.5 μm
latency (ms)	0.3	0.43
mean current amplitude (pA)	160.7	117.7
activation τ_1 (ms)	0.4	0.83
inactivation τ_2 (ms)	19.4	19.3
No response	n=2	n=10
RMP	-63.1 ± 1.3	-63.5 ± 1.7
mean soma size	29 ± 0.4 (19-31μm)	28.8 ± 1.8 (16-35μm)

Table 5. Physiological properties of cells exhibiting RA, SA or IA current and no response in all experiments All measured parameters are listed. unpaired t-test *P<0.05; **P<0.01; ***P<0.001.

4 DISCUSSION

The skin is one of the largest organs of the body and as such it exhibits a wide range of functions, of which mechanical protection might be one of the most ancient and important functions. At the molecular and cellular level the transduction of somatic sensation such as touch and pinch is poorly understood. Physiological and genetic studies on the nematode *C. elegan*s have suggested that cutaneous mechanotransduction is mediated by a complex of several proteins (Chalfie and Sulston 1981; Chalfie and Au 1989). In both invertebrates and vertebrates this mechanotransduction complex is localized to the afferent sensory nerve endings in the cutaneous layer (French 1992; French 1992; Gillespie and Walker 2001; Lewin and Moshourab 2004; Hu et al. 2006) and contains a mechanosensitive multimeric cation channel at its core, which is connected to the cytoskeleton intracellularly as well as to the extracellur matrix on the other side by accessory proteins, which have been shown to function as protein elements to mediate gating of the ion channel itself (Chelur et al. 2002; O' Hagan et al. 2005). Recent evidence has shown that an SLP3 is involved in gating mechanosensitive channels in mouse (Wetzel et al. 2007). This finding suggests that mechanotransduction components and mechanisms are conserved between *C. elegans* and mammals. Genetic analysis of touch sensation in *C. elegans* and research on the mechanosensitive hair cell in inner ear cochlea have suggested the existence of an extracellular link which tethers the mechanosensitive ion channels to the ECM and transduces mechanical force to the channels (Ernstrom and Chalfie 2002; Syntichaki and Tavernarakis 2004). So far there is no direct evidence showing that in the mouse an extracellular link is

essential for mechanotransduction (Lewin and Moshourab 2004; Hu et al. 2006). These results have prompted a question: whether an extracellular link is also conserved in the mouse sensory mechanotransduction system? In this study it was demonstrated that, as in *C. elegans* and *D. melanogaster,* an extracellular protein filament of ~100nm, synthesized by sensory neurons is essential for mechanotransduction in the mouse. It was also found that pharmacological and biochemical manipulation of this link could immediately and reversibly abolish the RA current expression of sensory neurons and in addition revealed the biochemical properties of this link. This cleavage and regeneration of the extracellular link could be clearly visualized and observed under electron microscopy. This was the first evidence to show that an extracellular mechanotransducer link exists and that it maybe essential for normal mechanotransduction.

This study also involved investigation of the role of ECM in sensory mechanotransduction. Genetic screens carried out in both *C. elegans* and *D. melanogaster* have suggested that extracellular proteins might be essential for the transducton of body touch and D. melanogaster bristle movement respectively (Du et al. 1996; Chung et al. 2001; Chalfie 2002). However, the evidence that extracellular proteins are necessary for gating mechanosensitive ion channels in flies and worms is indirect because acute ablation of candidate extracellular proteins was not shown to abolish mechanotransduction as demonstrated in vertebrate hair cells (Assad et al. 1991; Zhao et al. 1996; Goodyear and Richardson 2003; Siemens et al. 2004; Kazmierczak et al. 2007). Recent evidence suggests that extracellular proteins identified in genetic screens

for touch insensitive worms are not well placed *in vivo* to act as gating tethers for the MEC-4/MEC10 ion channel . In this study a co-culture models of sensory neurons and skin-derived epidermal keratinocytes or fibroblasts was established by cultivating sensory neurons on a monolayer of keratinocytes or fibroblasts. It was demonstrated that the molecular nature of the extracellular environment could profoundly modulate mechanosensitive channel gating in sensory neurons. Matrix proteins derived from keratinocytes have a profound inhibitory effect on sensory neuron mechanosensitivity. I found that laminin-332, which is exclusively expressed by keratinocytes could partially reproduce the inhibitory properties of keratinocyte-derived matrix. A variety of methods including TEM and a specialized microcontact printing technique were introduced and established to study the mechanisms by which mechanosensitivity inhibition takes place. The experimental data suggest that laminin-332 inhibition targets selectively on the expression of mechanosensitive RA current by inhibiting binding of the extracellular filament required for mechanosensitive channel gating through local contact, but not through an integrin-mediated pathway. In addition, it was also found that laminin-332 acts as an inhibitory factor for sensory neuron morphology by locally suppressing neurite growth/thickness in contact with a laminin-332 substrate. Laminin-332 inhibition for mechanosensitivity is selective for a subtype of neurons possessing RA-type mechanosensitive current. However, a laminin-332 substrate locally influences neurite morphology (growth/thickness) originating from all neurons in culture with no exception, suggesting that the underlying mechanism for laminin-332 mechanosensitivity inhibition is independent of its effect on neurite morphology.

4.1 Manipulation of the extracellular tether reveals its biochemical properties

Using a physiological assay that has been established *in vitro* to characterize mechanically gated channels in the neurites of cultivated mouse sensory neurons (Hu and Lewin 2006) and co-culture of sensory neurons on mouse 3T3 fibroblasts, it was found that mechanical stimulation of these neurites evoked fast mechanosensitive currents, as measured in the cell body. The amplitude and kinetic parameters of neuritic mechanosensitive currents were identical to those observed on a laminin substrate. The fibroblast substrate underneath the neurite and was then mechanically stimulated and it was found that short latency; fast activating mechanosensitive currents were also evoked in sensory neurons compared to direct stimulation of neurite. The gating kinetics (latency and activation time constant) of the mechanosensitive current was virtually identical to mechanical stimulation of the underlying fibroblast, suggesting that a physical link might transfer force from the stimulated fibroblast to mechanosensitive ion channels in the sensory neuron (Hu, Chiang et al 2009).

It was hypothesized that if the extracellular link is indeed required for mechanotransduction in mouse, destruction of the extracellular link should be able to abolish the mechanosensitivity of the sensory neurons. In mechanosensory hair cells, the tip link, which was suggested to be composed of cadherin-23 and protocadherin-15 (Kazmierczak et al. 2007) can be manipulated with BAPTA but not by the endopeptidase subtilisin (Bashtanov et al. 2004). The results showed that mechanically activated RA currents are sensitive to subtilisin

and a subtilisin-related, site specific protease “blisterase” purified from parasite *O. volvulus*, which cleaves a tetrabasic sequence with the motif RX(K/R)R but not by BAPTA as was found in hair cells. This ablation of mechanosensitivity could be completely recovered after further incubating the cells for 30 hrs in culture medium. Using a unique TEM, which I developed to maximize electron density of extracellular ultrastructure, an extracellular filament (length ~100 nm) can be readily observed and is destroyed concurrently with RA current abolishment. This tether reappeared with RA current recovery, suggesting that it is synthesized by cultured neurons on the laminin substrate. To identify the molecular basis of the tether, the neuronal extracellular proteins in culture were isolated and the composition was analyzed by mass spectrometry (data not shown in this study). Amongst all identified polypeptide hits, one of the most interesting candidates was a collagen, termed Col28 or Collagen XXVIII belonging to the class of von Willerbrand factor A (VWA) domain-containing protein, which was shown to be highly expressed in few neuronal cell types, especially in DRG neurons (Veit 2006). I hypothesized that Col28 comprises the molecular nature of the subtilisin-sensitive tether. To test the plausibility of this idea, I obtained VWA1 and VWA2 (Antibody against Col28) to localize immunoreactivity of this protein. The immunocytochemistry result shows a highly punctate expression manner of the Col28 immunoreactivity in sensory neurites, which was compatible with the hypothesis based on the randomness of the observed protein filaments under electron microscopy. However, after subtilisin treatment, the punctuate staining was still clearly observed, suggesting that Col28 was not abolished by subtilisin, which does not support this protein as composing the tether. I further analzed the sequence of Col28 and found that it does not possess the blisterase cleavage site

(RX(K/R)R) (data not shown in this study). It was also found in sequence analysis that amongst all identified polypeptides which numbered 800, only approximately 30 have a blisterase-specific site. The result suggests that blisterase specificity is a useful criterium to narrow down the range of identified candidates for the protein filament required for mechanosensitive channel gating. Ongoing investigations will shed a light on the identification of the molecular context of this tether although it is still a challenging task.

4.2 TEM study suggests correlation between a subtype of protein filaments and mechanically activated SA current

In control experiment, before proteases treatment, most observed attachments and links are randomly distributed over the interface. A frequency distribution ploted from control, subtilisin and subtilisin recovery groups were calculated and superimposed and subsequently fit to a Gaussian distribution. 75 nm was then chosen as the criteria for long tether considering absence and reappearance of the long links across different groups. For attachments less than 75 nm, two major types of Gaussian distribution can be distinguished (Fig. 13). Most cell-surface connections are in the form of very tight attachments, which is usually less than 15 nm. This subgroup correlates with the findings of cell-matrix adhesion complexes in other cell types. It was suggested the tight attachments, which are usually less than 30 nm are either direct integrin bindings or integrin-associated structures such as focal adhesions or hemidesmosomes

(Fernandez-Valle et al. 1998; McMillan et al. 1998). Apart from that, there are also many thick, electron-dense links with lengths around 50nm.

Interestingly, after subtilisin and blisterase treatment it was found that between the range of 30 nm and 75 nm the middle size tether links of length ~50 nm were intact, indicating that they are qualitatively insensitive to the protease subtilisin. The density of middle size links per μm^2 in control is 36.83 ± 3.707 (n=88), 39.02 ± 5.510 (n=58) in subtilisin treatment group, and 42.56 ± 5.230 (n=69) in subtilisin recovery group, which are also identical. However, in mechanically unresponsive SCG neurons that were used as a negative control in this study, the density of middle size links per μm^2 has significantly reduced to 19.40 ± 1.91 (n=99) ($P<0.01$ Unpaired t-test). The decrease of middle size link density is correlated with a reduction of mechanically activated SA current from 42% (19/45) in DRG to 13.3% (2/15) in SCG. This data is only suggestive and does not prove any fundamental link between the SA current shorter electron dense links. The tethers for sensory mechanotransduction channels may, like those of the hair cell tip link, be composed of more than one protein (Goodyear and Richardson 2003; Siemens et al. 2004; Sollner et al. 2004). Identification of the molecular composition of these proteins and their role in the sensory mechanotransduction complex in different subtypes of sensory neurons will be an important challenge for future work. These findings point towards an interesting direction for further investigation.

4.3 ECM proteins are important for mechanosensitive channel gating

Only the terminal endings of sensory neurons in the skin are mechanosensitive *in vivo*, and thus an experimental model of the cellular milieu was needed to mimic the receptor ending. To this end, co-cultures of sensory neurons with defined cell types normally encountered in the skin were established. Primary mouse skin keratinocytes that were first grown as a monolayer on glass coverslips were chosen. Sensory neurons were seeded on top of this monolayer and recordings were made once they had grown neurites. When cells were cultured on a keratinocyte monolayer, neuritea exhibited normal arborization. It was shown that the keratinocyte monolayer and keratinocyte-derived cell-free matrix alone could profoundly inhibit a RA mechanosensitive conductance and impede the latency and the activation time constant of SA mechanosensitive conductance (Fig. 19). In contrast when sensory neurons were recorded on a fibroblast cell monolayer the incidence and kinetics of mechanically activated channels was almost indistinguishable from that found on the laminin substrate. The dramatic changes in the physiological properties of mechanically activated channels on different cellular and non-cellular substrates observed in this study strongly support a critical role for the ECM in gating sensory channels. The experimental data also indicated that the latency and speed of channel gating was dependent on the extracellular environment. Due to the diversity of molecular composition, ECM proteins serve a wide variety of functions which include supporting cell anchorage, segregating tissues from one another and regulating cell-matrix communication (Iozzo 1998; Alberts et al. 2004). Mechanosensory signal

transduction responses in many cell types are known to involve integrin receptors although the time course of such changes are typically in the order of minutes and not μs as shown here (Fig. 7; Fig. 8; Fig. 20) (Jalali et al. 2001; Browe and Baumgarten 2003). Only recently was there research attempts discussing the possible coupling of mechanical stimulation and substrates interaction in sensory neurites *in vivo* and *in vitro* (Lucarz and Gerard 2007; Lin et al. 2009). The experimental results have revealed novel findings which will greatly facilitate our understanding about the role of ECM proteins in the sensory mechanotransduction complex.

4.4 Laminin-332 plays an inhibitory role selectively in expression of RA-type mechanosensitive currents

In a series of screening experiments on the ECM composition from laminin; 3T3 cells and keratinocytes, I have identified laminin-332, which was a molecule found in keratinocytes matrix but not in laminin nor in 3T3 matrix (Fig. 20 & Fig. 21). Laminin-332, a glycoprotein complex of three subunits: α_3 domain, β_3 domain, and γ_2 domain is a unique molecule in its biological activity and structure (Fig. 22) which was originally found as an anchoring filament component of keratinocytes (Carter et al. 1991; Rousselle et al. 1991). Previous findings from other groups have characterized the role of laminin-332 in signal transduction, keratinocyte differentiation and cell adhesion (Aberdam 1994; Pulkkinen 1994; Sasaki et al. 2004) by providing an attachment substrate for both adhesion and migration in a wide variety of cell types, including epithelial cells, fibroblasts, neurons and

leukocytes. These cells, compared to fibronectin, collagen, or vitronectin, will adhere to laminin-332 faster and spread to a larger extent. Laminin-332 is attracting attention as a substrate that may stimulate carcinoma cell migration (Marinkovich 2007), since it has been detected at the leading edge of invasive cancer tissue in several types of human carcinomas. Receptors for Laminin-332 include integrins $\alpha_3\beta_1$ and $\alpha_6\beta_4$ (Carter et al. 1991; Rousselle et al. 1991). The latter integrin is specialized in forming hemidesmosomes, which provide resistance to mechanical stress in many epithelia, including skin and gut. Impairment of laminin-332 in humans causes a severe and deadly blistering disease named Herlitz's JEB (Meneguzzi 1992; Marinkovich 1993). More recently, cell surface proteoglycans, such as syndecan-2 and syndecan-4 (Culp et al. 2006), have been identified as binding partners for laminin-332. The structural and functional properties of laminin-332 are well conserved across species. For instance, human cells adhere equally well to human and rat laminin-332. For most purposes, human and rat laminin-332 are interchangeable, likely based on the fact that integrin receptor specificity is largely conserved across species (Eble et al. 1998; Hormia 1998). However, so far to date there have been no publications aiming at discussing the role of laminin-332 in mechanotransduction and its interaction with the sensory mechanotransduction machinery. Here in this study I have shown for the first time that laminin-332 indeed plays a role in sensory mechanotransduction by modulating RA current expression. In this study I used a mixture of laminin with a concentration of laminin-332 30-fold lower than laminin and can still observe robust inhibition of RA-type current, suggesting that laminin-332 is a potent inhibitory factor for RA current expression (Fig. 24). In this study it is found that keratinocyte-derived

matrix not only inhibits RA current but also impedes SA gating kinetics. However, laminin-332 can only selectively reproduce keratinocyte matrix inhibitory function in terms of RA current expression, but not for the SA current gating kinetics (Fig. 23). This finding strongly suggests existence of other molecules in the keratinocyte-derived matrix that might modulate the SA conductance. Further study on the ECM composition of keratinocytes in comparison with laminin and 3T3 cells might shed a light on identification of molecules that contribute to modulation of SA current gating kinetics in keratinocytes.

Previously it was found in our lab that the I–V relation of mechanically activated conductance is indeed quite distinctive for the SA and RA current. The RA current shows a linear I–V relation with a reversal potential at approximately +80 mV and can be completely abolished when extracellular Na^+ ions are replaced by the impermeant cation $NMDG^+$ (Lechner et al. 2009). However, the SA current showed a clear reversal potential at around 0 mV under identical conditions and can be partially blocked by the TRP channel antagonist ruthenium red, indicating that a non-selective channel may underlie this current. It is demonstrated that the distinct biophysical properties of RA and SA currents are highly suggestive of different underlying ion channel entities (Hu and Lewin 2006). Here in this study, I found that laminin-332 selectively inhibits the expression of RA-type mechanosensitive current in both putative mechanoreceptors and nociceptors (judged by presence of hump in AP spikes) (Fig. 25), strengthening previous findings that distinct gating apparatus might underlie RA and SA current expressions.

4.5 Laminin-332 acts as a mechanosensitivity inhibitory factor by inhibiting binding of the tether to the substrate

The dramatic changes in the physiological properties of mechanically activated channels on different cellular and non-cellular substrates observed in this study strongly support a critical role for the ECM protein in gating sensory channels. The most interesting effect that I observed was a significant loss of mechanically activated RA current in cultured neurons on a rat laminin-332 substrate (Fig. 23). I have demonstrated from the data that laminin-332 selectively inhibits mechanosensitivity of neurons possessing RA current by turning this neuron subtype into mechanically unresponsive neurons. In addition laminin-332 substrate does not alter the proportion of mechanoreceptors and nociceptors in culture (Fig. 26). Qualitative changes in neurite arborization on laminin-332 substrate are not observed in comparison with laminin substrate. It can be concluded from these findings that the RA current suppression is not attributable to absence of neuron subtypes: mechanoreceptors and nociceptors but rather to another mechanism. TEM data show that a tether needed for conducting mechanically activated RA current has significant reduced from 4.9 ± 1.3 per μm^2 on laminin substrate (n=31) to 0.4 ± 0.2 per μm^2 on laminin-332 substrate (n=4) ($P<0.01$, Un-paired t-test) while the average length of the tether remains intact (Table 3). This finding provides a direct evidence for laminin-332 function. Previously it was found that the ~100 nm protein filament is necessary for RA type current conductance on a laminin substrate. Interestingly, the TEM data on laminin-332 substrate has strengthened correlation between the subtilisin/blisterase-sensitive filaments and RA-type current on laminin substrate,

suggesting that laminin-332 substrate might lack a binding site for the tether synthesized by sensory neurons. This effect might also conceivably be due to a signal provided by laminin-332 that suppresses the expression of a RA mechanosensitive channel or the extracellular tether needed for channel gating. It is however difficult to answer the question whether laminin-332 acts as a signal which consequently downregulates the expression profile of the channel or the extracellular tether given the fact that its molecular nature is yet to be revealed.

4.6 Laminin-332 inhibition takes place only if the sensory neurite has contact with the substrate independent of integrin receptors

Previous studies have suggested that cells sense cues that guide their growth and development by probing their microenvironment with surface membrane receptors that elicit intracellular signals when they bind their ligands. Cell interactions with ECM molecules differ from those with soluble regulatory factors, however, because in addition to ligand-induced signaling, cells also apply traction to their integrin receptors that mediate ECM adhesion (Marina et al. 1998). In this study, it was found that a keratinocyte-derived matrix and laminin-332 substrate could profoundly alter the RA current expression of neurons grown on it, however, keratinocyte-conditioned media and soluble laminin-332 added in culture media over 24 hours incubation did not suppress RA responses in sensory neurons cultured on the control substrate (Fig. 38). This result does not exclude the possibility that mechanosensitive channels or extracellular tethers are suppressed by an integrin-mediated trans-cellular signal. If such a signal should

exist it must act relatively rapidly to suppress the expression of mechanosensitive channels as recordings were made 24 hours after plating sensory neurons on the keratinocyte monolayer or on a laminin-332 substrate. I cannot therefore definitively exclude the possibility that the expression of the RA mechanosensitive channels or extracellur tethers is inhibited upon reception of laminin-332 signal. However, the changes that I observed in the latency and activation kinetics of SA responses on keratinocyte monolayer are more difficult to reconcile with such a model. Thus in this case the putative keratinocyte signal that is responsible for SA current modulation must induce changes in the molecular composition of the channel that impedes its ability to rapidly sense changes in membrane tension.

To further investigate laminin-332 function, a specialized methodology was established (Fig. 30; Fig. 31). This technique is modified to guide neurites originating from one soma to grow on different substrate arrays that are properly microfabricated at dimension of 25 μm, which is very wide at cellular level to avoid interference of signals from different substrates. Ii is demonstrated from my experimental data that different substrates distinctively modulate mechano-sensitivity of sensory neurites (Fig. 34; Fig. 35). This finding suggests that laminin-332 acts as a local inhibitory factor, but not as a signal, which globally inhibits the expression of the RA current. Laminins are a family of integral basement membrane glycoproteins, each containing α-, β- and γ- that assemble into characteristic heterotrimeric structures (Engel 1992; Colognato and Yurchenco 2000). The long arms of the three chains associate and form a helical coiled-coil region. The C-termini of α-domain are unique in that they form a large globular structure termed the G-domain, which is required for integrin-binding. To

date five α-, three β-, and three γ- domains have been identified, which assemble into at least fifteen laminin isoforms. Laminin-332 is unique for its β_3, and γ_2 domains, although a poorly characterized laminin isoform: laminin-522, which shares a common γ_2 domain with laminin-332 was recently identified (Aumailley and Yurchencho 2005). It was found in previous research that laminin-332 shares the common integrin-binding domain in the α_3 chain with laminin-6 (laminin-311), which are thought to cooperatively regulate cellular functions. These findings demonstrate that laminin-332 and laminin-6, in spite of having common integrin-binding domain have distinct biological activities due to distinctive β- and γ- domain combination (Hirosaki 2002), suggesting the importance of each α_3, β_3, and γ_2 domains in laminin-332 biochemical characteristics. The laminin proteins bind to several classes of membrane proteins, including integrins and dystroglycan (Li et al. 2003). It has been demonstrated that a laminin subunit laminin β2 can directly bind to the pore forming subunit of the voltage-gated calcium channel $Ca_v2.2$ (Nishimune et al. 2004). The $Ca_v2.2$-laminin β2 complex then acts as a stop signal for neurite outgrowth and sensory nerve innervation *in vivo* (Sann et al. 2008). To dissect the biochemical properties of domain functions in laminin-332, an antibody (CM6) that functionally blocks integrin binding to laminin-332 in α_3 chain was applied. It was found from the data that CM6 does not rescue laminin-332 inhibiton for RA current (Fig. 36), indicating that integrin-induced trans-cell signalling is not involved in laminin-332 inhibition of the mechanosensitive RA-type current expression. I have also examined the other two domains of laminin-332 and found that the two subunits of laminin-332 (β_3 and γ_2 domains) both do not have the ability to reproduce laminin-332 function to modulate RA current as of a complete laminin-332 isoform (Fig. 38). These

findings suggest that laminin-332 only functions in direct contact with sensory neurites on a laminin-332 substrate and each individual subunit of laminin-332 does not facilitate laminin-332 function as a complete isoform. In summary, the results strongly support a model for local inhibition by which laminin-332 acts as a local inhibitory factor to compete with the interaction partner of tether in laminin substrate and disassembly binding of the tether to ECM and subsequently results in impairment of RA mechanically activated current in mechanoreceptive neurons (Fig. 29). It is speculated that the helical coiled-coil region, in which three individual subunits long arms meet and tangle might play an important role. This question, however, cannot be addressed until an isolated coiled-coil region is generated and examined.

4.7 Laminin-332 inhibition of mechanosensitivity is independent of its inhibition of neurite outgrowth and might play a role in regulating sensory tissue function in the epidermis

In this study, it was noted that laminin-332 inhibition for RA current expression is coupled with a local neurite morphological inhibition in growth/thickness by laminin-332 substrate (Fig. 33; Fig. 35). My data show that laminin-332 inhibition for mechanosensitivity has a preference for a subtype of neurons, which exhibit mechanically activated RA-type current (Fig. 25; Fig. 26). However, I do not observe any preference of laminin-332 inhibition for neurite morphology (growth/thickness). My microcontact printing experimental results show that laminin-332 ubiquitously inhibits neurite growth/thickness of all cultured neurons

with various soma sizes (Fig. 33C). These results suggest that laminin-332 inhibition for mechanosensitivity and its ability to inhibit neurite outgrowth are two events, which may be independent of each other. Laminin-332 is the marker protein for keratinocytes, which is exclusively expressed by epidermal keratinocytes as compared to laminin and fibroblast-dreived matrix proteins, and its role in the sensory behavior is elucidated in this study. In recent years, findings from other groups have demonstrated that keratinocytes also express sensing proteins similar to those found in sensory neurons, such as TRPV1, TRPV3 and TRPV4 which enable them to sense thermal and noxious stimuli and perhaps osmotic variation in neurons. It was shown that keratinocytes have close contact with sensory neurons and exhibit a strong trophic effect toward sensory neurite in co-culture models (Chateau and Misery 2004; Chateau et al. 2007; Ulmann et al. 2007). Thus, keratinocytes synthesize key components, which endow them to be partners for sensory neurons. It was also found that stimulation of keratinocytes was followed by a release of extracellular ATP, which can act as a messenger onto target cells or followed by production of a calcium wave able to propagate to neighboring cells, such as DRG neurons and increase the intracellular Ca^{2+} concentration of DRG neurons (Koizumi et al. 2004). Thus it was proposed that keratinocytes cooperatively play an important role in the sensory system *in vivo* (Dhaka et al. 2006; Boulais et al. 2007). One limitation of these indirect mechanisms is that they are intrinsically slower than direct mechanical gating. In fact, direct gating was first proposed for hair cells because of their remarkable transduction speed (Corey and Hudspeth 1979), which is compatible with the experimental findings in this study. If keratinocytes or other epithelial cells do mediate sensory transduction, mechanisms of signal relay and specificity

between epithelial cells and neurons should be answered. One should ask: Does a molecule released from heat-activated keratinocytes excite the correct sensory neuron subtypes and is the time lapse short enough to allow discrimination of acute changes in skin temperature?

In this study, the ability of keratinocytes to interact with neurons *in vitro* has been elucidated. Previous research attempts have collectively discussed coupled behaviour of external stimulation and keratinocytes substrate interaction in nociceptive sensory nerve endings *in vivo* and *in vitro* (Chateau and Misery 2004; Chateau et al. 2007; Ulmann et al. 2007). In this study, I show for the first time that laminin-332 has its own role in directly modulating the sensory mechanoreceptive system. In adult mice, the cutaneous layer is innervated by a diversity of mechanosensitive neurons. Low threshold mechanoreceptors innervate a variety of structures found in the dermis of the skin (Merkel Cells, hair follicles, Meissners Corpuscles, etc) and do not normally make contact with keratinocytes localized in the epidermis. Nociceptive sensory neurons on the other hand normally provide a heavy innervation to the epidermis where their endings make contact with keratinocytes (Halata 1975; Breathnach 1977; Kruger 1996; Kruger et al. 2004; Zylka et al. 2005). Correlative to the findings in this study, I found that epidermal keratinocyte-derived laminin-332 protein selectively inhibits expression of mechanosensitive RA type current. However laminin-332 does not have any inhibitory effect on the expression of IA and SA currents, which are exclusively found in nociceptors, of which nerve endings innervate to epidermal layer in the skin. Thus, there is a possibility that laminin-332 might play a role in the development of sensory nerve endings innervation in the skin. *In*

vivo, laminin-332 plays an important role in keratinocytes function. It serves as an adhesion molecule by interacting with components in the cutaneous BMZs, such as: $\alpha_6\beta_4$, $\alpha_3\beta_1$ integrin receptors and type VII collagen, a component of anchoring fibrils extending from basement membrane to the underlying ECM (Spinardi et al. 1995; Xia 1996; Chen et al. 1999). Impairment of laminin-332 or gene mutation in any of its three sub-domains (α_3, β_3, and γ_2) leads to a lethal clinical snydrome: Herlitz's JEB, in which keratinocytes lose its anchorage to the dermal layer and severe blistering is caused upon subtle mechanical stimulation. It will be interesting to ask whether JEB patients have abnormalities in their somatosensation. To answer this question, further experimental effort has to be made to know if JEB patients have any somatosensation symptoms and to prove whether laminin-332 is involved in the developmental process of cutaneous sensory organ function.

4.8 Conclusions

- A subtilisin/blisterase-sensitive protein tether with a length of ~100nm is required for mechanically activated RA current expression
- The mechanically activated RA current is not supported and gating kinetics (latency and activation time constant) of SA current is impeded on a keratinocyte-derived matrix
- Laminin-332 is expressed by keratinocytes, but not present in EHS-derived matrix and fibroblast-derived ECM. It can potently reproduce the keratinocyte-mediated inhibition of RA current expression.

- Modulation of SA current gating kinetics by keratinocytes is not reproduced by laminin-332, suggesting that other molecules are involved.
- TEM results show that laminin-332 inhibition of RA current expression can be attributable to a lack of tether binding to the substrate.
- Microcontact printing and patch clamp experiments show that laminin-332 locally inhibits expression of RA current in contact with a laminin-332 substrate and an integrin-mediated pathway is not involved.
- Laminin-332 is also an inhibitory factor for cultured neurite outgrowth (growth/thickness), however, the mechanisms for modulation of mechanosensitivity and neurite morphology are likely two independent events although integrin-mediated pathway is not involved in both scenarios.

5 REFERENCES

Aberdam (1994). "Herlitz's junctional epidermolysis bullosa is linked to mutations in the gene (LAMC2) for the gamma 2 subunit of nicein/kalinin (LAMININ-5)." Nature Genet **6**: 299-304.

Adair, Xiong, Maddock, Simon, Goodman, Arnaout and Yeager (2005). "Three-dimensional EM structure of the ectodomain of integrin {alpha}Vß3 in a complex with fibronectin." The Journal of Cell Biology **168**(7): 1109-1118.

Alberts, Bray , Hopin, Johnson, Lewis, Raff, Roberts and Walter (2004). "Tissues and Cancer." Essential cell biology.

Alvarez de la Rosa, Zhang, Shao, White and Canessa (2002). "Functional implications of the localization and activity of acid-sensitive channels in rat peripheral nervous system." Proc Natl Acad Sci U S A **99**(4): 2326-31.

Assad, Shepherd and Corey (1991). "Tip-link integrity and mechanical transduction in vertebrate hair cells." Neuron **7**(6): 985-94.

Aumailley, Khal, Knoss and Tunggal (2003). "Laminin-5 processing and its integration into the ECM." Matrix Biol. **22**: 49-54.

Aumailley and Yurchencho (2005). "A simplified laminin nomenclature." Matrix Biology **24**(5): 326-332.

Baker, Hopkinson, Fitchmun, Andreason, Frasier, Plopper, Quaranta and Jones (1996). "Laminin-5 and hemidesmosomes: role of the alpha 3 chain subunit in hemidesmosome stability and assembly." Journal of Cell Science **109**(10): 2509-2520.

Bashtanov, Goodyear, Richardson and Russell (2004). "The mechanical properties of chick (Gallus domesticus) sensory hair bundles: relative contributions of structures sensitive to calcium chelation and subtilisin treatment." J Physiol **559**(Pt 1): 287-99.

Biel and Michalakis (2007). "Function and dysfunction of CNG channels: insights from channelopathies and mouse models." Molecular Neurobiology **35**(3): 266-277.

Boulais, Pereira, Lebonvallet and Misery (2007). "The whole epidermis as the forefront of the sensory system." Exp. Dermatol. **16**: 634-635.

Breathnach (1977). "Electron microscopy of cutaneous nerves and receptors." J. Invest. Dermatol **69**(1): 8-26.

Browe and Baumgarten (2003). "Stretch of beta 1 integrin activates an outwardly rectifying chloride current via FAK and Src in rabbit ventricular myocytes." J Gen Physiol **122**(6): 689-702.

Bushtanov, Goodyear, Richardson and Russel (2004). "The mechanical properties of chick (Gallus domesticus) sensory hair bundles_ relative contributions of structures sensitive to calcium chelation and subtilisin treatment." J Physiol **559**(1): 287-299.

Carter, Ryan and Gahr (1991). "Epiligrin, a new cell adhesion ligand for integrin-3-1 in epithelial basement membranes. Characterization of laminin 332 integrin specificity." Cell **65**: 559-610.

Cate, Baker and Gilbert (1995). "Occupational therapy and the person with diabetes and vision impairment." Am J Occup Ther **49**(9): 905-11.

Catherine B. Poole (2003). "Cloning and Biochemical Characterization of Blisterase, a Subtilisin-like Convertase from the Filarial Parasite, Onchocerca volvulus." Journal of Biological Chemistry **278**(38): 8.

Chalfie (2002). "Genetics of Sensory Mechanotransduction." Annual Review of Genetics **36**: 411-453.

Chalfie and Au (1989). "Genetic control of differentiation of the Caenorhabditis elegans touch receptor neurons." Science **243**(4894 Pt 1): 1027-33.

Chalfie, Horvitz and Sulston (1981). "Mutations that lead to reiterations in the cell lineages of C. elegans." Cell **24**(1): 59-69.

Chalfie and Sulston (1981). "Developmental genetics of the mechanosensory neurons of Caenorhabditis elegans." Dev Biol **82**(2): 358-70.

Chalfie, Sulston, White, Southgate, Thomson and Brenner (1985). "The neural circuit for touch sensitivity in Caenorhabditis elegans." J Neurosci **5**(4): 956-64.

Chalfie, Thomson and Sulston (1983). "Induction of neuronal branching in Caenorhabditis elegans." Science **221**(4605): 61-3.

Chateau, Dorange, Clement, Pennec, Gobin, Griscom, Baudrimont, Rougier, Chesne and Misery (2007). "In vitro reconstruction of neuro-epidermal connections." J. Invest. Derm. **127**: 979-981.

Chateau and Misery (2004). "Connections between nerve endings and epidermal cells: are they synapses?" Exp. Dermatol. **13**: 2-4.

Chelur, Ernstrom, Goodman, Yao, Chen, R and Chalfie (2002). "The mechanosensory protein MEC-6 is a subunit of the C. elegans touch-cell degenerin channel." Nature **420**(6916): 669-73.

Chen, Marinkovich, Jones, Li and Woodley (1999). "NC1 domain of type VII collagen binds to the beta3 chain of laminin 5 via a unique subdomain within the fibronectin-like repeats." J Invest Dermatol **112**: 177-183.

Chung, Zhu, Han and Kernan (2001). "nompA encodes a PNS-specific, ZP domain protein required to connect mechanosensory dendrites to sensory structures." Neuron **29**(2): 415-28.

Colognato and Yurchenco (2000). "Form and function: the laminin family of heterotrimers." Dev. Dyn. **218**: 213.

Condrescu, Opuni, Hantash and Reeves (2002). "Cellular regulation of sodium-calcium exchange." Ann N Y Acad Sci **976**: 214-23.

Corey and Garcia-Anoveros (1996). "Mechanosensation and the DEG/ENaC ion channels." Science **273**(5273): 323-4.

Corey and Hudspeth (1979). "Response latency of vertebrate hair cells." Biophys J **26**(3): 499-506.

Corey and Hudspeth (1983). "Kinetics of the receptor current in bullfrog saccular hair cells." J Neurosci **3**(5): 962-76.

Cueva, Mulholland and Goodman (2007). "Nanoscale organization of the MEC-4 DEG/ENaC sensory cechanotransduction channel in Caenorhabditis elegans touch receptor neurons." J. Neurosci. **27**(51): 14089-14098.

Culleya, Murphya, Babaiea, Nguyena, Pagela, Rousselleb and Clegg (2001). "Laminin-5 promotes neurite outgrowth from central and peripheral chick embryonic neurons." Neuroscience Letters **301**: 4.

Culp, Budgeon, Marinkovich, Meneguzzi and Christensen (2006). "Keratinocyte-Secreted Laminin 5 Can Function as a Transient Receptor for Human Papillomaviruses by Binding Virions and Transferring Them to Adjacent Cells." Journal of Virology **80**(18): 8940-8950.

Dhaka, Viswanath and Patapoutian (2006). "TRP ion channels and temperature sensation." Annu. Rev. Neurosci. **29**: 135-161.

Djouhri, Bleazard and Lawson (1998). "Association of somatic action potential shape with sensory receptive properties in guinea pig dorsal root ganglion neurones." J Physiol **513**(3): 857-872.

Draberova, Sulimenko, Kukharskyy and Draber (1999). "Monoclonal antibody NF-09 specific for neurofilament protein NF-M." Folia Biol (Praha) **45**(4): 163-165.

Drayna (2005). "Human Taste Genetics." Annual Review of Genomics and Human Genetics **6**: 217-235.

Drew, Rugiero, Cesare, Gale, Abrahamsen, Bowden, Heinzmann, Robinson, Brust, Colless, Lewis and Wood (2007). "High-threshold mechanosensitive ion channels blocked by a novel conopeptide mediate pressure-evoked pain." PLoS ONE **2**(6): e515.

Drew, Wood and Cesare (2002). "Distinct mechanosensitive properties of capsaicin-sensitive and -insensitive sensory neurons." J Neurosci **22**(12): RC228.

Driscoll and Tavernarakis (1997). "Molecules that mediate touch transduction in the nematode Caenorhabditis elegans." Gravit Space Biol Bull **10**(2): 33-42.

Du, Gu, William and Chalfie (1996). "Extracellular proteins needed for C. elegans mechanosensation." Neuron **16**(1): 183-94.

Eble, Wucherpfennig, Gauthier, Dersch, Isberg and Hemler (1998). "Recombinant soluble human alpha3beta1 integrin: purification,processing, regulation, and specific binding to laminin-5 and invasin in a mutually exclusive manner." Biochemistry **37**(31): 10945-10955.

Ekblom, Lonai and & Talts (2003). "Expression and biological role of laminin-1." Matrix Biol **22**: 35–47.

Engel (1992). "Laminins and other strange proteins." Biochemistry **31**: 10643.

Ernstrom and Chalfie (2002). "Genetics of sensory mechanotransduction." Annu Rev Genet **36**: 411-53.

Falk-Marzillier, Susan, Domanico, Mullen and Quaranta (1998). "Characterization of a Tight Molecular Complex between Integrin α6β4 and Laminin-5 Extracellular Matrix." Biochemical and Biophysical Research Communications **251**(1): 49-55.

Fernandez-Valle, Wood and Bunge (1998). "Localization of focal adhesion kinase in differentiating Schwann cell/neuron cultures." Microsc Res Tech **41**(5): 416-30.

Flock, Cheung, Flock and Utter (1981). "Three sets of actin filaments in sensory cells of the inner ear. Identification and functional orientation determined by gel electrophoresis, immunofluorescence/electron microscopy. ." J. Neurocytol. **10**: 133-147.

French (1992). "Mechanotransduction." Annu Rev Physiol **54**: 135-52.

Furness and Hackney (1985). "Cross-links between stereocilia in the guinea pig cochlea." Hear Res **18**: 177-188.

Gara, Grumati, Urciuolo, Bonaldo, Kobbe, Koch, Paulsson and Wagener (2008). "Three Novel Collagen VI Chains with High Homology to the 3 Chain." J Biol Chem. **283**(16): 10658-10670.

Garcia-Anoveros and Corey (1997). "The molecules of mechanosensation." Annu Rev Neurosci **20**: 567-94.

Garcia-Anoveros, Ma and Chalfie (1995). "Regulation of Caenorhabditis elegans degenerin proteins by a putative extracellular domain." Curr Biol **5**(4): 441-8.

Garcia-Anoveros, Samad, Zuvela-Jelaska, Woolf and Corey (2001). "Transport and localization of the DEG/ENaC ion channel BNaC1alpha to peripheral mechanosensory terminals of dorsal root ganglia neurons." J Neurosci **21**(8): 2678-86.

Gillespie and Walker (2001). "Molecular basis of mechanosensory transduction." Nature **413**(6852): 194-202.

Goodman, Ernstrom, Chelur, O'Hagan, Yao and Chalfie (2002). "MEC-2 regulates C. elegans DEG/ENaC channels needed for mechanosensation." Nature **415**(6875): 1039-42.

Goodman and Schwarz (2003). "Transducing touch in Caenorhabditis elegans." Annu Rev Physiol **65**: 429-52.

Goodyear and Richardson (1992). "Distribution of the 275 kD Hair Cell Antigen and Cell Surface Specialisations on Auditory and Vestibular Hair Bundles in the Chicken Inner Ear." THE JOURNAL OF COMPARATIVE NEUROLOGY **325**: 243-256.

Goodyear and Richardson (1999). "The ankle-link antigen: an epitope sensitive to calcium chelation associated with the hair-cell surface and the calycal processes of photoreceptors." J Neurosci **19**(10): 3761-72.

Goodyear and Richardson (2003). "A novel antigen sensitive to calcium chelation that is associated with the tip links and kinocilial links of sensory hair bundles." J Neurosci **23**(12): 4878-87.

Gu, Caldwell and Chalfie (1996). "Genetic interactions affecting touch sensitivity in Caenorhabditis elegans." Proc Natl Acad Sci U S A **93**(13): 6577-82.

Halata (1975). "The mechanoreceptors of the mammalian skin ultrastructure and morphological classification." Springer-Verlag Berlin: 1-75.

Hamill and Martinac (2001). "Molecular basis of mechanotransduction in living cells." Physiol Rev **81**(2): 685-740.

Hargrave (1992). "Rhodopsin and phototransduction: a model system for G protein-linked receptors." The FASEB Journal **6**: 2323-2331.

Hasko and Richardson (1988). "The ultrastructural organization and properties of the mouse tectorial membrane matrix." Hear Res **35**(1): 21-38.

Hirokawa and Tilney (1982). "Interactions between actin filaments and between actin filaments and membranes in quick-frozen and deeply etched hair cells of the chick ear." J Cell Biol **95**: 249-261.

Hirosaki (2002). "Laminin-6 Is Activated by Proteolytic Processing and Regulates Cellular Adhesion and Migration Differently from Laminin-5." The journal of Biological Chemistry **277**(51): 49287-49295.

Hormia (1998). "The epithelium-tooth interface--a basal lamina rich in laminin-5 and lacking other known laminin isoforms." J. Dent. Res. **77**(7): 1479-1485.

Howard and Bechstedt (2004). "Hypothesis: a helix of ankyrin repeats of the NOMPC-TRP ion channel is the gating spring of mechanoreceptors." Curr Biol **14**(6): R224-6.

Howard and Bechstedt (2004). "Hypothesis: A helix of ankyrin repeats of the NOMPC-TRP ion channel is the gating spring of mechanoreceptors." Current Biology **14**(6): 224-226.

Howard and Hudspeth (1988). "Compliance of the hair bundle associated with gating of mechanoelectrical transduction channels in the bullfrog's saccular hair cell." Neuron **1**(3): 189-199.

Hu and Lewin (2006). "Mechanosensitive currents in the neurites of cultured mouse sensory neurones " Journal of Physiology **577** 815-828

Hu, Milenkovic and Lewin (2006). "The high threshold mechanotransducer: a status report." Pain **120**(1-2): 3-7.

Huang, Gu, Ferguson and Chalfie (1995). "A stomatin-like protein necessary for mechanosensation in C. elegans." Nature **378**(6554): 292-5.

Hunt and Ottoson (1973). "Receptor potential and impulse activity in isolated mammalian spindles. ." J. Physiol. **230**: 19-50.

Iozzo (1998). "Matrix proteoglycans: from molecular design to cellular function." Annu. Rev. Biochem. **67**: 609-652.

Itzhak and Driscoll (1999). "DEG/ENaC channels: A touchy superfamily that watches its salt " BioEssays **21**(7): 568-578.

Iwasaki, Kaoru, Yoshinori, Yukio, Masakazu, Kiyotoshi and Takao (2005). "Electron tomography reveals diverse conformations of integrin Alpha2bBeta3 in the active state." Journal of Structural Biology **150**: 259-267.

Jacobs and Hudspeth (1990). "Ultrastructural correlates of mechanoelectrical transduction in hair cells of the bullfrog's internal ear." Cold Spring Harb Symp Quant Biol **55**: 547-561.

Jalali, del Pozo, Chen, Miao, Li, Schwartz, Shyy and Chien (2001). "Integrin-mediated mechanotransduction requires its dynamic interaction with specific extracellular matrix (ECM) ligands." Proc Natl Acad Sci U S A **98**(3): 1042-6.

Jasmin and Ohara (2004). "Anatomical Identification of Neurons Responsive to Nociceptive Stimuli." Pain Research **99**: 1543-1894.

Kachar, Parakkal, Kurc, Zhao and Gillespie (2000). "High-resolution structure of hair-cell tip links." Proc Natl Acad Sci U S A **97**(24): 13336-41.

Kariya and Miyazaki (2004). "The basement membrane protein Laminin-5 acts as a soluble cell motility factor." Exp. Cell Res. **297**: 508-520.

Kazmierczak, Sakaguchi, Tokita, Wilson-Kubalek, Milligan, Muller and Kachar (2007). "Cadherin 23 and protocadherin 15 interact to form tip-link filaments in sensory hair cells." Nature **449**(7158): 87-91.

Kernan, Cowan and Zuker (1994). "Genetic dissection of mechanosensory transduction: mechanoreception-defective mutations of Drosophila." Neuron **12**(6): 1195-206.

Kim Bak Jensen (2003). "Identification of Keratinocyte-specific Markers Using Phage Display and Mass Spectrometry." Molecular & Cellular Proteomics **2**: 9.

Kloda and Martinac (2002). "Mechanosensitive channels of bacteria and archaea share a common ancestral origin." Eur Biophys J **31**(1): 14-25.

Koerber (1992). Functional Heterogeneity of Dorsal Root Ganglion Cells.

Koerber, Druzinsky and Mendell (1988). "Properties of somata of spinal dorsal root ganglion cells differ according to peripheral receptor innervated." J Neurophysiol **60**: 1584-1596.

Koizumi, Fujishita, Shigimato, Tsuda and Inoue (2004). "Ca2+ waves in keratinocytes are transmitted to sensory neurons: the involvement of extracellular ATP and P2Y2 receptor activation." Biocehm. J. **380**: 329-338.

Koltzenburg, Stucky and Lewin (1997). "Receptive properties of mouse sensory neurons innervating hairy skin." J Neurophysiol **78**(4): 1841-50.

Kruger (1996). "The functional morphology of thin sensory axons: some principles and problems." Prog. in Brain Res. **113**: 255-272.

Kruger, Light and Schweizer (2004). "Axonal terminals of sensory neurons and their morphological diversity " Journal of Neurocytology **32**(3): 205-216.

Kumar, Chaudhry, Reid and Boriek (2002). "Distinct signaling pathways are activated in response to mechanical stress applied axially and transversely to skeletal muscle fibers." J Biol Chem **277**(48): 46493-503.

Kumar, Yin and Paulaitis (2002). "Relating Interactions between Neurofilaments to the Structure of Axonal Neurofilament Distributions through Polymer Brush Models." Biophysical Journal **82**(5): 2360-2372.

Kung (2005). "A possible unifying principle for mechanosensation." Nature **436**: 647-654.

Kunneken, Pohlentz, Schmidt-Hederich, Odenthal, Smyth, Peter-Katalinic, Bruckner and Eble (2004). "Recombinant human Laminin-5 domains. Effects of heterotrimerization, proteolytic processing, and N-glycosylation on α3/β1 Integrin binding. ." J. Biol. Chem. **279**: 5184-5193.

Lai, Hong, Kinnell, Chalfie and Driscoll (1996). "Sequence and transmembrane topology of MEC-4, an ion channel subunit required for mechanotransduction in Caenorhabditis elegans." J Cell Biol **133**(5): 1071-81.

Langer, Koitschev, Rexhausen and Ruppersberg (2001). "Lateral Mechanical Coupling of Stereocilia in Cochlear Hair Bundles." Biophysical Journal **80**(6): 2608-2621.

Laurent (1999). "A systems perspective on early olfactory coding." Science **286**: 723-728.

Lawson (1992). "Morphological and Biochemical Cell Types of Sensory Neurons." Sensory neurons: Diverity, Development, and Plasticity, edited by S.A. Scott, New York: Oxford University Press: 27-59.

Lawson (2002). "Phenotype and function of somatic primary afferent nociceptive neurones with C-, Adelta- or Aalpha/beta fibres." Exp Physiol **87**: 239-244.

Lechner, Frenzel, Wang and Lewin (2009). "Developmental Waves of mechanosensitivity acquisition in sensory neuron subtypes during embryonic development." The EMBO Journal **in press**.

Legan, Goodyear and Richardson (2001). "The 275 kD hair-cell antigen and the glomerular mesangial cell phosphatase rPTP-GMC1 have an identical distribution on the haircell's apical surface " Assoc Res Otolaryngol Abstr **24**: 138.

Legan, Rau, Keen and Richardson (1997). "The mouse tectorins. Modular matrix proteins of the inner ear homologous to components of the sperm-egg adhesion system." J. Biol. Chem. **272**: 8791-8801.

Lewin and Moshourab (2004). "Mechanosensation and pain." J Neurobiol **61**(1): 30-44.

Li, Edgar, Fassler, Wadsworth and Yurchenco (2003). "The role of laminin in embryonic cell polarization and tissue organization." Dev. Cell **4**: 613-624.

Lin, Cheng, LeDuc and Chen (2009). "Understanding Sensory Nerve Mechanotransduction through Localized Elastomeric Matrix Control." PLoS ONE **4**(1): 1-9.

Loewenstein (1959). "The generation of electric activity in a nerve ending." Ann N Y Acad Sci **81**: 367-87.

Loewenstein and Skalak (1996). "Mechanical transmission in a Pacinian corpuscle- An analysis and a theory." J. Physiol. **182** 346–378.

Lotz, Nusrat, Madara, Ezzell, Wewer and Mercurio (1997). "Intestinal epithelial restitution. Involvement of specific laminin isoforms and integrin laminin receptors in wound closure of a transformed model epithelium." American Journal of Pathology **150**: 747-760.

Lucarz and Gerard (2007). "Current considerations about Merkel cells " European Journal of Cell Biology **86**(5): 243-251.

Lundquist (1996). "The mec-8 gene of C. elegans encodes a protein with two RNA recognition motifs and regulates alternative splicing of unc-52 transcripts." Development **122**(5): 1601-1610.

Lynch (1997). "Nonsyndromic deafness DFNA1 associated with mutation of a human homolog of the Drosophila gene diaphanous. ." Science **278**: 1315-1318.

Lynn (1975). "Somatosensory receptors and their CNS connections." Annu Rev Physiol **37**: 105-27.

Mannsfeldt, Carroll, Stucky and Lewin (1999). "Stomatin, a MEC-2 like protein, is expressed by mammalian sensory neurons." Mol Cell Neurosci **13**(6): 391-404.

Marina, Christopher, Chen and Ingber (1998). "Cellular control lies in the balance of forces." Current Opinion in Cell Biology **10**(2): 232-239.

Marinkovich (1993). "The basement membrane proteins kalinin and nicein are structurally and immunologically identical." Lab. Invest. **69**: 295–299.

Marinkovich (2007). "Laminin 332 in squamous-cell carcinoma." Nature Reviews Cancer **7**: 370-380.

Markin and Hudspeth (1995). "Gating-spring models of mechanoelectrical transduction by hair cells of the internal ear." Annu Rev Biophys Biomol Struct **24**: 59-83.

Martin and Timpl (1987). "Laminin and other basement membrane components." Annu. Rev. Cell Biol. **3**: 57-85.

Masunaga, Ishiko, Tomita, Aberdam, Ortonne, Nishikawa and Shimizu (1996). "Localization of Laminin-5 in the epidermal basement membrane " The Journal of Histochemistry and Cytochemistry **44**(11): 1223-1230.

Mcgee, Goodyear, Legan and Walsh (2006). "The very large G-protein-coupled receptor VLGR1: a component of the ankle link complex required." J Neurosci **26**: 6543-6553.

McMillan, McGrath, Tidman and Eady (1998). "Hemidesmosomes show abnormal association with the keratin filament network in junctional forms of epidermolysis bullosa." J Invest Dermatol **110**(2): 132-7.

Mendrick and Kelly (1993). "Temporal expression of VLA-2 and modulation of its ligand specificity by rat glomerular epithelial cells in vitro." Lab Invest **69**(6): 690-702.

Meneguzzi (1992). "Kalinin is abnormally expressed in epithelial basement membranes of Herlitz's junctional epidermolysis bullosa patients." Exp. Dermatol. **1**: 221-229.

Mianchi (2007). "Mechanotransduction: Touch and Feel at the Molecular Level as Modeled in Caenorhabditis elegans." Molecular Neurobiology **36**: 254-271.

Michel, Goodyear, Richardson and Petit (2005). "Cadherin 23 is a component of the transient lateral links in the developing hair bundles of cochlear sensory cells. ." Dev Biol **280**: 281-94.

Mombaerts (2004). "Genes and ligands for odorant, vomeronasal and taste receptors." Nature Reviews Neuroscience **5**: 263-278.

Nagel and Thurm (1991). "Structures transmitting stimulatory force to the sensory hairs of vestibular ampullae of fishes and frog " Cell and Tissue Research **265**: 567-578.

Nishimune, Sanes and Carlson (2004). "A synaptic laminin-calcium channel interaction organizes active zones in motor nerve terminals." Nature **432**: 580-587.

O' Hagan, Chalfie and Goodman (2005). "The MEC-4 DEG/ENaC channel of Caenorhabditis elegans touch receptor neurons transduces mechanical signals." Nature Neuroscience **8**(1): 43-50.

Ohara, Gahara, Miyake, Teraoka and Kitamura (1993). "Neurofilament deficiency in quail caused by nonsense mutation in neurofilament-L gene." J Cell Biol **121**(2): 387-395.

Ohara O (1993). "Neurofilament deficiency in quail caused by nonsense mutation in neurofilament-L gene." J Cell Biol **121**(2): 387-395.

Osborne and Comis (1990). "Action of elastase, collagenase and other enzymes upon linkages between stereocilia in the guinea-pig cochlea." Acta Otolaryngol **110**(1-2): 37-45.

Osborne, Comis and Pickles (1984). "Morphology and cross-linkage of stereocilia in the guinea-pig labyrinth examined without the use of osmium as a fixative." Cell and Tissue Research **237**: 43-48.

Paladini and Coulombe (1998). "Directed expression of keratin 16 to the progenitor basal cells of transgenic mouse skin delays skin maturation." J Cell Biol **142**(4): 1035-51.

Patel (1998). "A mammalian two pore domain mechano-gated S-like K+ channel." The EMBO Journal **17**(15): 4283-4290.

Patel, Lazdunski and Honore (2001). "Lipid and mechano-gated 2P domain K(+) channels." Curr Opin Cell Biol **13**(4): 422-8.

Patricia Rousselle (1995). "Structural Requirement for Cell Adhesion to Kalinin (Laminin-5)." The journal of Biological Chemistry **270**: 5.

Paulsson, Aumailley, Deutzmann, Timpl, Beck and Engel (1987). "Laminin-nidogen complex. Extraction with chelating agents and structural characterization." Eur J Biochem **166**(1): 11-9.

Pickles, Brix, Comis, Gleich, Koppl, Manley and Osborne (1989). "The organization of tip links and stereocilia on hair cells of bird and lizard basilar papillae." Hear Res **41**(1): 31-41.

Pickles, Comis and Osborne (1984). "Cross-links between stereocilia in the guinea pig organ of Corti, and their possible relation to sensory transduction." Hear Res **15**(2): 103-112.

Price, Lewin, McIlwrath, Cheng, Xie, Heppenstall, Stucky, Mannsfeldt, Brennan, Drummond, Qiao, Benson, Tarr, Hrstka, Yang, Williamson and Welsh (2000). "The mammalian sodium channel BNC1 is required for normal touch sensation." Nature **407**(6807): 1007-11.

Price, McIlwrath, Xie, Cheng, Qiao, Tarr, Sluka, Brennan, Lewin and Welsh (2001). "The DRASIC cation channel contributes to the detection of cutaneous touch and acid stimuli in mice." Neuron **32**(6): 1071-83.

Pulkkinen (1994). "A homozygous nonsense mutation in the beta 3 chain gene of laminin 5 (LAMB3) in Herlitz junctional epidermolysis bullosa." Genomics **24**: 357–360

Richardson, Bartolami and Russell (1990). "Identification of a 275-kD protein associated with the apical surfaces of sensory hair cells in the avian inner ear." J Cell Biol **110**(4): 1055-66.

Rousselle, Lunstrum, Keene and Burgeson (1991). "Kalinin: an epithelium-specific basement membrane adhesion molecule that is a component of anchoring filaments." Journal of Cell Biology **114**: 567-576.

Rowe (2002). "Synaptic transmission between single tactile and kinaesthetic sensory nerve fibers and their central target neurones." Behav Brain Res **135**(1-2): 197-212.

Ryan (1996). "The functions of laminins: lessons from in vivo studies. ." Matrix Biol. **15**: 369–381.

Sann, Xu, Nishimune, Sanes and Spitzer (2008). "Neurite outgrowth and in vivo sensory innervation mediated by a Cav2.2-Laminin beta2 stop signal." The Journal of Neuroscience **28**(10): 2366-2374.

Sasaki, Fassler and Hohenester (2004). "Laminin: the crux of basement membrane assembly. ." J. Cell Biol **164,**: 959–963

Scott (2005). "Taste Recognition: Food for Thought " Neuron **48**(3): 455-464.

Sidi, Friedrich and Nicolson (2003). "NompC TRP channel required for vertebrate sensory hair cell mechanotransduction." Science **301**(5629): 96-9.

Siemens (2004). "Cadherin 23 is a component of the tip link in hair-cell stereocilia." Nature **428**: 950-955.

Siemens, Lillo, Dumont, Reynolds, Williams, Gillespie and Muller (2004). "Cadherin 23 is a component of the tip link in hair-cell stereocilia." Nature **428**(6986): 950-5.

Sollner, Rauch, Siemens, Geisler, Schuster, Muller and Nicolson (2004). "Mutations in cadherin 23 affect tip links in zebrafish sensory hair cells." Nature **428**(6986): 955-9.

Spinardi, S., Cullen, Milner and Giancotti (1995). "A recombinant tail-less integrin beta 4 subunit disrupts hemidesmosomes, but does not suppress alpha 6 beta 4-mediated cell adhesion to laminins." J Cell Biol **129**: 473-487.

Storm (2003). "Calmodulin-Regulated Adenylyl Cyclases: Cross-Talk and Plasticity in the Central Nervous System." Molecular Pharmacology **63**(3): 463-468.

Sukharev and Anishkin (2004). "Mechanosensitive channels: what can we learn from simple model systems?" Trends in Neuroscience **Vol.27 No.6**: 345-351.

Sukharev, Blount, Martinac, Blattner and Kung (1994). "A large-conductance mechanosensitive channel in E. coli encoded by mscL alone." Nature **368**(6468): 265-8.

Syntichaki and Tavernarakis (2004). "Genetic models of mechanotransduction: the nematode Caenorhabditis elegans." Physiol Rev **84**(4): 1097-153.

Takagi (2002). "Global Conformational Rearrangements in Integrin Extracellular Domains in Outside-In and Inside-Out Signaling." Cell **110**(5): 599-611

Tavernarakis, Shreffler, Wang and Driscoll (1997). "unc-8, a DEG/ENaC family member, encodes a subunit of a candidate mechanically gated channel that modulates C. elegans locomotion." Neuron **18**(1): 107-19.

Tilney (1989). "Preliminary biochemical characterization of the stereocilia and cuticular plate of hair cells of the chick cochlea." J. Cell Biol. **109**(1711-1723).

Timpl (1979). "Laminin-a glycoprotein from basement membranes." J. Biol. Chem. **254**: 9933–9937.

Tobin and Bargmann (2004). "Invertebrate nociception: behaviors, neurons and molecules." J Neurobiol **61**(1): 161-74.

Tomaselli, Doherty, Emmett, Damsky, Walsh and Reichardt (1993). "Expression of beta 1 integrins in sensory neurons of the dorsal root ganglion and their functions in neurite outgrowth on two laminin isoforms." J Neurosci **13**(11): 4880-8.

Tsuruta, Hopkinson, Lane, Werner, Cryns and Jones (2003). "Crucial role of the specificity-determining loop of the Integrin β4 subunit in the binding of cells to Laminin-5 and outside-in signal transduction." J. Biol. Chem. **278**: 38707-38714.

Ulmann, Rodeau, Danoux, Contet-Audonneau, Pauly and Schlichter (2007). "Trophic effects of keratinocytes on the axonal development of sensory neurons in a coculture model." Eur. J. Neurosci. **26**(1): 113-125.

Veit (2006). "Collagen XXVIII, a Novel von Willebrand Factor A Domain-containing Protein with Many Imperfections in the Collagenous Domain." The journal of Biological Chemistry **281**(6): 3494-3504.

von Philipsborn, Lang, Andre´ Bernard, Loeschinger, David, Lehnert, Bastmeyer and Bonhoeffer (2006). "Microcontact printing of axon guidance molecules for generation of graded patterns." Nature Protocol **VOL.1 NO.3**: 7.

Walker (2000). "A Drosophila mechanosensory transduction channel." Science **287**: 2229-2234.

Walz (2003). "Structure of integrin alpha5beta1 in complex with fibronectin." The EMBO Journal **22**: 4607-4615.

Wetzel, Hu, Riethmacher, Benckendorff, Harder, Eilers, Moshourab, Kozlenkov, Labuz, Caspani, Erdmann, Machelska, Heppenstall and Lewin (2007). "A stomatin-domain protein essential for touch sensation in the mouse " Nature **445**(7124): 206-209.

Xia (1996). "Anchorage Mediated by Integrin a6134 to Laminin-5 (Epiligrin) Regulates Tyrosine Phosphorylation of a Membrane-associated 80-kD Protein." J. Cell Biol. **132**: 727-740.

Zhang (2004). "MEC-2 is recruited to the putative mechanosensory complex in C. elegans touch receptor neurons through its stomatin-like domain. ." Curr Biol **14**(21): 1888-1896.

Zhang, Jones, Brody, Costa and Brookes (2004). "Thermosensitive Transient Receptor Potential Channels in Vagal Afferent Neurons of the Mouse." Am J Physiol Gastrointest Liver Physiol.

Zhang and Randall (1996). "Laminin 5 deposition promotes keratinocyte motility." Experimental Cell Research **227**(2): 309-322.

Zhao, Yamoah and Gillespie (1996). "Regeneration of broken tip links and restoration of mechanical transduction in hair cells." Proc Natl Acad Sci U S A **93**(26): 15469-74.

Zheng, Sekerkova, Vranich, Tilney, Mugnaini and Bartles (2000). "The deaf jerker mouse has a mutation in the gene encoding the espin actin-bundling proteins of hair cell stereocilia and lacks espins." Cell **102**(3): 377-85.

Zylka, Rice and Anderson (2005). "Topographically distinct epidermal nociceptive circuits revealed by axonal tracers targeted to Mrgprd." Neuron **45**(1): 17-25.

6 APPENDIX

6.1 List of Figures

6.2 List of Tables